Study of α-β Phase Transition in K_2ZnBr_4

by

Masaki TAKESADA

Research Institute for Electronic Science,

Hokkaido University, Sapporo

1995

ACKNOWLEDGEMENTS

The author wishes to express his sincere thanks to Professor Toshirou Yagi of Hokkaido University for his guidance and discussions through out the course of this work. He is grateful to Professor Hiroyuki Mashiyama of Yamaguchi University for his valuable discussions and comments. It is a pleasure to thanks Professor Shuichi Kinoshita of Osaka University of his critical discussion and suggestion. He wishes to express his appreciation to Professor Yuhji Tsujimi and Dr. Masaru Kasahara of Hokkaido University and Dr. Hironobu Kasano of Yamaguchi University for their encouragements and useful criticism. It is a honor to thank Dr. Masashi Yamaguchi of Hokkaido University for his continual experimental advice and suggestion. He wishes to thank Dr. Eisuke Suzuki and Dr. Pho Kaung of Hokkaido University for their discussion. He is grateful to Mr. Takeshi Kado of Hokkaido University for technical assistance and advice. Thanks go to Miss Rui Kageyama for drawing of tables of this thesis. He thanks members of the laboratory for their continuous encouragements. Finally, he would like to thank his parents for their never ending support.

ABSTRACT

The mechanism of the α-β phase transition in K_2ZnBr_4 is investigated by means of X-ray diffraction and Brillouin scattering. The transition is a first order and reconstructive one accompanied with a large amount of atomic displacements. By X-ray study an interesting relation were found between the unit cell axes of the α and β phases. The relation can not be explained by an ordinal group theoretical method applicable to the second order phase transition in orthorhombic Rb_2ZnCl_4-group crystals. In order to explain the transition mechanism, an intermediate body-centered cubic and a hexagonal closed-packed structure are considered as virtual states between the α and β phases as the virtual intermediate states model (VIS model).

The Brillouin scattering spectra have been observed near the transition point (T_t=458K) as a function of temperature. After the transition, the spectra of high-temperature β phase take different values of the frequency shift in each experimental run in contrast to the good reproducibility in low α phase. A characteristic discrete distribution of the frequency shift of the longitudinal acoustic mode in the β phase was observed by Brillouin scattering experiment repeated many times on heating run through T_t. On the other hand, the transverse mode shows negligibly small anomalous behavior near T_t. The results are well explained by the elastic properties calculated in terms of the VIS model. Furthermore the space groups of the virtual intermediate states are concluded as $Im\bar{3}m$ and $P6_3/mmc$ by the both results of X-ray and Brillouin scattering studies.

CONTENTS

LIST OF FIGURES

Figure

Figure

Figure

LIST OF TABLES

Table

CHAPTER 1 INTRODUCTION

Phase transition phenomena exist widely in nature. They have been generally classified into two parts; first order transition and second order one. For the latter case, due to its continuous behavior near the transition point, a group-subgroup relationship holds between the high and low symmetry phases which take place on each side of the transition. This relationship defines the symmetry of the lower temperature phase as a subgroup of the symmetry group of the high temperature phase. The most characteristic point of the transition is that it is accompanied with infinitesimal displacements of the atoms from one equilibrium position to another at the transition. For these transition, many successful studies have been carried out theoretically and experimentally in recent few decades in terms of an application of the symmetry and thermodynamic concepts of the Landau theory.

On the other hand, for the first order transition, a finitary atomic displacement and strong discontinuous properties appear in addition to breakdown of group-subgroup relationship between the two phases. (Strictly speaking, although a part of first order phase transitions has the group-subgroup relationship, we pay attention to the first order phase transition which do not have the relationship, here.) Due to these difficulties few studies have been reported for the first order phase transition. However, although the most of elements,[1)] a number of alloys[1,2)], many of dielectrics[2)] and ferroelectrics belong to this category. In particular the reconstructive phase transition which are accompanied by large atomic displacements is

usually accepted as the transition where no symmetry relation holds between the relevant phases. By V. Dmitriev etal. some theoretical studies have been reported for only some reconstructive phase transitions.[3] But these reports can not explain the characteristic of the reconstructive phase transition enough.

In contrast to the preceding idea, the present study adds a new light to the study of the reconstructive phase transition. Here, we consider as the following; a physical relation should exist between the two phases in each side of the reconstructive phase transition due to a restraint in the cause of composing their crystal structures. Then the present study treats the reconstructive phase transition changed from a solid phase to the other one. We chose here ferroelectric K_2ZnBr_4 crystal as a typical example of the reconstructive phase transition, the α-β transition. The relationship between the crystallographic axes of the low temperature α and high temperature β phases is observed by using X-ray diffraction and Brillouin scattering. In order to explain the axis relation obtained by X-ray study, the virtual intermediate states model (the VIS model) is newly proposed as a mechanism of the α-β transition. The VIS model is assumed the group-subgroup relation between the α phase and a virtual intermediate state (VIS), and between the β phase and the other VIS, respectively. The Burgers' relation between body-centered cubic (bcc) and a hexagonal closed-packed structure (hcp) structure is applied to a relationship between the two VIS. By the VIS model it becomes possible that the reconstructive phase transition is considered continuously. Furthermore, the VIS model is confirmed by Brillouin scattering study.

In § 1.1 the studies of the A_2BX_4 type compounds are briefly described. The historical studies of the α-β transition are summarized in § 1.2. The purpose of the present study is described in §1.3.

§ 1.1 A_2BX_4 type Ferroelectrics

Ferroelectrics of A_2BX_4 type compounds generally have either a phase transition sequence based on the β-K_2SO_4 type structure[4] or the Sr_2GeS_4 type structure[5]. The β-K_2SO_4 type compounds have the isomorphous structure with the space group Pmcn and indicate a similar sequence of phase transitions each other.[4,6,7] In A_2BX_4 type compounds, it is well known that the sequence is realized in the case of A is K or Rb, B is Zn or Co and X is Cl or Br. In this case the compounds undergo the phase transition from the normal phase with β-K_2SO_4 structure (Pmcn) to the incommensurate phase followed by the commensurate phase of threefold cell expansion along the c-axis (ferroelectric, $P2_1cn$).[7-9] We abbreviate normal, incommensurate and commensurate as N, INC and C, and for the compounds K_2ZnBr_4, K_2CoBr_4, Rb_2ZnCl_4 and Rb_2ZnBr_4 as KZB, KCB, RZC and RZB, hereafter. These compounds are known as the Rb_2ZnCl_4 group compounds (the RZC group compounds) expect for KZB and KCB.[8] By Shimizu et al. the phase transition sequences were summarized in ref.10 as shown in Fig.1.1.

Some of the latter Sr_2GeS_4 type compounds in A_2BX_4 ferroelectrics have been investigated by several authors mainly on the halide compounds for X=Br or I.[5,10-17] Gesi first observed ferroelectricity of the Sr_2GeS_4 type compound of Tl_2ZnI_4 and

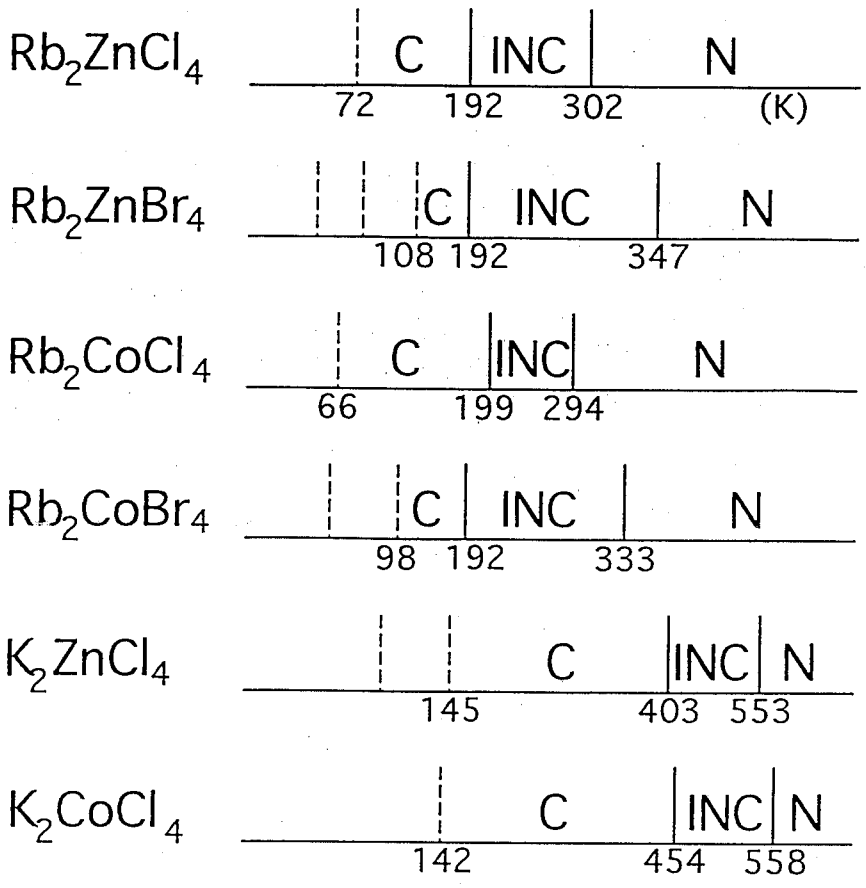

Fig. 1.1 β-K_2SO_4 type ferroelectric crystals, where A=Rb or K, B=Zn or Co and X=Cl or Br, and their phase transition sequences. N: normal phase, INC: incommensurate phase, C: commensurate phase. Each crystal shows ferroelectricity along the a-axis below its incommensurate-commensurate transition point. [Shimizu et al.[10)]]

found a phase transition from a paraelectric Sr_2GeS_4 structure phase with space group $P2_1/m$ to a ferroelectric phase with $P2_1$.[5] It was also pointed out by Gesi that there is a possibility of finding other ferroelectric materials in the Sr_2GeS_4 type compounds. Recently, the analogous ferroelectricity and phase transition sequence have been reported in some other compounds.[10,15-17]

Some compounds among these A_2BX_4 type ferroelectrics, KCB[9,17-19], KZB[9,10,16,19,20], Rb_2ZnI_4[14,20], Rb_2MnI_4[21,22] (RMI) and Rb_2FeI_4[23] (RFI), have both phase transition sequences based on the Sr_2GeS_4 and β-K_2SO_4 type structures (α and β sequences, respectively). The α sequence is the low temperature stable one and the β sequence the high temperature stable one. Furthermore, a phase transition between the two sequences takes place and is called as the α-β transition. The α-β transition is a first order and reconstructive one. For example the successive transitions of KZB on the α and β sequences are summarized in Fig.1.2[20,24] The β sequence changes again to the α sequence below 440K. If the crystal is quenched rapidly, the crystal system remains in the β sequence. But below 440K, the β sequence is metastable and reverses to the α sequence. On the β sequence, the crystal successively performs the N-INC and INC-C phase transitions as the RZC-group ferroelectrics.[8]

As shown in Fig.1.2, the phases on each sequence are denoted as α_I and α_{II} in α sequence and β_I, β_{II}, β_{III} and β_{IV} in the β sequence, respectively. The α-β transition takes place between α_I and β_{II} phases. Hereafter α_I and β_{II} phases are denoted as α and β phases for simplicity. The mean structure of disordered-α phase is shown in Fig.1.3(a).[16] Hereafter we call this structure as α

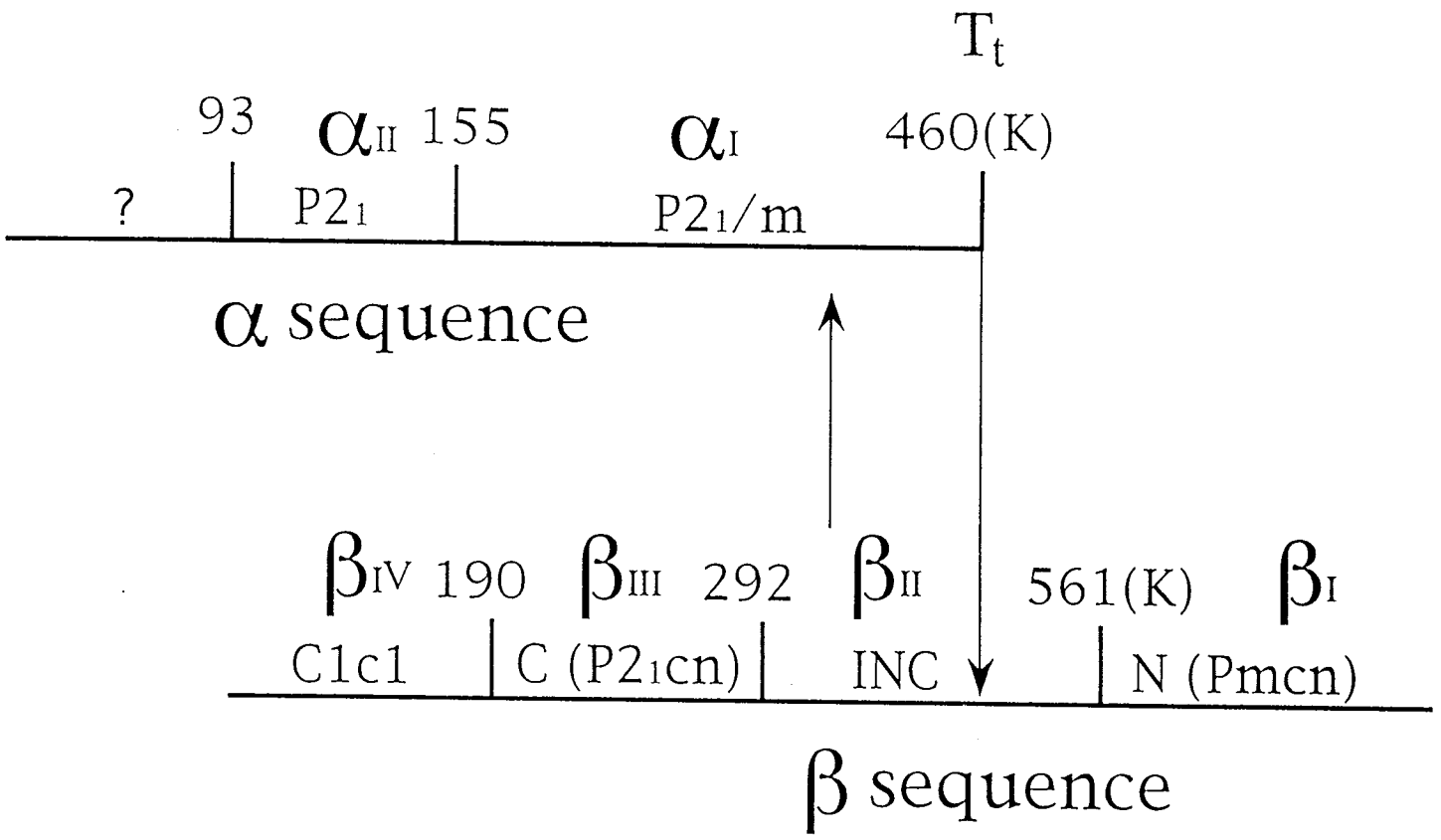

Fig. 1.2 The phase sequences and the space groups realized in K_2ZnBr_4.

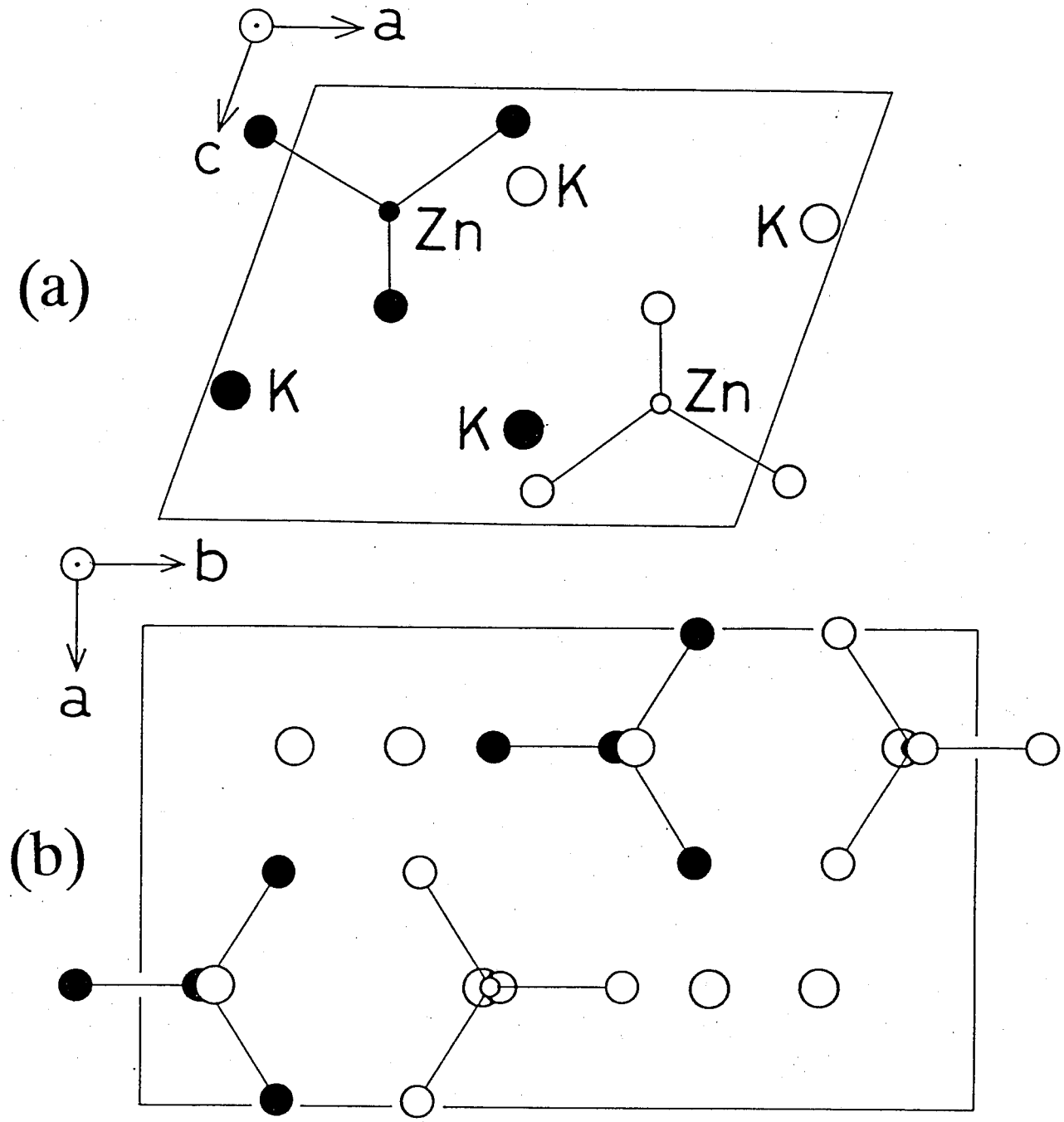

Fig. 1.3 The α and β structures of K_2ZnBr_4. (a)The b axis of this monoclinic unique axis is perpendicular both to the a and c axes. Filled circles (K-atom) and filled $ZnBr_4$ tetrahedron lie on one mirror plane (z=1/4), and open circles lie on the other mirror plane (z=3/4).

(b) β structure takes the pseudo-hexagonal structure. The c axis is the pseudo-hexagonal axis and is perpendicular to the plane. The filled and open circles showing the tetrahedra ($ZnBr_4$) indicate the different layers on which the center Zn-atoms sit.

structure. That is, the α structure is the Sr_2GeS_4 type structure, monoclinic one. Similarly, β structure shown in Fig.1.3(b) is given as the mean structure of disordered β_I phase.[20] The β structure is the β-K_2SO_4 type structure, orthorhombic one. The phase transition accompanies a considerably large atomic displacement because of the difference between the two crystal structures.[20,24]

In summary, the interesting points of the α-β transition are as follows: from a structural viewpoint, the succession of phases on the β sequence and also the crystal structure of β phase[20] are similar to those of the RZC group. On the other hand the α sequence shows a quite different sequence and structure from the RZC group. In addition to this, the α-β transition is the reconstructive one, so a considerable amount of atomic displacement is expected.

§1.2 Historical Review of the Studies of α-β Phase Transition

A few studies have been reported on the α-β transition: Shimizu et al. have been reported some anomalous quantities for the α-β transition at T_t by the differential thermal analysis (DTA) measurement and dielectric measurement of KCB[17,19], KZB[10,19], RMI[22,23] and RFI[23]. The results of KZB are shown in Figs.1.4(a) and (b).[17] In the curve 2 (the dielectric constant) of Fig.1.4(a) and the curve 1 (DTA trace) of Fig.1.4(b), the anomaly observed around 470K indicates the α-β transition on heating run. The characteristic of the α-β transition is the strong endothermic anomaly as shown in Fig.1.4(b). The curves 1 and 2 in Fig.1.4(a) indicate a cooling and heating runs in the α

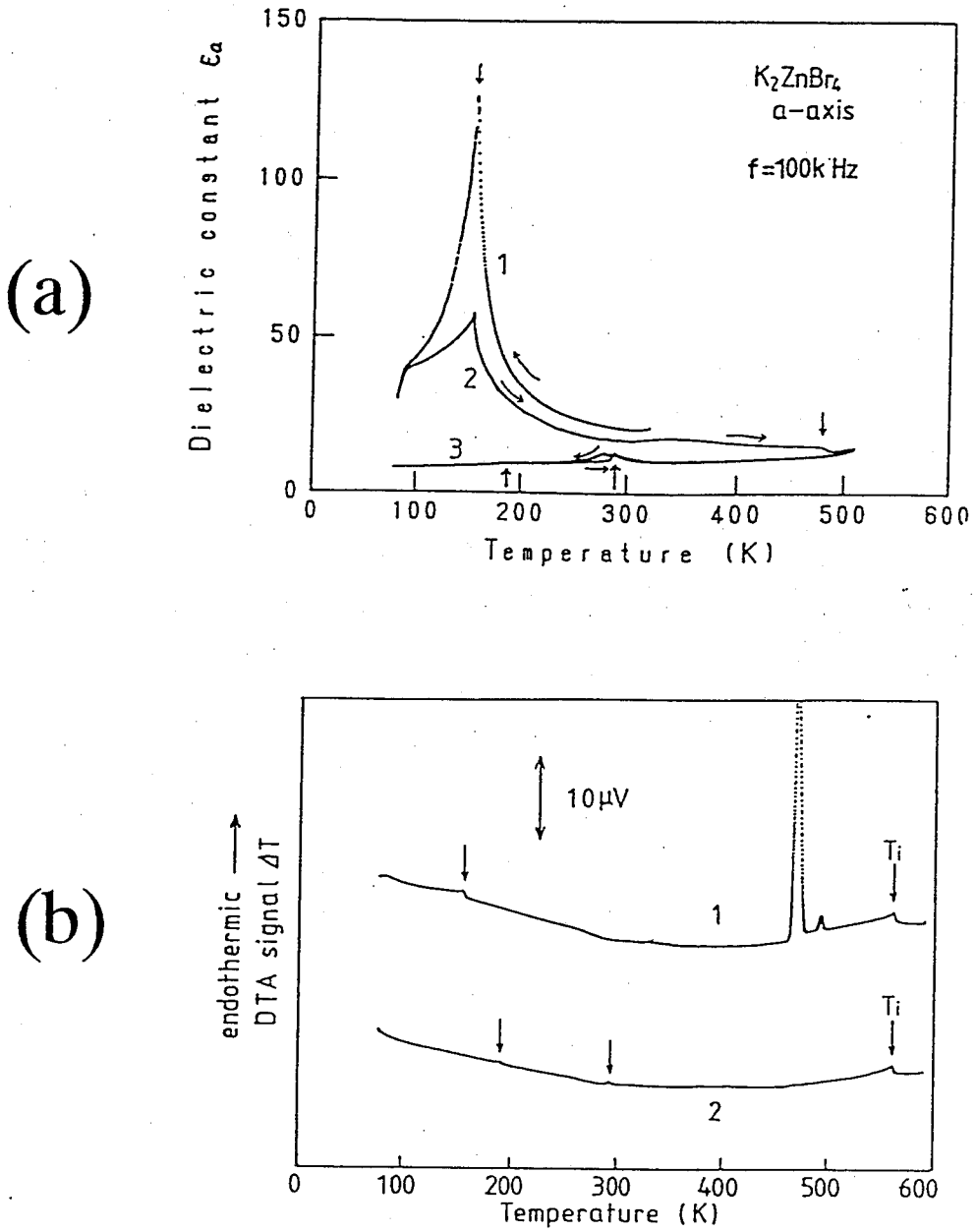

Fig. 1.4 (a) Temperature dependence of dielectric constant, ε_a, along the a-axis of K_2ZnBr_4. (b) DTA trace of K_2ZnBr_4 on heating. [Shimizu et al.[19)]]

sequence, respectively. The anomaly observed around 155K indicates a phase transition from paraelectric α_I phase with $P2_1/m$ to ferroelectric α_{II} phase with $P2_1$, which is characteristic of the α sequence. The curve 3 in Fig.1.4(a) shows the heating and cooling runs on the β sequence below 440K. The curve 2 in Fig.1.4(b) also indicates the heating on the β sequence. Thus the high temperature stable β sequence is easily supercooled to realize all other phases on the sequence.

The α-β transition from α to β phase has been interested because of the long time behavior of the transition process. In KCB[17] and KZB[25], the time-dependent recovering process from the metastable β to the α phases has been investigated in the region between 470K and room temperature by measuring of dielectric constant as shown in Figs.1.5(a) and (b).[25] In Fig.1.5.(a), the curve obtained at each quenching temperature shows a gradual approach toward the value of the α phase. Figure 1.5(b) shows the plot of incubation time obtained in Fig.1.5(a) as a function of holding temperature. Here the incubation time is defined as necessary time to start to change to the α sequence. As shown in Fig.1.5(b), the supercooled sample in the temperature region around room temperature recovers most quickly.

By Mashiyama et al[20] the temperature dependence of the unit cell of KZB is given in both of the α and β sequence as a function of temperature. The unit cell volume of the β phase is just twice the α phase within the experimental errors in the whole temperature range as shown in Fig.1.6.[20] Finally the history of studies about the α-β transition is summarized in Table 1.1. However, there is no report about the reconstructiveness of the α-β transition.

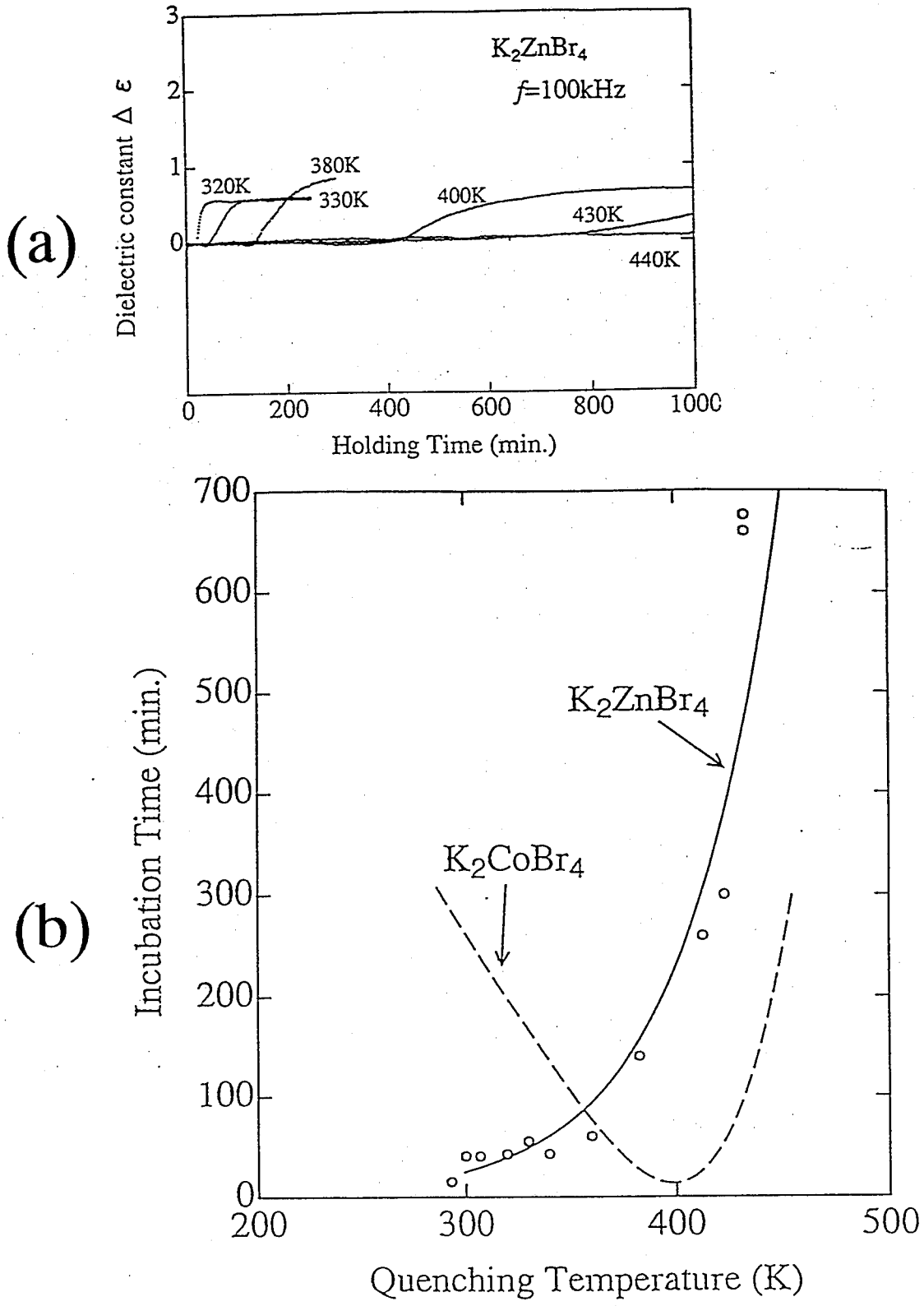

Fig. 1.5. (a) Time dependence of the dielectric constant (c-direction) after the sample was quenched to temperatures shown in the figure, from above the α-β transition. (b) Open circles indicate the incubation time as a function of quenching temperature for K_2ZnBr_4. Broken curve indicates the data of K_2CoBr_4. [Shimizu et al.[25)]]

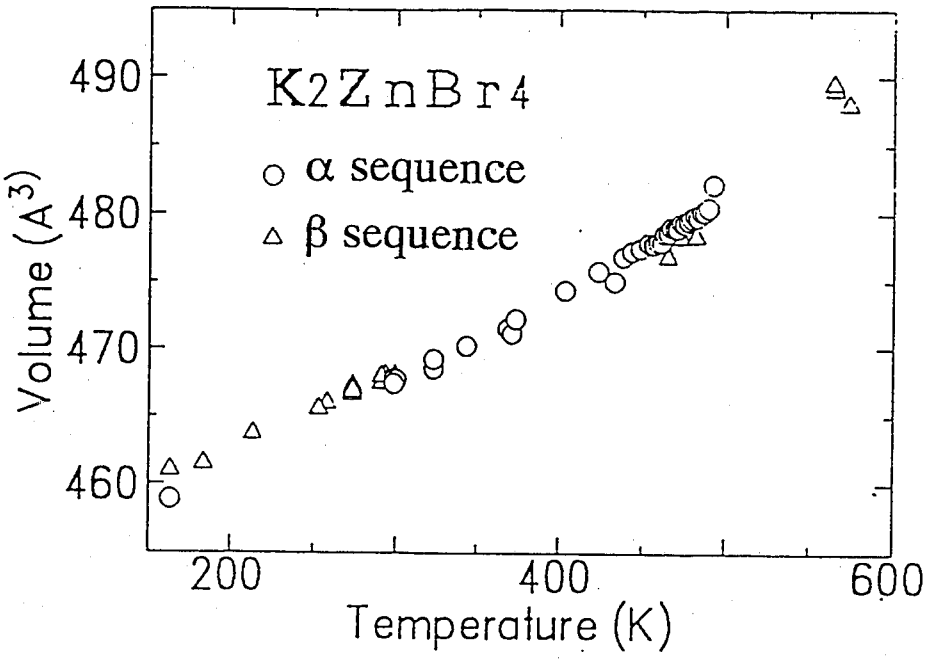

Fig. 1.6. The temperature dependence of the unit cell volume. The half volume of the basic cell of the β sequence is plotted as the β phase one. [Mashiyama et al.[20)]]

HISTORICAL SUMMARY

year	compond	subjects	authors	Ref.No.
1975	K_2CoBr_4	α-β Transition (by DTA) first report	H. J. Seifert et al.	17
1978	Rb_2MnI_4	α-β Transition (by DTA andX-ray)	H. J. Seifert et al.	20
1984	Rb_2ZnI_4	ferrooelectricity in Sr_2GeS_4 type compound ?	K. Geshi	13
1985	Tl_2ZnI_4	ferrooelectricity in Sr_2GeS_4 type compound		
		first report (by dielectric mesurement)	K. Geshi	4
1986	K_2CoBr_4	α-β Transition (by X-ray)	J.Warczewski et al.	29
1990	K_2CoBr_4	Time dependent Phase Transition		
		(by dielectric measurement)	H. Suzuki et al.	16
1990	K_2ZnBr_4	New ferroelectric with α-β Transition		
		(by DTA and dielectric measurements)	F. Shimizu et al.	9
1991	K_2ZnBr	N-INC-C Tansition in the β sequence		
	& K_2CoBr_4	(by X-ray)	H.Mashiyama et al.	8
1992	K_2ZnBr_4	αI-αII Transition in the α sequence		
		and structures of the αI & αII Phase (by X-ray)	H.Kasano et al.	15
1992	K_2ZnBr_4			
	& K_2CoBr_4	dielectric measurement in the α and β sequence.	F.Shimizu et al.	18
1993	Rb_2MnI_4	α-β Transition (by DTA)	F.Shimizu et al.	21
1994	K_2ZnI_4	ferrooelectricity in Sr_2GeS_4 type compound	F.Shimizu et al.	14
		(DTA,dielectric and pyroelectric charge method)		
1994	Rb_2MnI_4			
	& Rb_2FeI_4	α-β Transition (by dielectric and DTA)	F.Shimizu et al.	22
1994	K_2ZnBr_4	α-β Transition (by Brillouin scattering)	M.Takesada et la.	25
1994	K_2ZnBr_4			
	&Rb_2ZnI_4	α-β Transition (by X-ray)	H.Mashiyama et al.	19
1994	K_2ZnBr_4	α-β Transition (by Brillouin scattering)	M.Takesada et la.	26
1994	K_2ZnBr_4	αI-αII Transition in the α sequence	M.Jochum et al.	36
1994	K_2ZnBr_4	α-β Transition (by X-ray)	M.Takesada et la.	23
1994	K_2ZnBr_4	α-β Transition (by Brillouin scattering)	M.Takesada et la.	27
1994	K_2ZnBr_4	Time dependent α-β Phase Transition.	F.Shimizu et al.	24
1994	K_2ZnBr_4	α-β Transition (by Brillouin scattering)	M.Takesada et la.	28

Table 1.1 Historical summary of the studies of the α–β transition.

§ 1.3 Purpose of the Present Study

The purpose of the present study is to elucidate a mechanism of the α-β transition in KZB by means of X-ray diffraction and Brillouin scattering. The X-ray study is performed to investigate a reconstructiveness of the α-β transition and to propose a model as the mechanism of the reconstructive first-order α-β transition. The relation between crystal axes of the α and β phases is obtained by repetitions of heating and cooling experimental runs. By X-ray study, however, it is very difficult to obtain the relation between the single domain α phase and the first heated β one, because it is rare to realize a single domain β phase in a first heated crystal from α phase. Then the final result obtained by X-ray study includes unknown factors. As well known, in order to assign the crystal axes by X-ray diffraction, we need a whole single domain crystal as a specimen.

On the other hand by Brillouin scattering study, it is possible to obtain the relation between the α phase and the first heated β phase, since the focal position can be easily selected to be a single domain area in the crystal. In order to elucidate the mechanism of the α-β transition, the temperature dependence of the acoustic modes are observed by Brillouin scattering near the α-β transition point T_t. Furthermore in order to get the relation between the phases which take place on each side of the reconstructive α-β transition, repetition of the warming runs using as-grown single crystal was carried out in many times under careful temperature control. A characteristic distribution of the frequency shifts ($\Delta\nu$) in the β phase are elucidated. By the Brillouin scattering study the model of the α-β transition is

confirmed.

In the chapter 2, the experimental procedures are described for X-ray study and Brillouin scattering one. In chapter 3, the axis relation between the α and β phases are given experimentally by X-ray study. Then the characteristic distribution of $\Delta\nu$ in the β phase are obtained by Brillouin scattering study. In chapter 4, using the relation obtained by X-ray study, a new model is proposed as the mechanism of the α-β transition. Then the model is confirmed by the results of the characteristic distribution obtained by the Brillouin scattering study. These results have already published in ref. 24 for X-ray study and refs. 26, 27, 28 and 29 for Brillouin studies.

CHAPTER 2. EXPERIMENTAL PROCEDURE

§ 2.1 Crystal Growth and Habit

Crystal growth was performed by evaporation method from aqueous solutions.[10] The reagents of KBr with the purity of 100% and $ZnBr_2$ with the purity of 97% were dissolved with stoichiometric ratio in water. In order to reduce dust, aqueous solution was filtered with a micron filter (Gelman HT Tuffryn) 0.2μm pore size. The saturated solution was slowly evaporated at about 380K for several weeks. The crystals were transparent, colorless and strongly deliquescent. Habit of obtained single crystal is shown in Fig.2.1.1. The crystal has clear cleaved (10-1) plane.

§ 2.2 X-ray diffraction Study

The block of single crystal was cut in ligroin liquid under a polarizing microscope. The specimens for X-ray diffraction were prepared by enclosing the small block in a glass capillary in vacuum. The specimen was mounted on a four-circle diffractmeter (Rigaku AFC5). Temperature of the specimen was controlled by blowing hot air.

First, setting parameters (UB-matrix) of the α phase were obtained, namely the unit-cell orientation was determined at room temperature using the program system of peak-search (PKS). Second, with monitoring intensity of a Bragg reflection, the specimen was heated from room temperature to above the α-β transition point. The Bragg reflection of the α phase completely disappeared at the transition point. Then the unit-cell orientation of the β structure was determined. Again the specimen

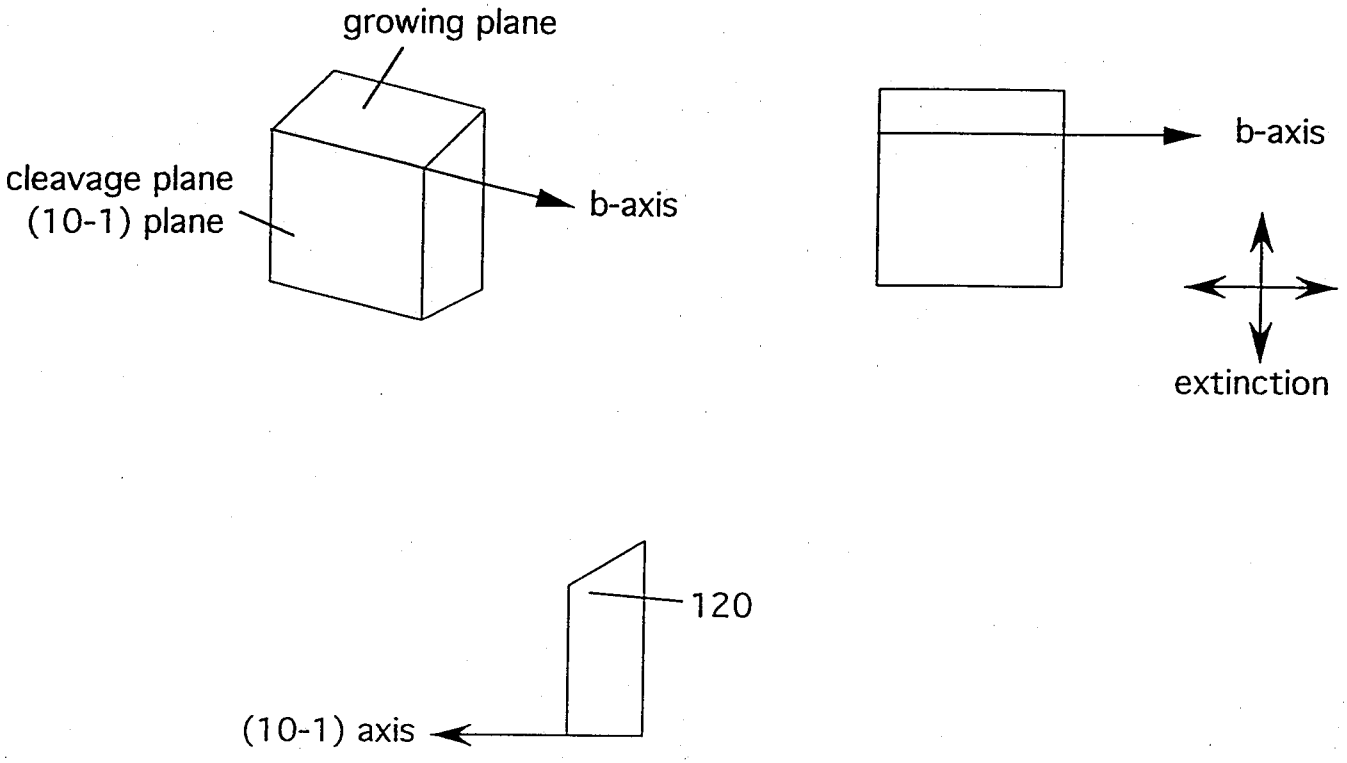

Fig. 2.1.1 Crystal habit of K_2ZnBr_4

was cooled through the α-β transition. Bragg reflections were searched to determine the unit cell orientation of the α structure. These processes were repeated several decades times. Sometimes the sample contained domains with different orientations, then we could not determine the UB-matrix, though.

In order to elucidate the relation between crystal axes of two phases, we use angles between β and α structures as illustrated in Fig.2.2.1, where $\theta(a_\beta, a_\alpha)$, $\theta(a_\beta, b_\alpha)$ and $\theta(a_\beta, c_\alpha)$ indicate angles between the a_β- and a_α-axes, the a_β- and b_α-axes and the a_β- and c_α-axes, respectively. That is, the angles between axes in one and in the other structures are represented by a 3x3 matrix with nine angles. Hereafter we call this matrix the α-β axis relation. In addition to this, we can obtain the α-α axis relation, if crystal is cooled to the α phase again. The β-β axis relation is also obtained if the crystal is warmed again up to the β phase. From all α and β unit-cell orientations, the α-β, α-α and β-β relations were calculated within all combinations.

The accuracy to determine the axes of a unit cell is ascertained as the followings; First, there are no difference between structures of each β phase or α phase. Second, there is no possibility that the wrong cell is assigned by using reflections of different domains in a sample (See Appendix 2.2).

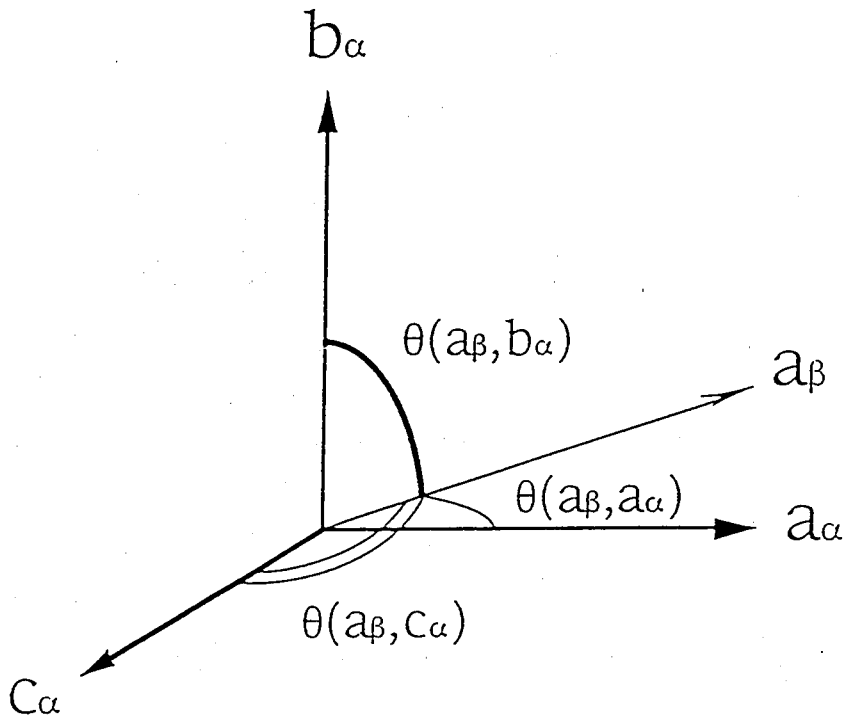

$$\begin{array}{c} \\ a_\beta \\ b_\beta \\ c_\beta \end{array} \begin{array}{c} \begin{array}{ccc} a_\alpha & b_\alpha & c_\alpha \end{array} \\ \begin{pmatrix} \theta(a_\beta,a_\alpha) & \theta(a_\beta,b_\alpha) & \theta(a_\beta,c_\alpha) \\ \theta(b_\beta,a_\alpha) & \theta(b_\beta,b_\alpha) & \theta(b_\beta,c_\alpha) \\ \theta(c_\beta,a_\alpha) & \theta(c_\beta,b_\alpha) & \theta(c_\beta,c_\alpha) \end{pmatrix} \end{array}$$

Fig. 2.2.1 Angles between the unit cell vectors of the α and β structures.

§ 2.3 Brillouin Scattering Study

Optical setup for Brillouin scattering is schematically shown in Fig.2.3.1. An Ar^+ ion laser was used as a light source, which was operated at λ_o=514.5nm with a longitudinal single mode at an average power of 50-60mW. The incident light was focused with lens 1 (L1, f=70mm). Then the scattered light was collected by the lens 2 (L2, f=70mm), and analyzed by the piezoelectrically scanned Fabry-Perot interferometer (Burleigh, DAS-1) on the five-pass stage. The analyzed light was detected by the photomultiplier (HAMAMATSU Photonics R585). In order to avoid a serious damage of the photomultiplier tube, due to elastically scattered light, the shutter was used as shown in Fig.2.3.1, where the shutter was synchronized with the scanning of the Fabry-Perot interferometer. The Brillouin scattering spectra were observed from room temperature to 520K as functions of temperature. Temperature of the sample cell was controlled by regulating an electric current by Ohkura EC61 with chromel-alumel thermocouples set near the specimen in the light scattering cell shown in Fig.2.3.2 (see Appendix 2.3). The temperature was stabilized within the error of ±0.03K.

The single crystal obtained by the evaporation method has a cleaved (10-1) plane with the size of 2x3mm^2 and thickness of about 1mm. The specimen was set in the light-scattering cell filled with silicone oil in order to avoid absorption of moisture, and reduce the strong elastic component in the spectra, and improve the thermal homogeneity around the specimen in the cell. The scattering geometry is shown in Fig.2.3.3 (see Appendix 2.3.2). The phonon wave vector q was selected to be parallel to

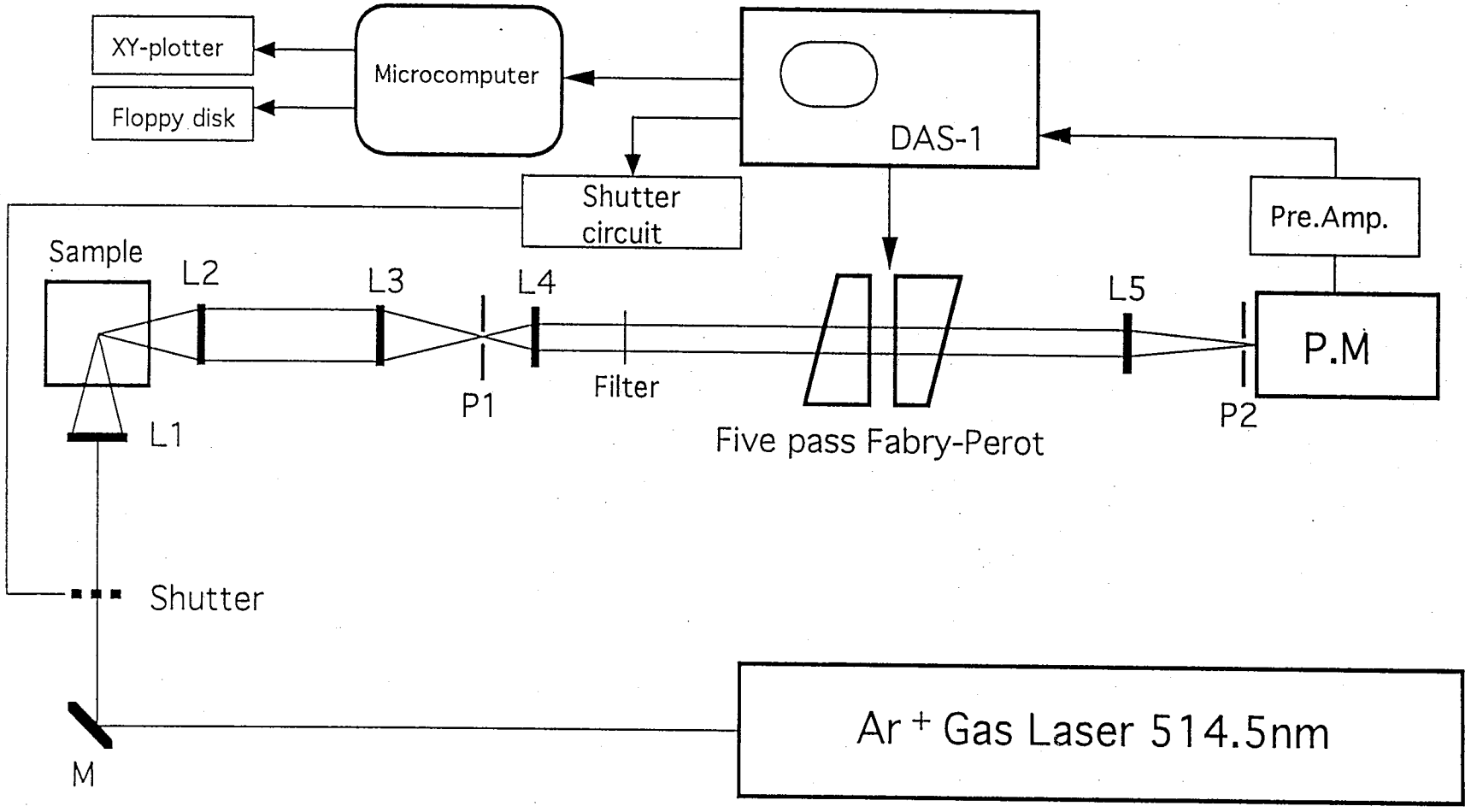

Fig. 2.3.1 Optical set up for Brillouin scattering. L1-5 show lenses with 70, 70, 150, 50, and 250mm, respectively. A1-4: aperture of 0.2, 7, 7 and 0.5mmø, respectively.

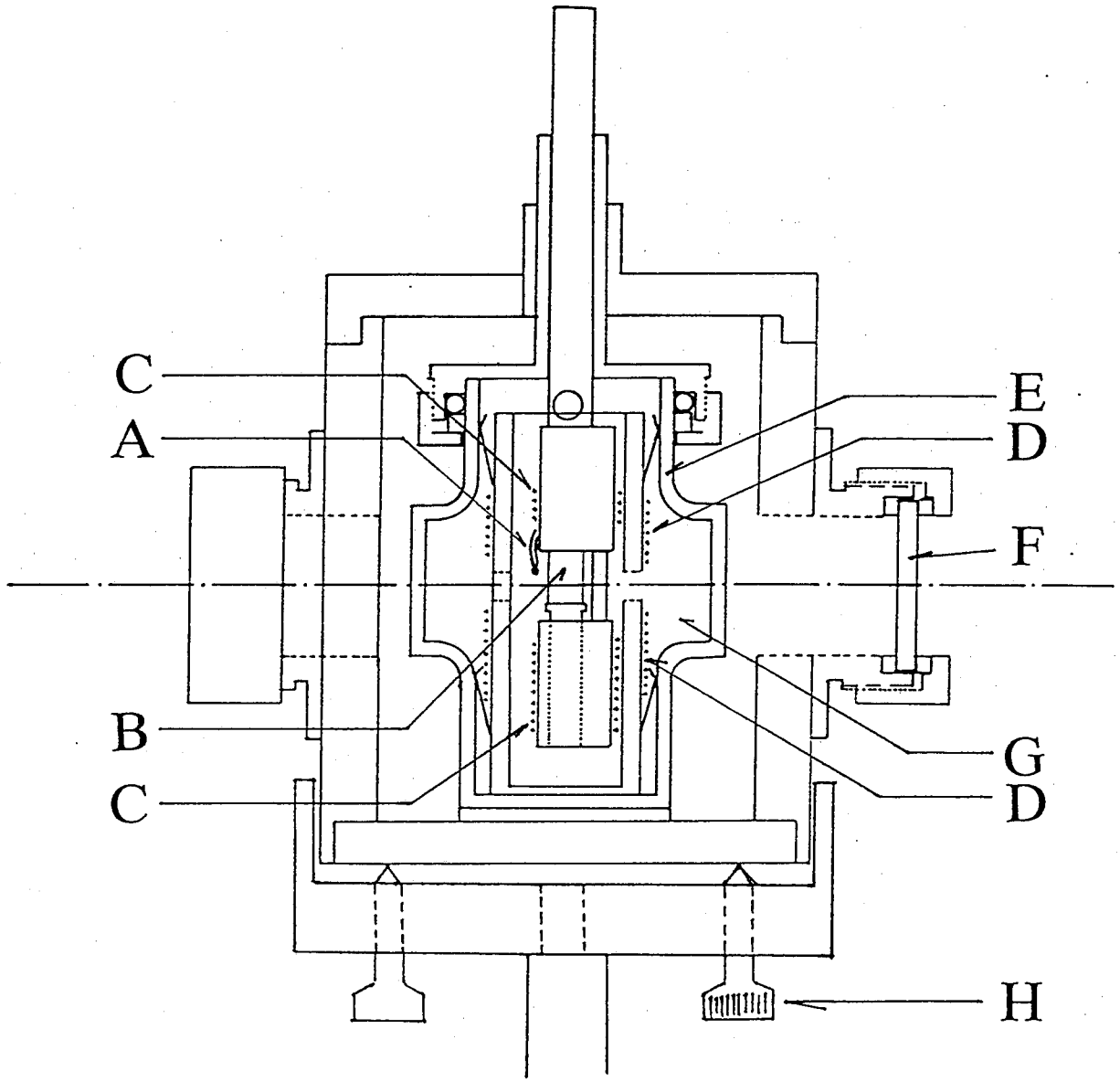

Fig. 2.3.2 Sample cell for light scattering measurement. (A)Chromel-alumel thermocouples set, (B)Sample, (C, D)Manganin heater, (E)Glass cell, (F)Glass window, (G)Silicone oil and (H)Goniometer.

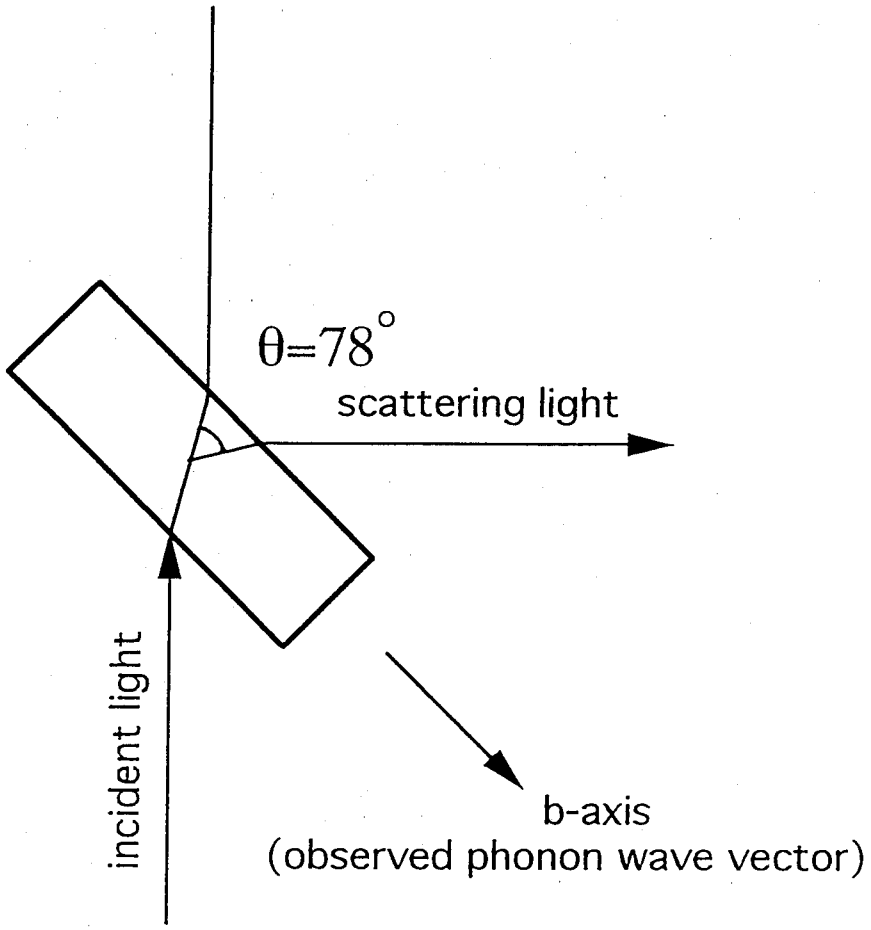

Fig. 2.3.3 Scattering geometry for Brillouin scattering measurement. The scattering angle θ is calculated by using the refractive index n_s=1.4025 (see Appendix 2.3.2).

the b-axis at room temperature in the α phase. The scattering angle θ is approximately 78 degrees shown in Fig.2.3.3 (see Appendix 2.3.2). The polarization of incident light was parallel to the a-axis. The magnitude of observed phonon wave vector q is 2.422×10^{-2} [nm^{-1}] at room temperature as described in Appendix 2.3.2.

CHAPTER 3. EXPERIMENTAL RESULT

§ 3.1 X-ray diffraction Study

It is surprising enough that a relation between the crystal axes of α and β phases change at every time passing through the transition. Examples of axis relations are shown as matrixes in Table 3.1. On the data 1 of the α-β axis relations in Table 3.1 the b_α-axis is parallel to the c_β-axis, since the angle between b_α and c_β-axis is 0 degree. Similarly, in data 2 the b_α -axis is almost parallel to the a_β-axis. In data 3 there is no such relation. Thus, the relation of the unit cell orientation between α and β phases seems to be very complicated. The α-α and β-β axis relations are also shown in Table 3.1. Generally, the crystal axes change their directions drastically. Examining the α-α and β-β axis relations, however, we obtain the following feature; though the crystal axes are almost parallel to the original crystal axes through the α-β-α transition or the β-α-β transition, they often turns approximate by some ten degrees. The data 6 is such a case. Reconstructivity of the α-β transition is expected from these feature. These phenomena will be discussed in §4.1.2. It should be noted here that the crystals did not crack through the α-β transition although crystal axes changed so much. The volume per chemical formula was almost the same in both α and β phases as shown in Fig.1.6.[20)]

	Experimental result			
	data 1			
		aα	bα	cα
	aβ	38	89	148
	bβ	128	91	121
	cβ	90	0	90
	data 2			
		aα	bα	cα
	aβ	83	172	87
α-β	bβ	133	91	25
	cβ	135	97	114
	data 3			
		aα	bα	cα
	aβ	68	146	122
	bβ	21	76	91
	cβ	97	120	32
	data 4			
		aα	bα	cα
	aα	178	89	73
	bα	90	177	92
	cα	72	92	36
α-α	data 5			
		aα	bα	cα
	aα	122	35	91
	bα	145	124	78
	cα	90	97	19
	data 6			
		aβ	bβ	cβ
	aβ	12	102	89
	bβ	102	166	83
	cβ	91	95	173
	data 7			
		aβ	bβ	cβ
	aβ	58	146	81
	bβ	149	120	88
	cβ	86	97	170
β-β	data 8			
		aβ	bβ	cβ
	aβ	48	137	99
	bβ	80	69	156
	cβ	42	54	69
	data 9			
		aβ	bβ	cβ
	aβ	116	153	92
	bβ	56	104	142
	cβ	44	111	53

Table 3.1. Experimental results of axis relations between α-β, α-α, β-β phases.

§ 3.2 Brillouin Scattering Study

The observed Brillouin scattering spectrum is composed of three clear peaks: one longitudinal acoustic mode (LA) and two transverse acoustic modes (TA1 and TA2), as shown in Fig.3.2.1. The frequency shifts of the three modes were determined by comparison with the spectra observed in two free spectral ranges (FSR) of the Fabry-Perot interferometer; one was 30.8GHz and the other 66.0GHz. The three pairs of the peaks in the α phase were assigned as LA, TA1 and TA2 modes according to the value of the frequency shifts. These mode assignments were confirmed by an inelastic neutron scattering as shown in Fig.3.2.2 (see Appendix 3.2). The temperature dependence of the spectra was observed using the FSR of 15GHz.

The frequency shifts have been observed in both α and β phases as functions of temperature as shown in Fig.3.2.3, where the different marks indicate different experimental runs. In the α phase, the frequency shifts of the different runs show a common gradual decrease with increasing temperature to T_t. Both LA and TA2 modes indicate a discrete jump at T_t, though the TA1 mode does not show any anomaly at T_t within experimental error. The most striking feature shown in Fig.3.2.3 is the temperature dependence of LA mode in the β phase; the frequency shift of these modes indicate a different value in this phase in each experimental run. Obviously this is not due to the experimental factors because the data points in the α phase show good reproducibility within experimental error.

Furthermore, in order to investigate the distribution of temperature dependence of the LA mode, the Brillouin scattering

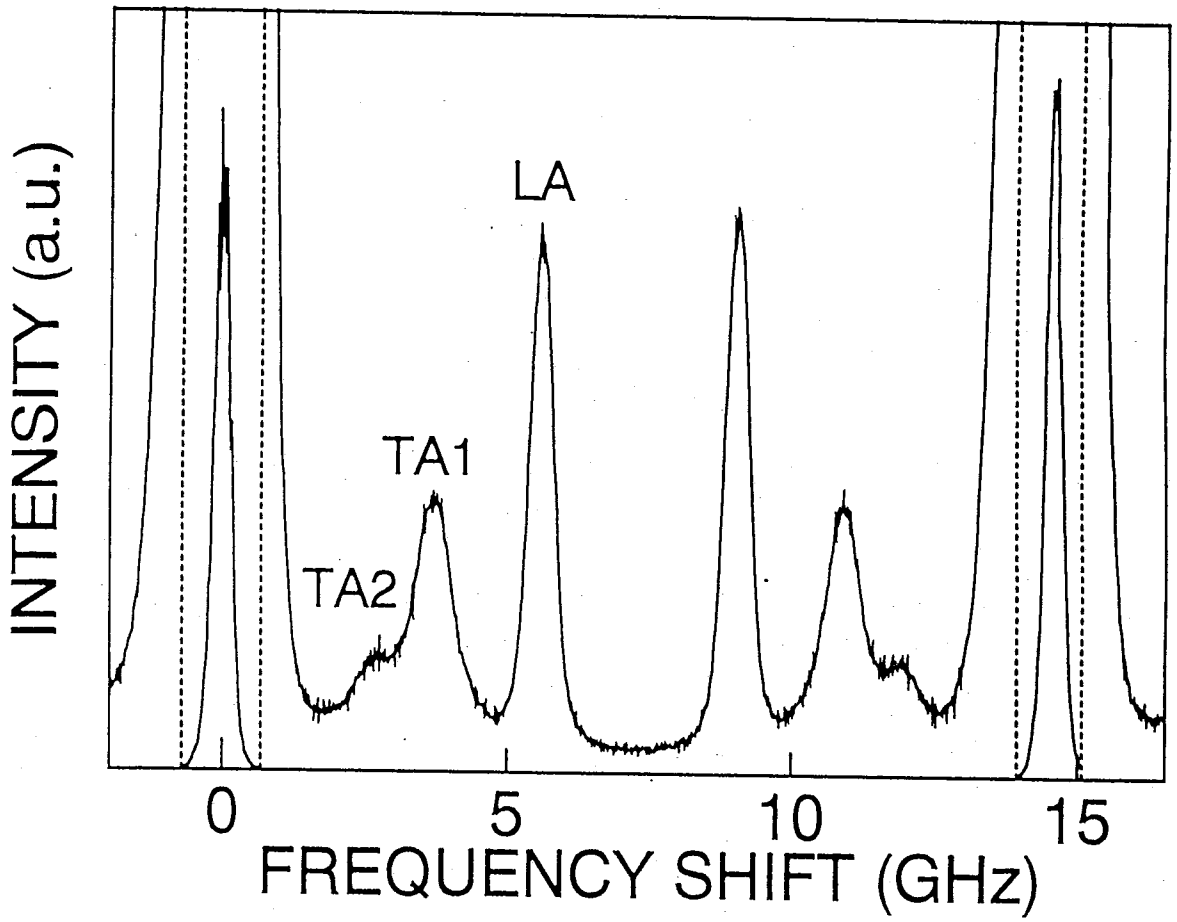

Fig. 3.2.1 Brillouin scattering spectra of K_2ZnBr_4 observed at 433K (α phase). The phonon-wave vector is parallel to the b-axis. The free spectral range (FSR) is 14.6GHz. LA, TA1 and TA2 indicate the longitudinal acoustic mode and two transverse acoustic modes, respectively.

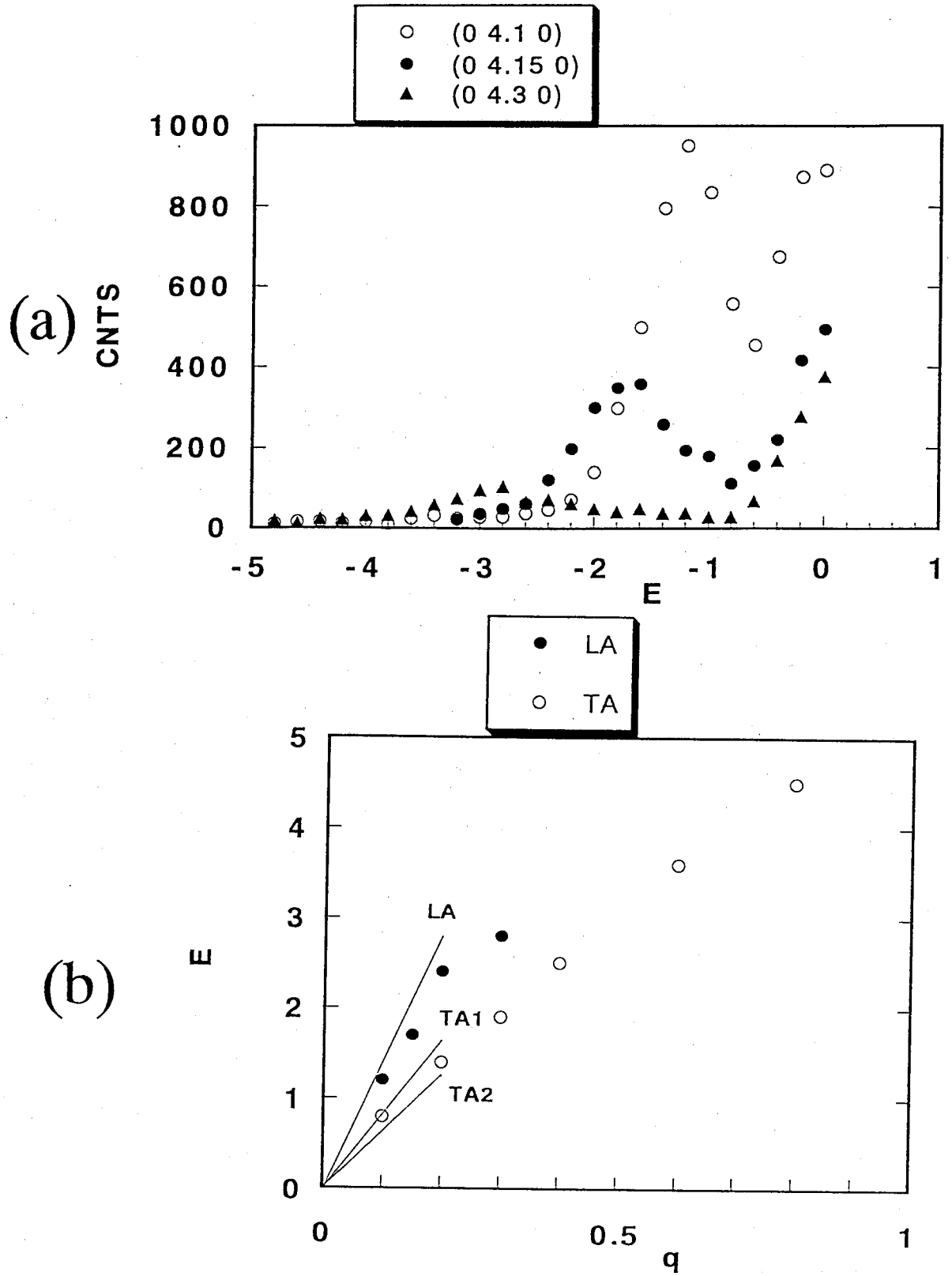

Fig. 3.2.2 (a)Scattering intensity at room temperature with constant Q=(0 4+q 0). (b)Phonon dispersion of the LA and TA modes along [010] in the α phase of KZB at room temperature. Three linear lines indicate the LA, TA1 and TA2 modes obtained by Brillouin scattering study.

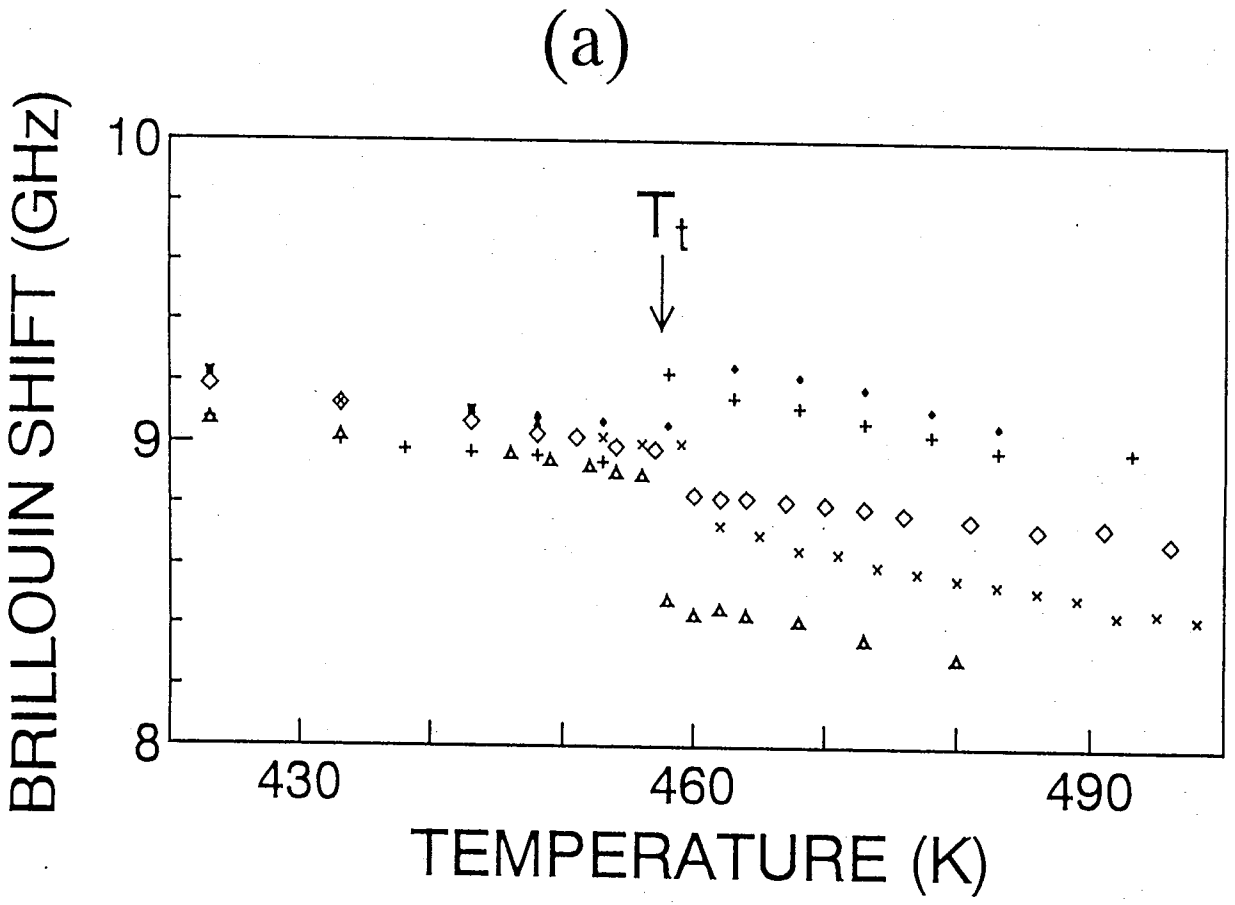

Fig. 3.2.3 Temperature dependence of the Brillouin scattering frequency shift on heating runs of the longitudinal mode LA (a), transverse modes TA1 and TA2 (b). The different marks show different experimental runs upon heating.

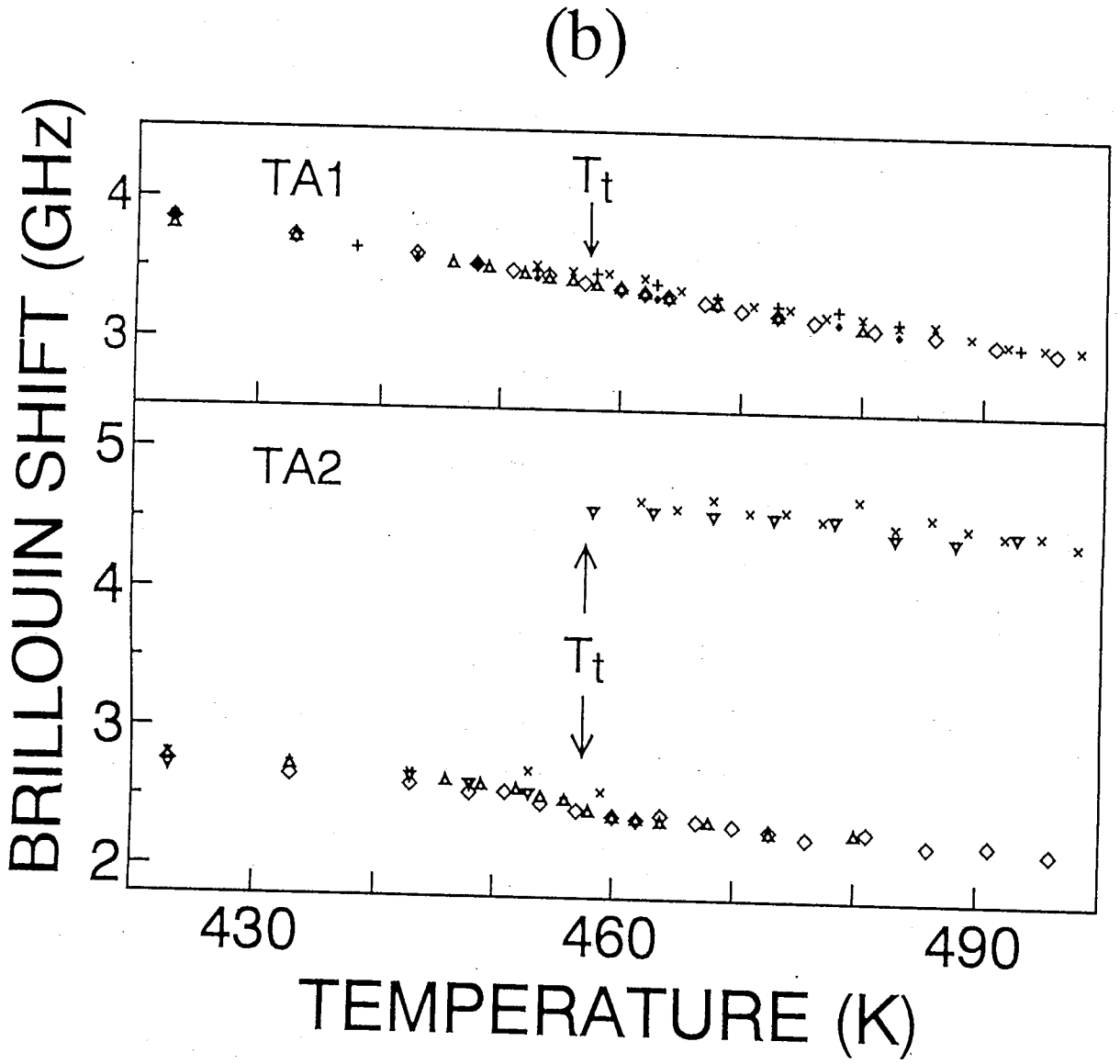
(b)
BRILLOUIN SHIFT (GHz)
TA1
T_t
TA2
T_t
4
3
5
4
3
2
430
460
490
TEMPERATURE (K)

spectra have been observed in many repeated runs in both α and β phases as a function of temperature, where we investigate only the LA and TA1 modes due to the poor intensity of TA2 mode as shown in Fig.3.2.1. The temperature dependences of the frequency shift ($\Delta\nu$) of LA and TA1 modes are shown in Figs.3.2.4(a) and 3.2.4(b), respectively. In these figures, in order to reduce systematic experimental errors, the temperature dependences of $\Delta\nu$ were normalized to the value of the α phase at 458K (T_t). The LA mode in the β phase shows a discrete distribution as shown in Fig.3.2.4(a) in contrast to the TA1 mode shown in Fig.3.2.4(b). The TA1 mode does not show any anomalous behavior at the α-β transition within experimental error as shown in Fig.3.2.4(b).

The temperature dependence of the Brillouin frequency shift upon heating and cooling is compared in Fig.3.2.5 in order to confirm the first-order property of the α-β transition. Figure 3.2.5 indicates that only the LA mode shows a clear jump at T_t. Upon cooling there is an anomaly of the temperature dependence of the Brillouin shift at about 353K indicating the transition from the β phase to α phase. A large thermal hysteresis of about 100K was observed although 30K hysteresis was reported previously by DTA.[10] This result supports the similarity in the phase transition sequence between K_2ZnBr_4 and K_2CoBr_4, as described above.[10]

The temperature dependence of the peak width (FWHM) of the LA mode was investigated as shown in Fig.3.2.6. The temperature dependence does not show any anomaly within experimental error.

Finally, in order to show the stability of this experimental system, position dependence of the frequency shift and FWHM of the LA mode were observed as shown in Fig.3.2.7. A standard

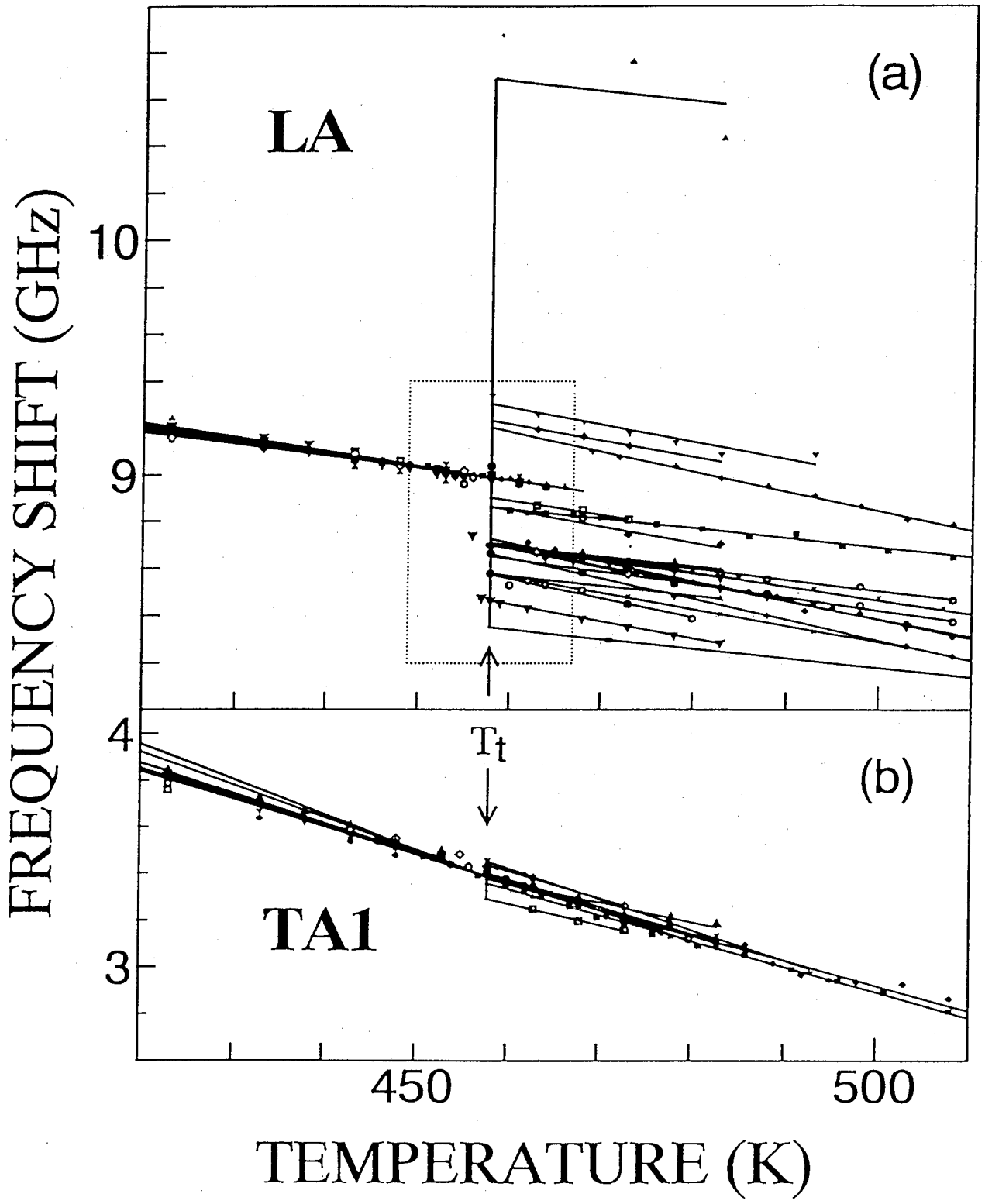

Fig. 3.2.4 Temperature dependence of the Brillouin frequency shift of LA mode (a) and TA mode (b). The marks indicate each of the experimental runs on heating. Each line is given by the least squares fit.

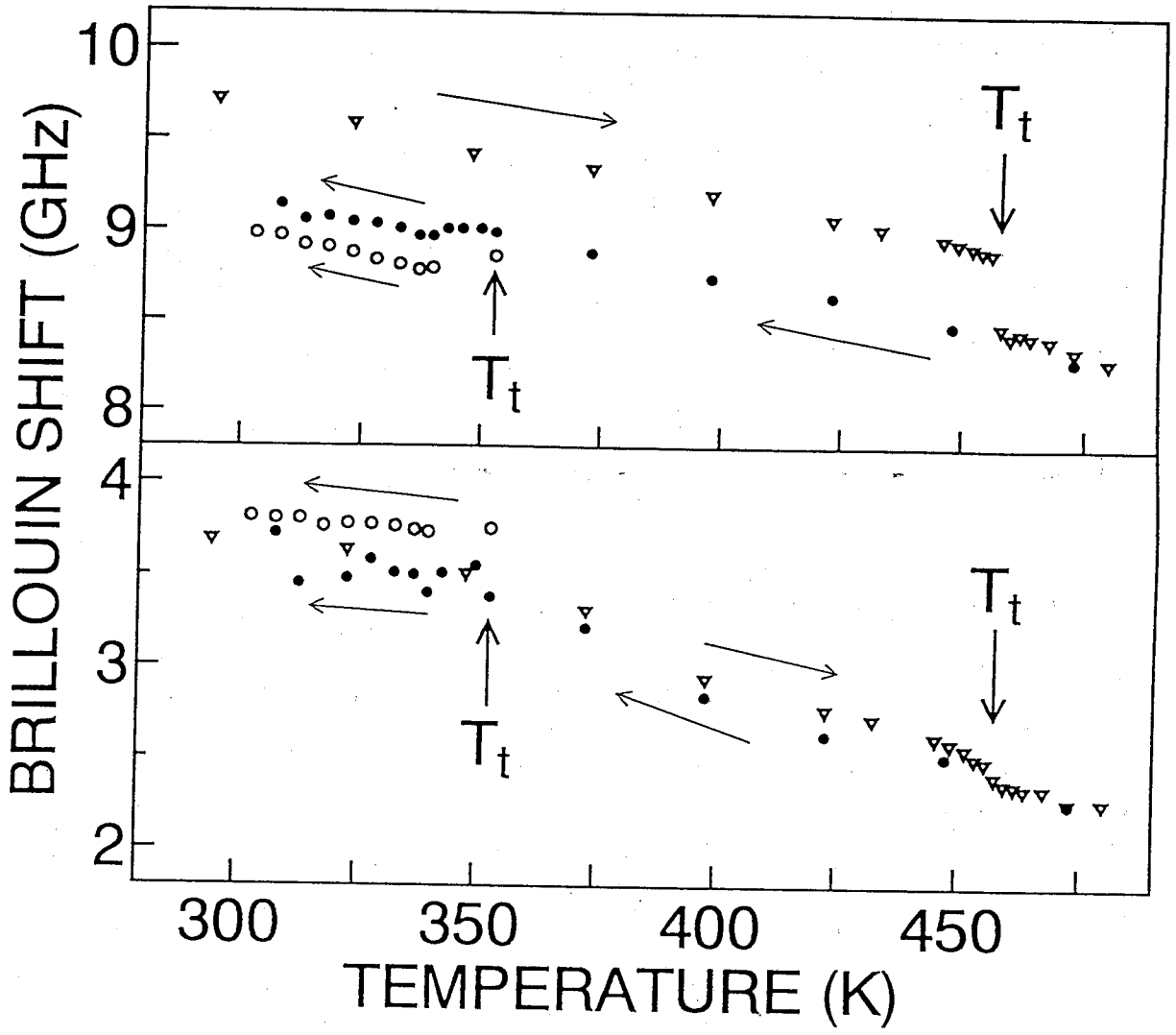

Fig. 3.2.5 Thermal hysteresis of the Brillouin frequency shift of LA (upper) and TA1 (lower) modes. The triangles and circles denote heating and cooling, respectively. The solid and open circles indicate the two domains of the α phase appearing upon cooling.

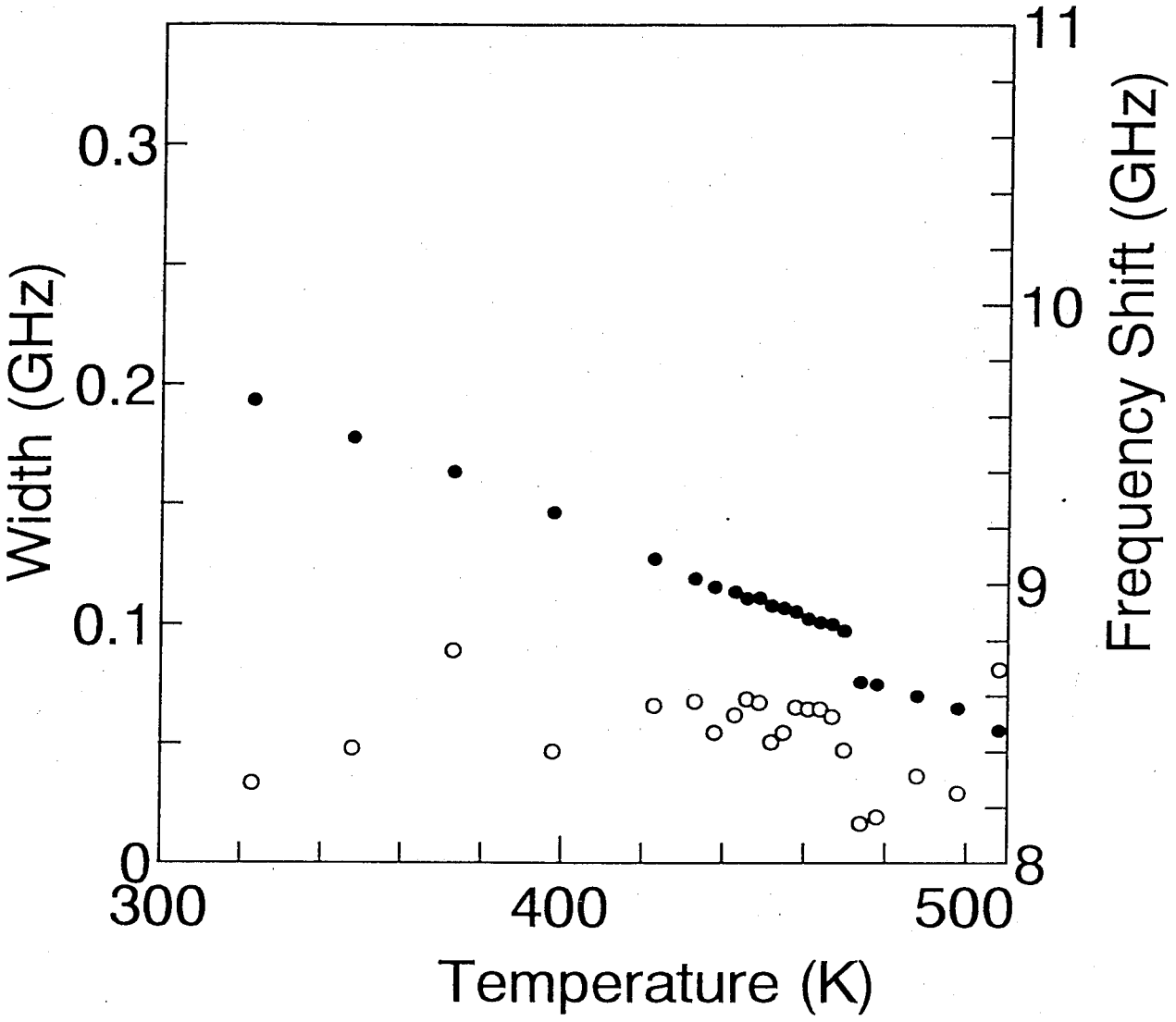

Fig. 3.2.6 Temperature dependence of a peak width (FWHM) and frequency shift of the LA mode, open and closed circles, respectively.

deviation of results of the frequency shift and FWHM of the LA mode in Fig.3.2.7 are 0.0156GHz and 0.0172GHz, respectively. Therefore an experimental error of the frequency shift of the LA mode should be considered within about 0.04GHz.

In summary, we obtained the Brillouin scattering spectra of K_2ZnBr_4 near the first-order α-β transition as functions of temperature. Upon heating the temperature dependence of the frequency shifts in the β phase showed an obvious difference in each experimental run in contrast to the good reproducibility in the α phase. The temperature dependence of the LA mode indicates a discrete distribution in the β phase by many times repetitions of experimental runs.

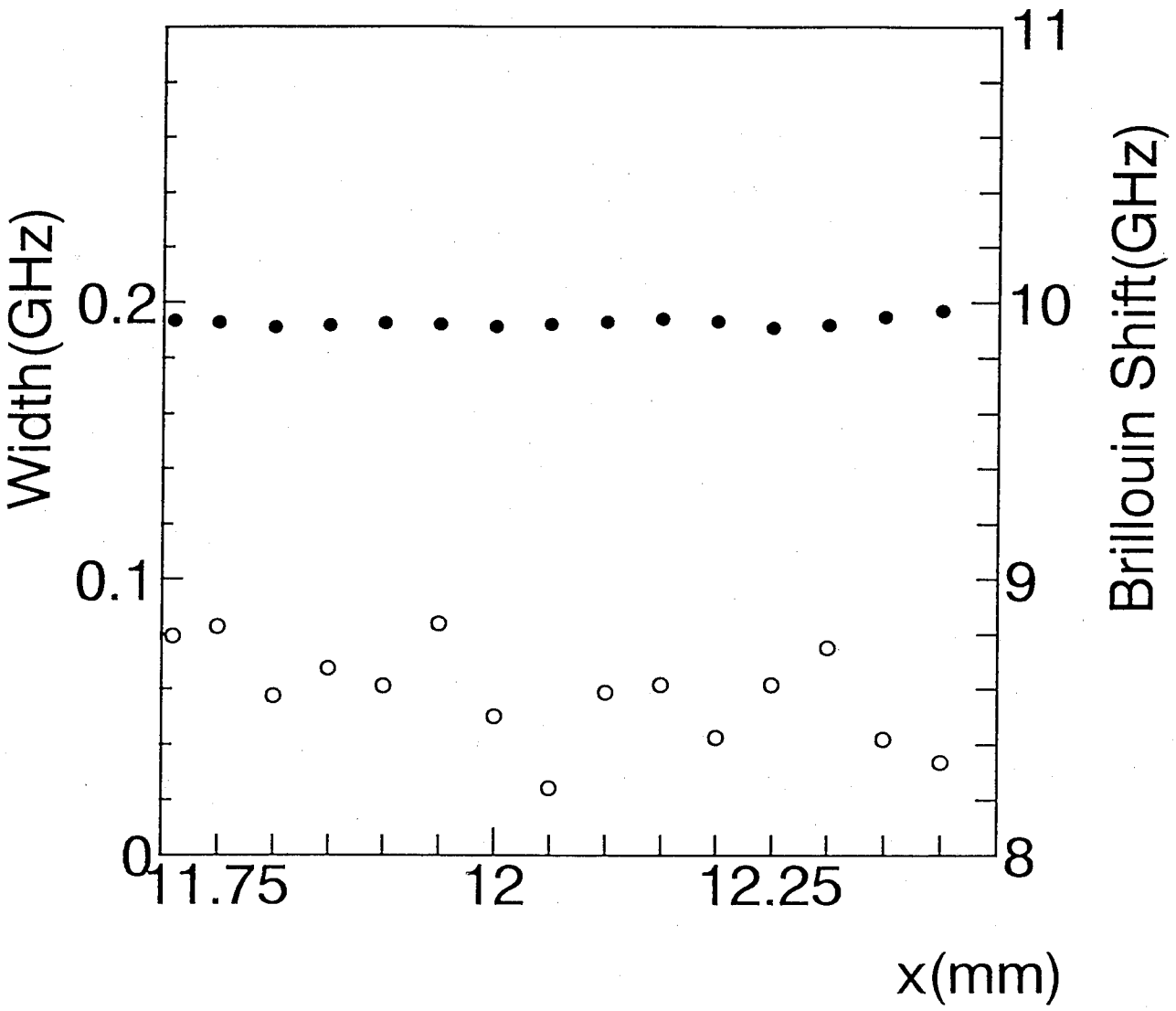

Fig. 3.2.7 Position dependence of the frequency shift and the Peak width of the LA mode.

CHAPTER 4. DISCUSSION

§ 4.1 α-β transition from the view point of the crystal structure

4.1.1 X-ray diffraction Study

Investigating the α-β and β-β axis relations in Table I, we have to recognize that the α-β transition can not be explained by a simple model accompanied with the symmetry breaking from the prototype phase[29] as the second order phase transition (See Appendixes 4.1.1 and 4.1.2). The feature of the axis relation is summarized as follow; The α-β axis relation can not be determined uniquely by the reason explained in Appendix 4.1.1. The β-β axis relation indicates that the c-axis of the β phase may change its direction to some dozen of possible directions through the β-α-β transition, though the c-axis is the unique axis of a pseudo-hexagonal structure as discussed in Appendix 4.1.2. Data 8 and 9 in Table I are good examples of such case. Investigating the α-α axis relations in Table I, we note that the α-α axis relation (data 4) indicates the existence of monoclinic domains, which will be discussed in §4.1.4.

4.1.2 Proposal of VIS model

In order to explain the complicated feature of the axis relation appeared in the α-β transition, a model is newly proposed in the present study. In this model, it is assumed that the structural change undergoes through two virtual intermediate states during the α-to-β transition or β-to-α transition; a body-centered cubic (bcc) state and a hexagonal close-packed (hcp) state. Namely, the phase transition proceeds as the following,

$$\alpha \rightleftharpoons (\text{bcc}) \rightleftharpoons (\text{hcp}) \rightleftharpoons \beta.$$

Hereafter, we call this model as VIS model (Virtual Intermediate States model). The relation between the hcp and β structures (the hcp-β relation) is easily understood, since the β phase is a pseudo-hexagonal structure. The α-bcc relation is explained in Appendix 4.1.3 with taking account of similarity between the α structure shown in Fig.4.1.1 and the bcc structure in Fig.4.1.2(b). The bcc-hcp relation is understood by an application of the method given in the Burgers' model[30] shown in Fig.4.1.3 as discussed in Appendix 4.1.3. For considering the model, we approximate the crystal structures of the α and β sequences as α and β structures, respectively.

In Fig.4.1.4 we demonstrate the transition from β to α structure with paying attention on Zn atoms placed at the centers of $ZnBr_4$ tetrahedra. Figure 4.1.4 is drawn according to the relations discussed in Appendix 4.1.3 with taking account of the periodicity of all of a crystal. This figure indicates one of the possible movements. For example, while filled circles A, B, C and D moves to the positions A', B', C' and D', respectively. Angle β, which is defined as shown in Fig.4.1.4, changes from 106 degrees to 109 degrees which is realized in the bcc structure. Then the length of a, b, c axes becomes the lattice constants of the α structure as shown in Fig.4.1.1. A schematic illustration of the hcp-bcc axis relation is given by Fig.4.1.5.

Considering the bcc structure as a virtual intermediate state, we can explain the small variations in the crystal axes observed after the α-β-α or β-α-β transition as mentioned in §3.1. That is, we can consider two types of transformations

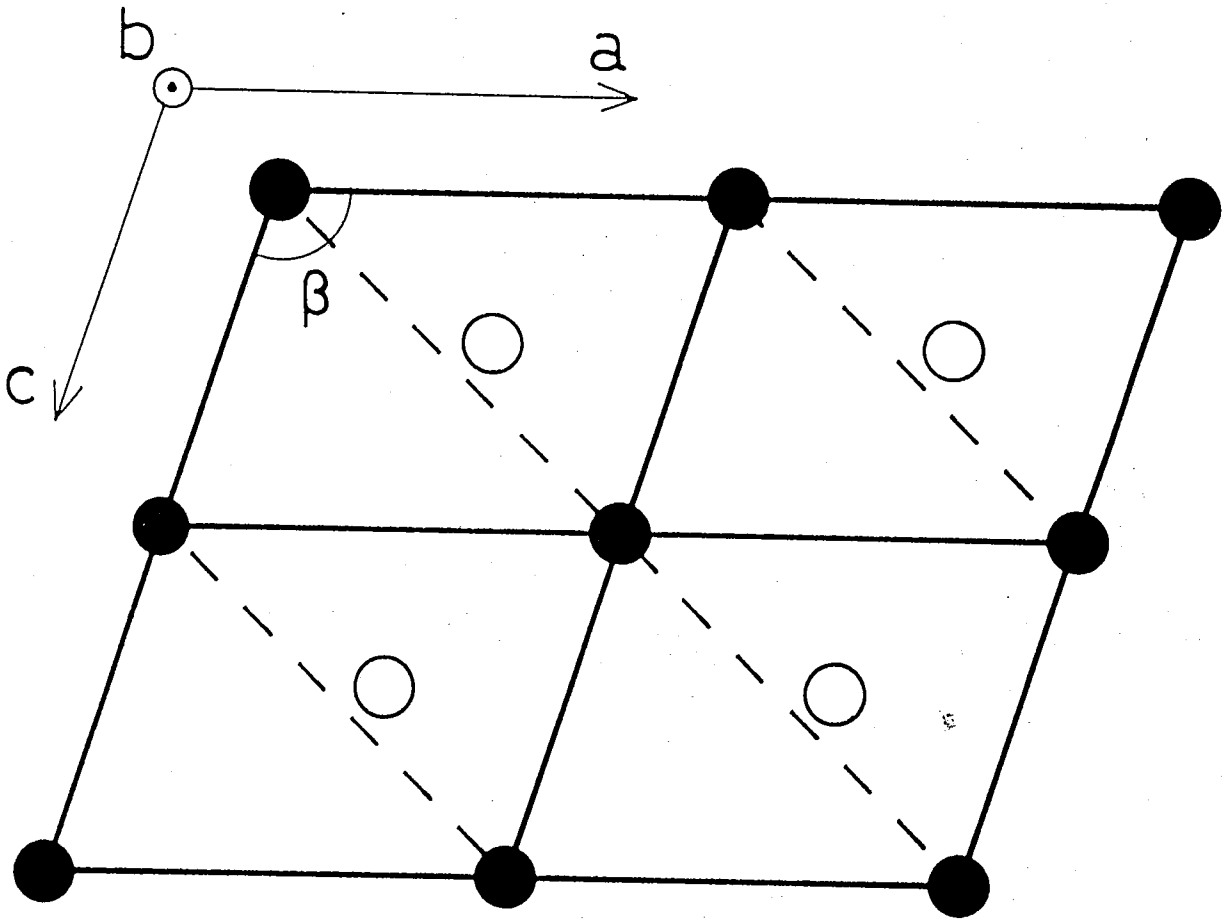

Fig. 4.1.1 The b-axis projection of the α structure. The angle of β is about 109 degrees. Only Zn atoms are drawn. The closed and open circles indicate the difference of the layer on which Zn atoms sit.

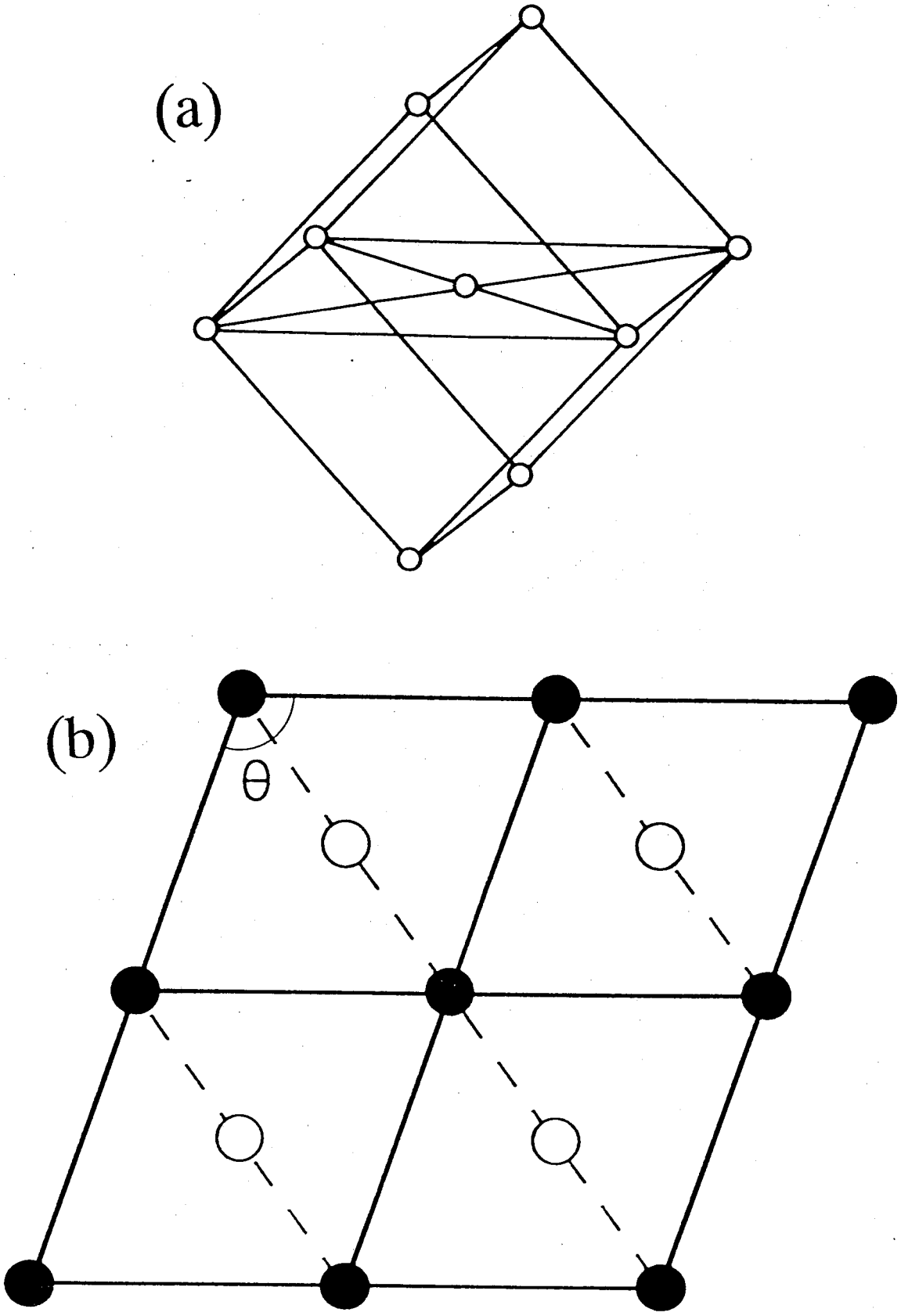

Fig. 4.1.2 The bcc structure. The projection of the structure from the [110] direction is shown in (b). The angle θ is 109.47 degrees.

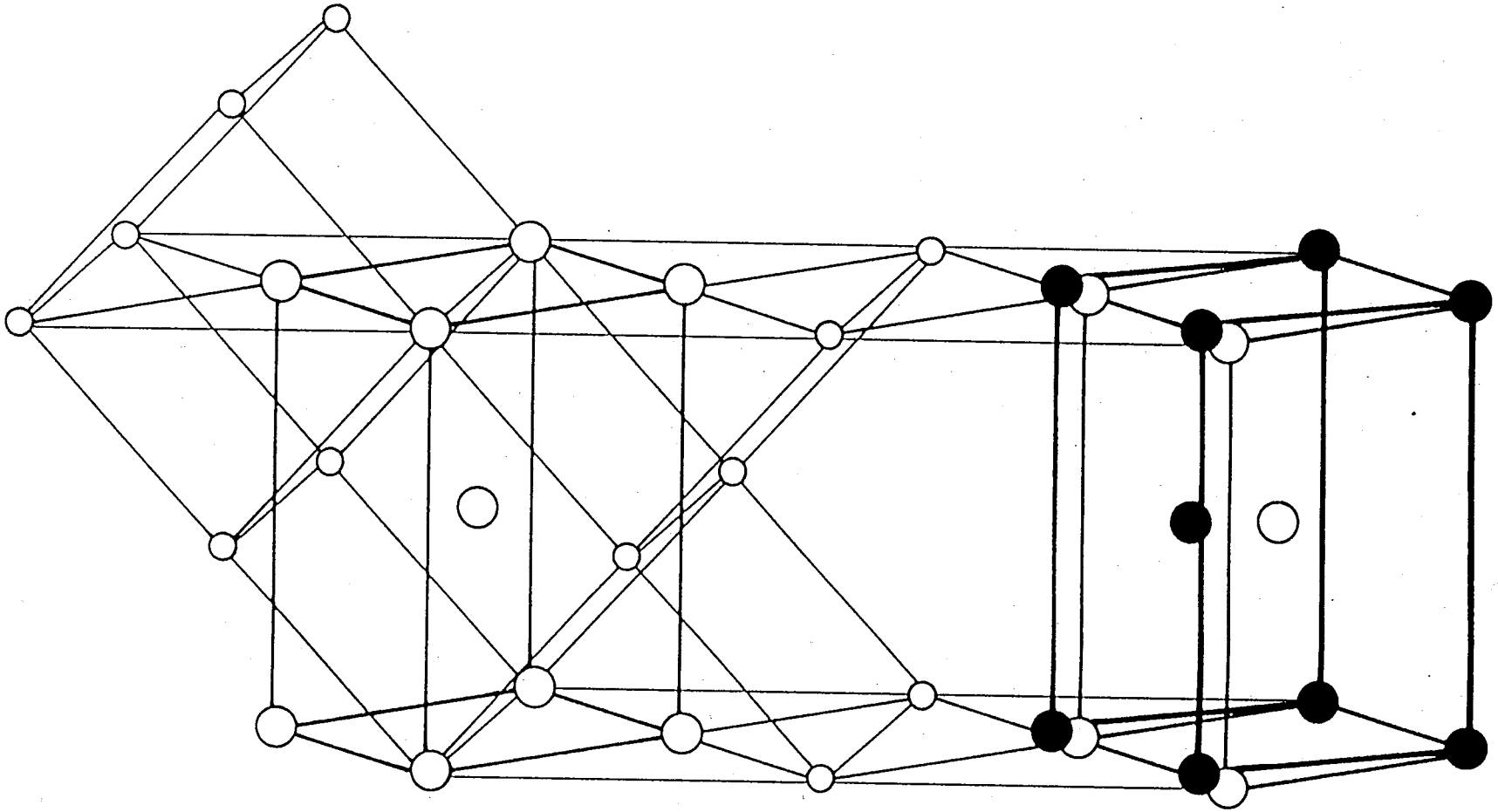

Fig. 4.1.3 The three dimensional picture of the relation between the bcc and hcp structures. The open circles are the bcc structure. The solid circles are the hcp structure.

Fig. 4.1.4 The atomic displacements at the β-to-α transition. Solid circles indicate the hcp structure or the β structure. If atoms move from ABCD to A'B'C'D', the β structure transforms into the α structure approximately. Solid line cell and broken line cells indicate unit cells of the β structure and the approximate α structure, respectively. The unique axes of both the hcp and α structures are perpendicular to the plane.

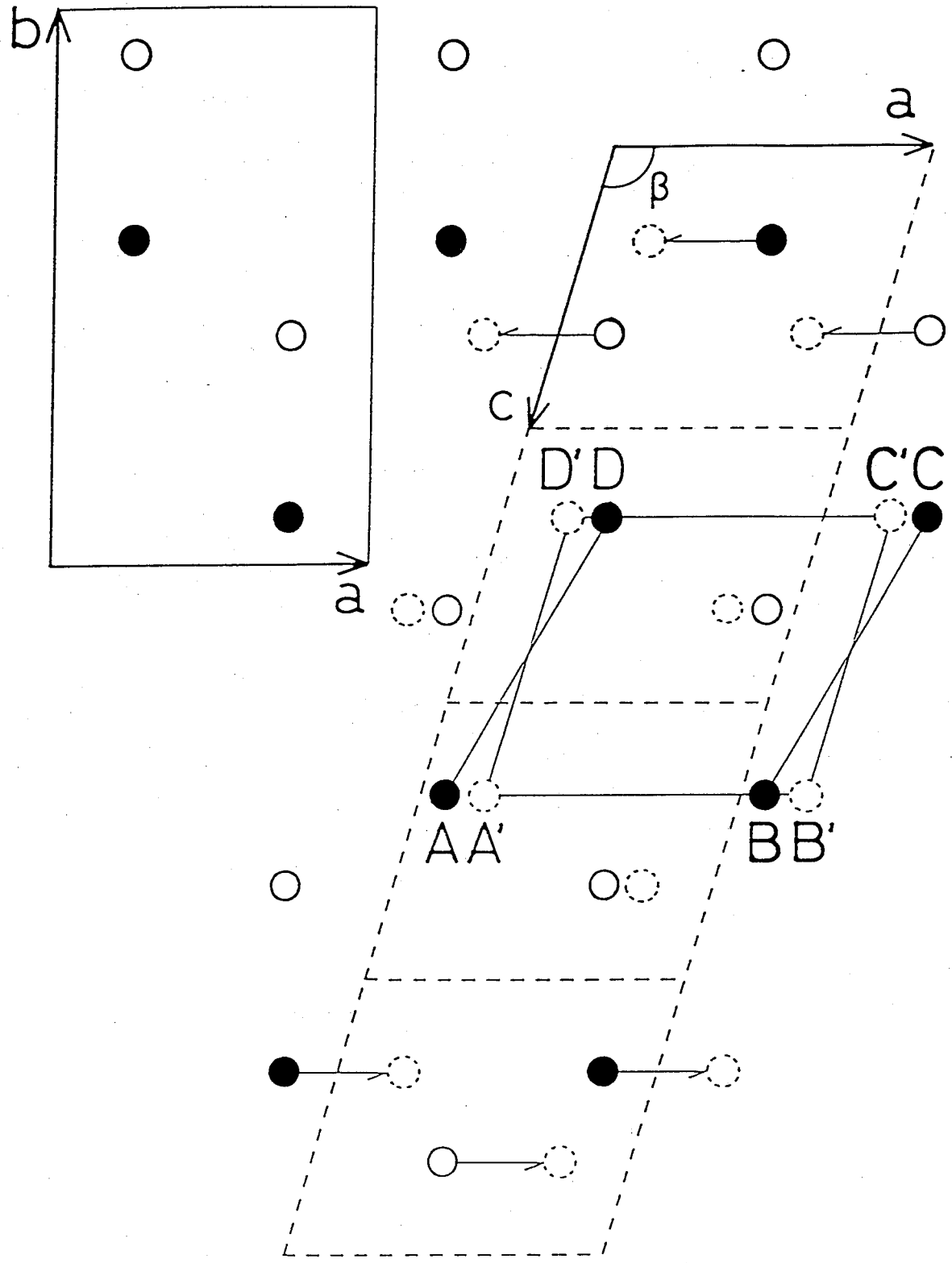
b
a
a
β
c
D'D
C'C
AA'
BB'

Fig. 4.1.5 The relation between the bcc structure and the hcp structure. Solid line cells and broken line cells indicate the bcc and hcp structures, respectively; bcc: the projection of the bcc structure from the [110] direction, hcp: the hcp structure projected along the unique axis. There are two equivalent types for the transformation; type-A and type-B.

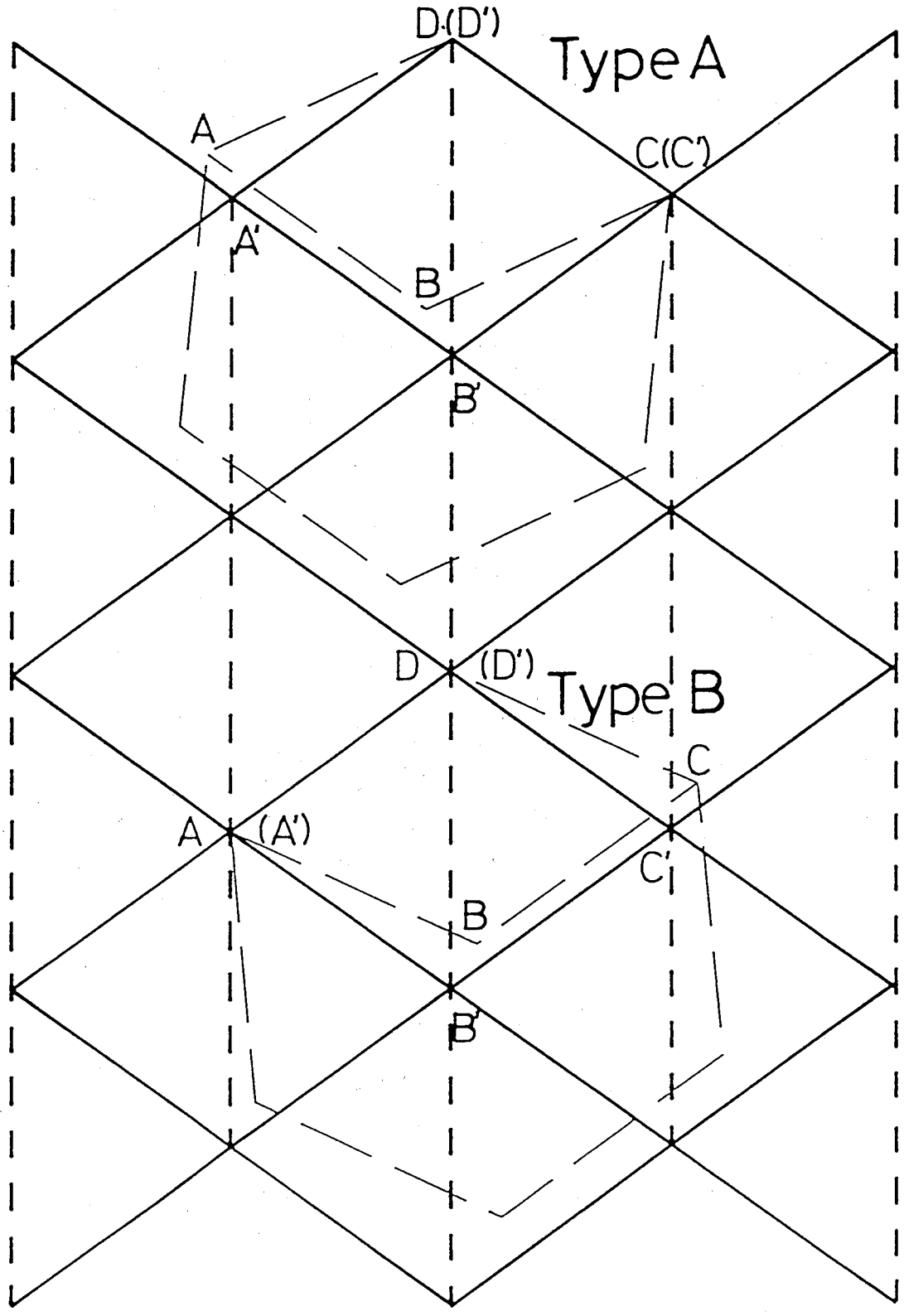
D(D')
Type A
A
C(C')
A'
B
B'
D
(D')
Type B
C
A
(A')
C'
B
B'

indicated as type-A and type-B as shown in Fig.4.1.5. Type-A indicates that the direction of the a_α-axis is kept through the α-to-β transition as in Fig.4.1.4, while type-B indicates that one of the c_α-axis in α structure is kept. If type-A change to type-B, then the crystal axes have to turn about ten degrees around the [110] axis of the bcc or b_α-axis (unique axis). This may explain the small change (about ten degrees) in the direction of the β structure as in the case of data 6 in Table 3.1.

4.1.3 Calculation of Axis Relation according to VIS model

In this subsection, we calculate the possible axes relations, which are defined in §2.2, in the α-β transition. It is well known that in the bcc structure there are six axes identical to [110] axis. Using the axis relation between the virtual bcc and hcp states given in Fig.4.1.5, the α-β axis relation is calculated in the case that the sample undergoes the α-to-β transition only once. Though, if sample is cooled again to the α phase from β phase, we observe the increase of number of the possible α-β axis relations after passing through the transition by warming run again.

The β-β axis relations given in §2.2 is calculated here as the relation between cell-orientations of the β phases which can be given through the α-to-β transition from the single α phase for the first time. The α-α axis relations are calculated within the restriction that, after α-to-β transition, the β phase transforms to the α phase at low temperature, only according to the atomic displacements shown in Fig.4.1.4. That is, all possible α-α axis relations are not calculated here to avoid

complexity. Furthermore we take account of either type-A or type-B axis relation illustrated in Fig.4.1.5. Thus, a difference of the angles between type-A and type-B relations is neglected for simplicity. Therefore, we have to take account of the difference between the experimental result and the result calculated here becomes considerably large. Furthermore if the second and the third α-β transitions are repeated, the difference may become twice or three times. The calculated results are given in Table 4.1.1.

The right matrix calculated from the VIS model should be compared with the experimental result of the left matrix. $\Delta\theta$ given in parentheses shows the difference between the VIS model and the experimental results. We can conclude that the VIS model reproduces the experimental results very well.

In Table 4.1.2, $\Delta\theta$ for all the experimental results is summarized. The results can be classified into three groups according to the angle between two c_β-axes or between b_α-axis and c_β-axis; the angle of 0 or 180 degrees, 60 or 120 degrees, and 90 degrees. Furthermore, each group is divided into three sub groups according to the experimental errors of θ, $\Delta\theta$. Most cases are $\Delta\theta<30°$, which seems to support the VIS model.

There are some cases for which $\Delta\theta$ is over 30 degrees in Table 4.1.2. The reason of such a large discrepancy is considered as the following. The calculated axis relations are derived under the condition that a specimen is exposed only once α-to-β transition. However most of the experimental results were the relation between two phases which were exposed on several times of α-β transitions as mentioned in § 2.2.

	Experimental result				VIS model			
	data 1							
		aα	bα	cα		aα	bα	cα
	aβ	38	89	148	aβ	49(11)	90(1)	156(8)
	bβ	128	91	121	bβ	139(11)	90(1)	114(7)
	cβ	90	0	90	cβ	90(0)	0(0)	90(0)
	data 2							
		aα	bα	cα		aα	bα	cα
	aβ	83	172	87	aβ	76(7)	155(17)	113(26)
α-β	bβ	133	91	25	bβ	122(11)	115(24)	31(6)
	cβ	135	97	114	cβ	145(10)	90(7)	109(5)
	data 3							
		aα	bα	cα		aα	bα	cα
	aβ	68	146	122	aβ	71(3)	145(1)	123(1)
	bβ	21	76	91	bβ	19(2)	73(3)	96(5)
	cβ	97	120	32	cβ	90(7)	120(0)	34(2)
	data 4							
		aα	bα	cα		aα	bα	cα
	aα	178	89	73	aα	180(2)	90(1)	74(1)
	bα	90	177	92	bα	90(0)	180(3)	90(2)
	cα	72	92	36	cα	74(2)	90(2)	32(4)
α-α	data 5							
		aα	bα	cα		aα	bα	cα
	aα	122	35	91	aα	125(3)	41(6)	99(8)
	bα	145	124	78	bα	145(0)	120(4)	60(18)
	cα	90	97	19	cα	78(12)	78(19)	31(12)
	data 6							
		aβ	bβ	cβ		aβ	bβ	cβ
	aβ	12	102	89	aβ	0(12)	90(12)	90(1)
	bβ	102	166	83	bβ	90(12)	180(14)	90(7)
	cβ	91	95	173	cβ	90(1)	90(5)	180(7)
	data 7							
		aβ	bβ	cβ		aβ	bβ	cβ
	aβ	58	146	81	aβ	60(2)	150(4)	90(9)
	bβ	149	120	88	bβ	150(1)	120(0)	90(2)
	cβ	86	97	170	cβ	90(4)	90(7)	180(10)
β-β	data 8							
		aβ	bβ	cβ		aβ	bβ	cβ
	aβ	48	137	99	aβ	49(1)	139(2)	90(9)
	bβ	80	69	156	bβ	68(12)	71(2)	150(6)
	cβ	42	54	69	cβ	49(7)	56(2)	60(9)
	data 9							
		aβ	bβ	cβ		aβ	bβ	cβ
	aβ	116	153	92	aβ	109(7)	161(8)	90(2)
	bβ	56	104	142	bβ	62(6)	100(4)	150(8)
	cβ	44	111	53	cβ	35(9)	107(4)	60(7)

Table 4.1.1. Experimental axis relations between α-β, α-α, β-β phases and the calculated axis relations by the use of VIS model against experimental results. The numbers in parenthesis indicate the difference angle ($\Delta\theta$) between the calculated axis relation and the experimentally observed one.

The angle between unique axes		0°(180)	60°(120)	90°	Total
	The number of data	6	17	2	25
β-β	$\Delta\theta$				
	~15°	3	9	0	12
	15°~30°	3	7	2	12
	30°~	0	1	0	1
	The number of data	18	54	30	102
α-β	$\Delta\theta$				
	~15°	6	16	6	28
	15°~30°	9	33	23	65
	30°~	3	5	1	9

Table 4.1.2. The numbers of observed axis relations that agree with the VIS model.

4.1.4 Monoclinic domains of α phase

Now we demonstrate that two monoclinic domains in the α phase are created from the orthorhombic β phase. In Fig.4.1.6, the chain rectangle indicates the unit cell (c-projection) of the β phase. The crosses are the atomic positions of zinc atoms. They are on the two layers of the hcp structure. If zinc atoms move according the solid arrows within each layer, then a monoclinic unit cell (a,c) indicated by solid lines is realized. This case has been explained in Fig.4.1.4. On the other hand, if atoms move according the broken arrows, then we get another monoclinic unit cell (a',c'). These two kinds of cells take the identical α structure and therefore they are the monoclinic domains. When the ratio a/c is 1.28 and the monoclinic angle β is 109.0°, the ratio a'/c' of the counter part is also 1.28 and β' is 108.3°. Therefore these two kind of domains can be constructed with less strain. In this way the VIS model can explain the co-existence of the monoclinic domains with the common a and b axes. Indeed the co-existence of such monoclinic domains was often recognized by observing the reflections with l=half integer in samples exposed to the α-β-α transition.

The result of data 4 in Table 4.1.1 is a good example. The angle between the a axes of α phases before and after the α-β-α transition is 178 degrees. The angle between b axes is 177 degrees. That is, both a axes and b axes are approximately parallel with each other. On the other hand, the angle between the c axes is 36 degrees. This result indicates that the c axis direction turns in the real space without changing both a and b axes directions like as Fig.4.1.6.

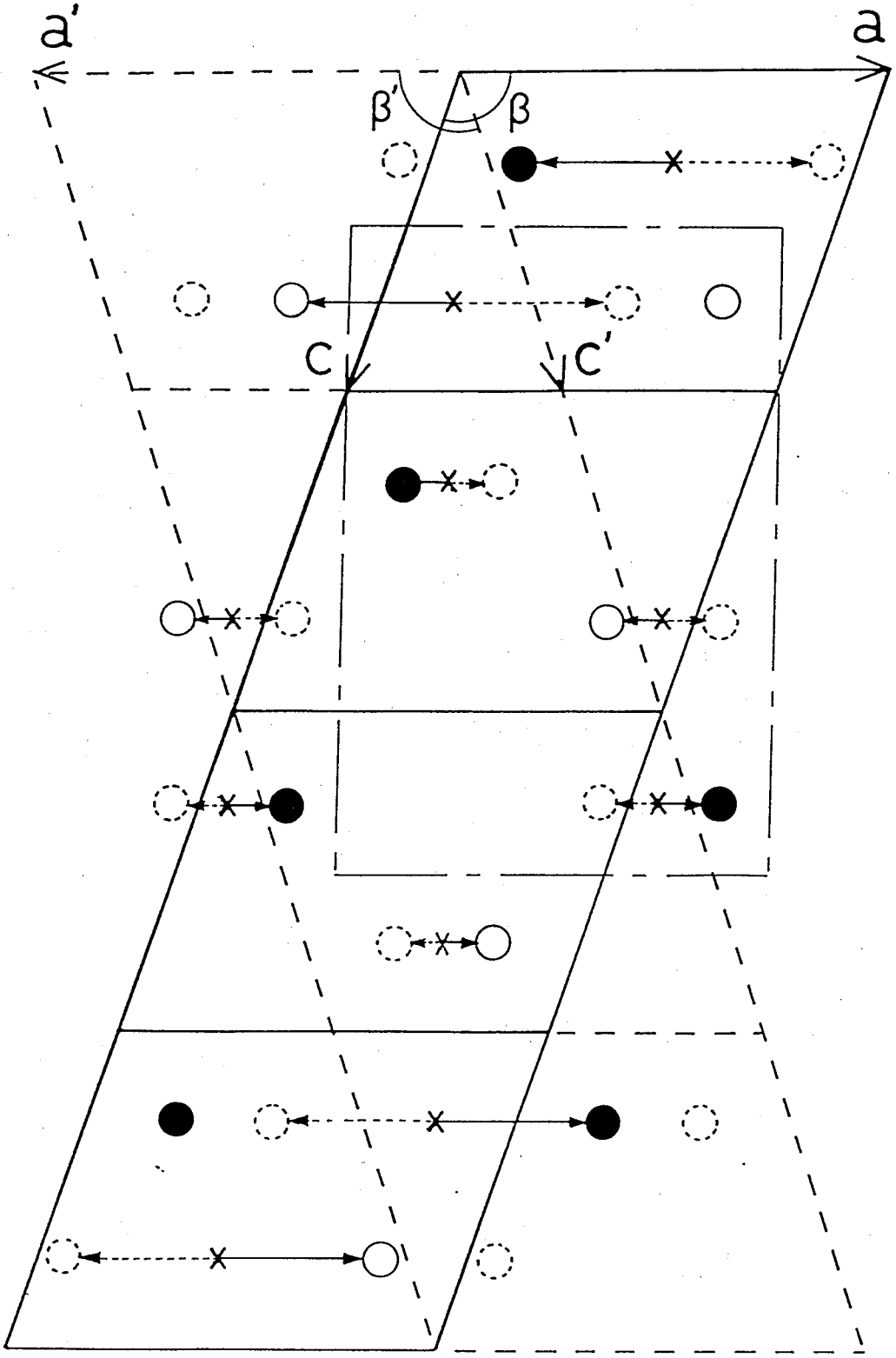

Fig. 4.1.6. Two type of domains of the α structure created after the β-to-α transition.

§ 4.1.5 Remarks

For many A_2BX_4-type ferroelectrics with β-K_2SO_4 structure in the high temperature phase, it is widely considered that $P6_3/mmc$ is the space group of the prototype phase. However, the α-β transition in KZB and KCB can not be explained by assuming that $P6_3/mmc$ is the prototype. In order to explain the change of the axis relation through α-β transition, we consider the bcc and hcp structures as the virtual intermediate states. It is also demonstrated that this VIS model explains the monoclinic domain very well.

§4.2 Discussion from the View Point of Elastic Property

4.2.1 α-β Transition studied by Brillouin Scattering.

The LA mode in the β phase shows a discrete distribution as shown in Fig.3.2.4(a) in contrast to the TA1 mode shown in Fig.3.2.4(b). The most interesting feature, shown inside the broken-line of Fig.3.2.4(a), is emphasized in Fig.4.2.1(a), where an expanded scale was employed. The distribution are roughly classified as denoted by the alphabetical letters into nine groups as shown in Fig.4.2.1(a). In addition to these nine groups, we found totally ten groups of $\Delta\nu$ in the β phase as shown in Fig.4.2.1(b). This distribution is considered to be caused by the distribution of the direction of the crystal axes induced by the reconstructive α-β transition.

On the other hand, the TA1 mode does not show any anomalous behavior at the α-β transition as shown in Fig.3.2.1(b). This indicates that the polarization vector of TA1 mode has a minor correlation with the atomic displacement due to the transition. In addition to the temperature dependences of LA and TA2 modes, the present result clearly shows the anisotropy of the atomic displacement of the VIS model.

We can see in Fig.3.2.5 that there is an obvious difference between the two series of the temperature dependence of LA mode upon heating and cooling in the α phase. The result indicates that the direction of the unique axis changes due to the α-β transition, since the direction of this LA mode is parallel to the unique axis of the monoclinic α phase of a virgin crystal. This result can be also explained by the VIS model with the relation between the unique axis of α phase and the [110] axis of

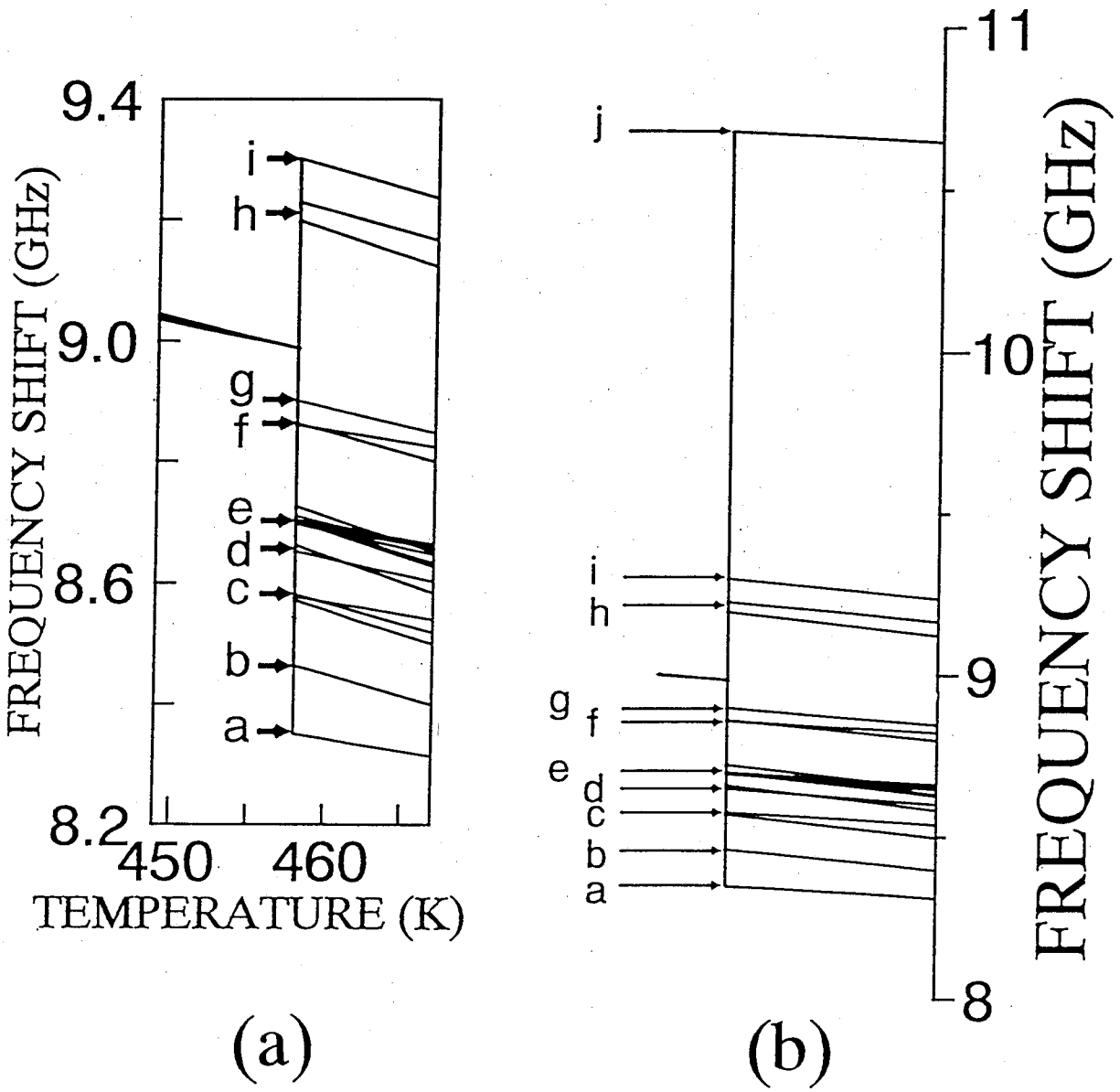

Fig. 4.2.1 (a)Discrete distribution of the Brillouin frequency shift of LA mode inside the broken-line(a), and of all results(b) of Fig. 3.2.3. Alphabetical letters indicate the name of the group of the Brillouin frequency shift in the β phase.

the bcc structure. That is, from the comparison of the temperature dependences of the frequency shifts observed upon heating and cooling, we confirmed the change of unique axis direction in the α phase due to the α-β transition.

4.2.2 Calculation of the frequency shift in terms of VIS model

The results are discussed by using the VIS model. The distributions of the LA and TA1 modes are calculated according to the VIS model. Here the VIS model is explained in detail to give appropriate help to a recognition of the model calculation: From a microscopical viewpoint the VIS model assumes the bcc and hcp states as the VIS in a boundary between α and β phases at T_t. Then the α-β transition are demonstrated according to the VIS model. Firstly, the monoclinic α phase changes to the virtual bcc state with the monoclinic axis of the α phase (the b-axis) transforming to the [110] axis of the bcc structure, where there are equivalent six directions of the <110> axis of the bcc structure. Then the virtual bcc state changes to the virtual hcp state with the one of the six <110> axes transforming to the hexagonal axis. Finally the virtual hcp state changes to the pseudo-hexagonal β phase with the hexagonal axis transforming to the pseudo-hexagonal axis (the c-axis of the orthorhombic β phase). It is possible for the c-axis of the β phase to have the equivalent six directions after the α-β transition thermodynamically because of the six <110> axes of the bcc structure.

In order to help to understand the VIS model, the directions of q relative to the crystallographic system of the β phase are shown in Fig.4.2.2. Six arrows show the directions of q in the β

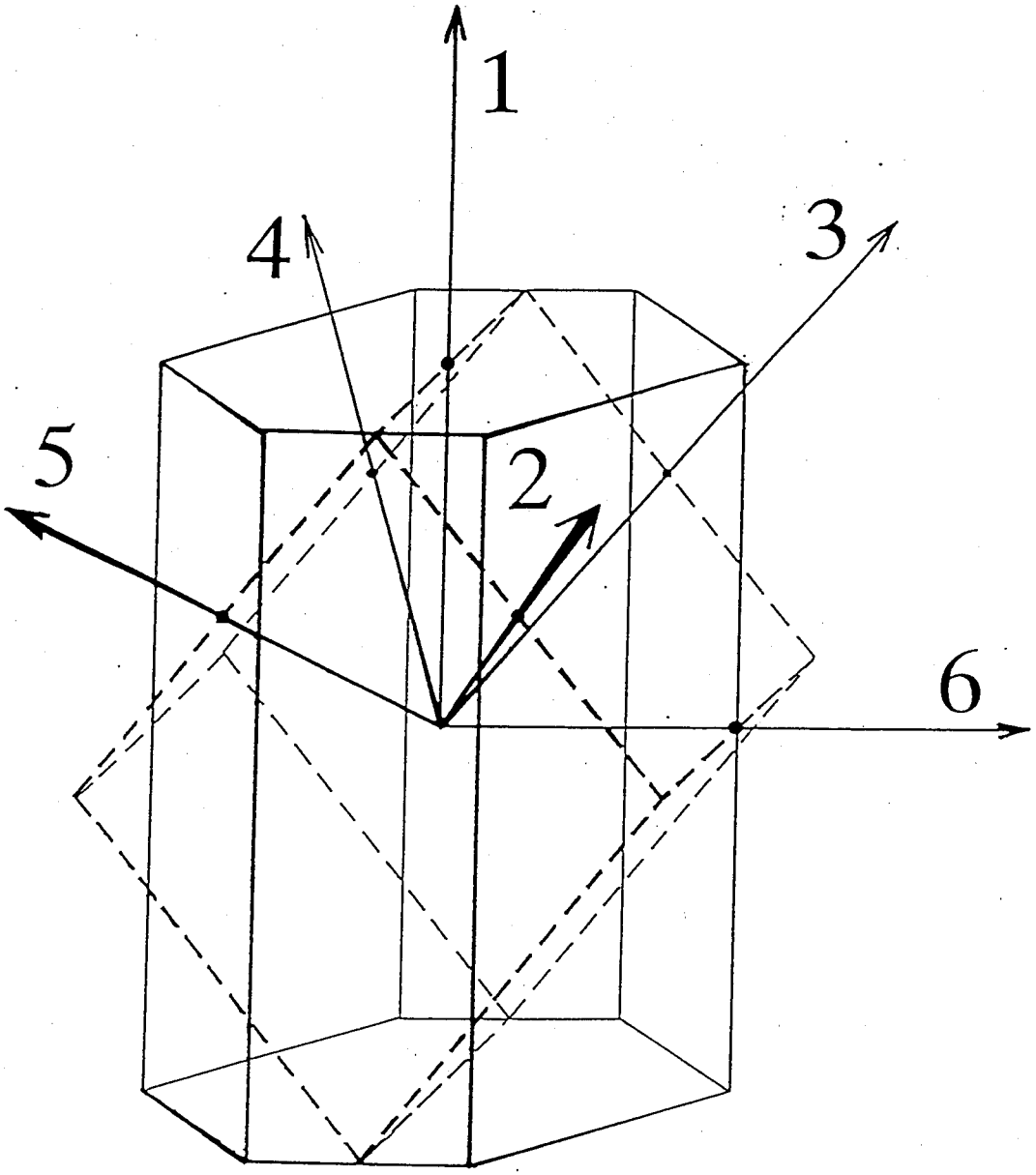

Fig. 4.2.2 Arrows (1-6) indicate the directions of the observed wave vector q relative to the crystallographic system in the β phase. Broken lines indicate the bcc structure of the VIS. Solid lines indicate the hexagon of the pseudo-hexagonal structure of the β phase. Small arrows, a, b and c, show the crystal axes of the β phase.

phase after the α-β transition. Strictly speaking, the VIS model gives thirty one possible directions (see Appendix 4.2) in the α-β transition as described §4.1.

If we obtain a complete set of the components of the elastic stiffness tensor and the refractive indices of the β phase, we can calculate each of $\Delta\nu$ in the β phase along the directions of q on condition that includes the thirty-one arrows. The tensor has not been fully obtained for KZB. However, Rb_2ZnCl_4 (RZC) has both of the structure and the phase transition sequence similar to the β sequence of KZB, and its elastic stiffness tensor and its refractive indices have been reported.[31)]

The distribution of $\Delta\nu$ of LA mode shown in Fig.4.2.1(b) is calculated using the elastic stiffness tensor of RZC. Here the refractive indices n was assumed as $n=(n_a+n_b+n_c)/3$. For one direction of q in the β phase, we were able to solve the elastic equations and obtained $\Delta\nu$ of LA and TA modes. The calculated result of LA mode is shown in Fig.4.2.3(a), where the characteristic ten different values of $\Delta\nu$ appears. The values of $\Delta\nu$ denoted as a-c, d-i and j in Fig.4.2.3(a) correspond to the wave vectors expressed by the arrows of 6 (group III), 2-5 (group II) and 1 (group I) in Fig.4.2.2, respectively, where the names of groups, groups I, II and III, correspond to the names described in Appendix 4.2. Now we can compare the calculated result of LA mode with the experimental one as shown in Fig.4.2.3(b). It is clear that the characteristics distributions of $\Delta\nu$ shown in Figs.4.2.3(a) and 4.2.3(b) are similar well each other. This good coincidence suggests that the origin of the characteristic distribution of $\Delta\nu$ shown in Fig.4.2.1(a) is caused

by the virtual bcc and hcp structures of the VIS model in the α-β transition. Here in Figs.4.2.3(a) and 4.2.3(b) the difference between the observed and calculated results seems to be caused by the difference in the elastic properties between KZB and RZC.

In Fig.4.2.1(b) TA1 mode does not show any anomaly at T_t within the experimental error. On the other hand the calculated result shows a distribution over 0.5GHz as shown in Fig.4.2.4. This difference is also caused by a difference between the elastic properties of both crystals. For a more conclusive evidence, however, we need a farther study.

4.2.3 Characteristic distribution of frequency shift $\Delta\nu$ of the LA mode in A_2BX_4 Type Compounds

The distributions of $\Delta\nu$ of the LA and TA1 modes are investigated by performing the calculation of $\Delta\nu$ using the elastic stiffness tensor of the RZC and RZB of the RZC group compounds, which have the phase transition sequence and the structure similar to the β phase of KZB as mentioned above and the elastic stiffness tensors and the refractive indices n are known.[31] The model calculations of LA and TA1 modes of RZC have been already shown in 4.2.2. In order to compare with the characteristic of the RZC-group compounds, we also calculate about $(NH_4)_2SO_4$ (ASO) compound[32] which shows a different phase transition sequence from the RZC-group compounds.

The refractive indices n was assumed as $n=(n_a+n_b+n_c)/3$. The calculated results show in Figs.4.2.5(a) and 4.2.5(b). The each calculated result of LA and TA1 modes by using the elastic stiffness tensors of RZC, RZB and ASO indicates a characteristic independent ten-lines distribution of the $\Delta\nu$ based on an

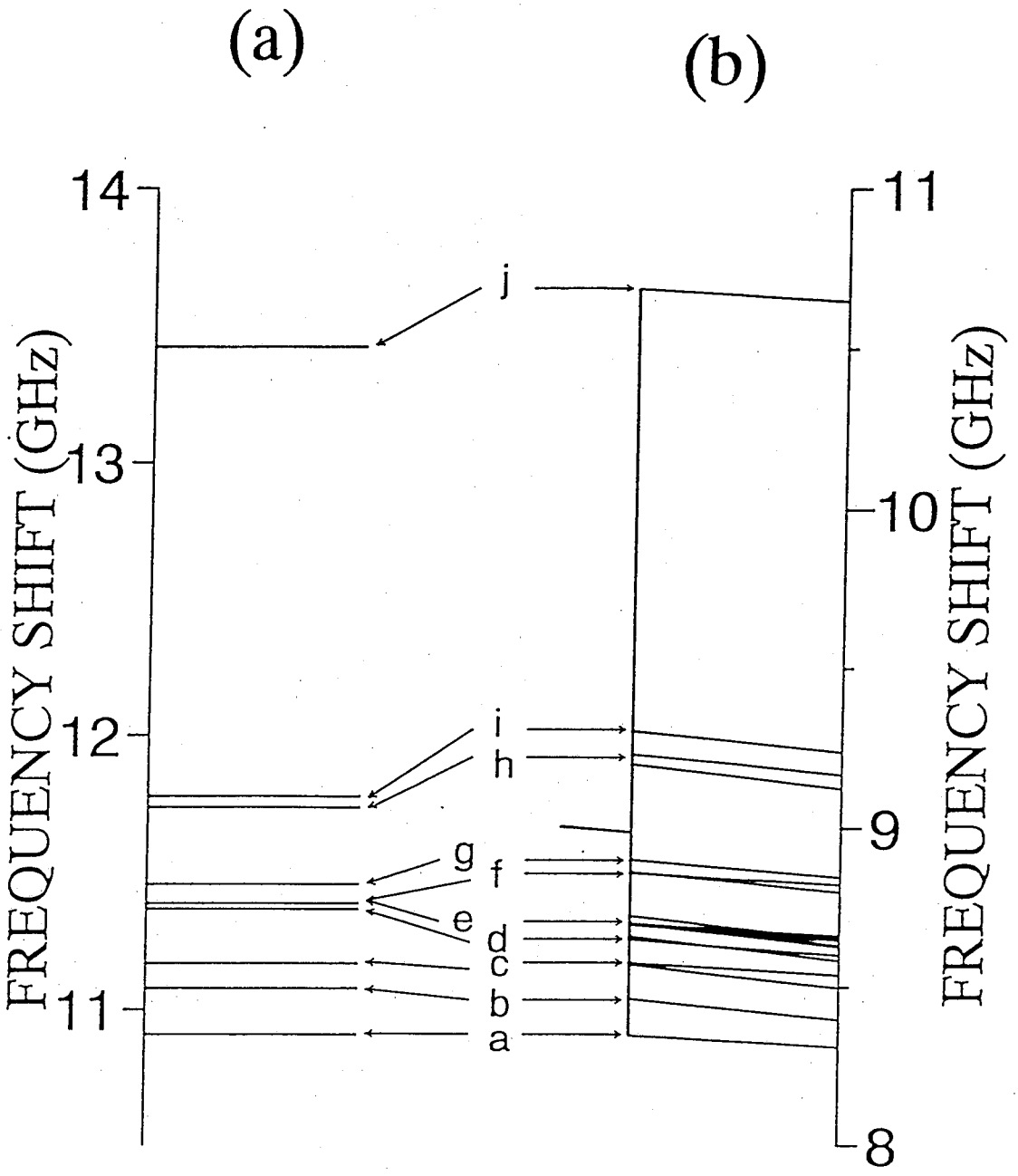

Fig. 4.2.3(a) Brillouin frequency shift of LA mode of Rb_2ZnCl_4 calculated in terms of the VIS model. Alphabetical letters indicate the name of the group of the Brillouin frequency shift. Notice that the group j is very similar to the case of KZB. (b) The present experimental result of LA mode. Arrows indicate correspondence between the groups of calculated and observed results.

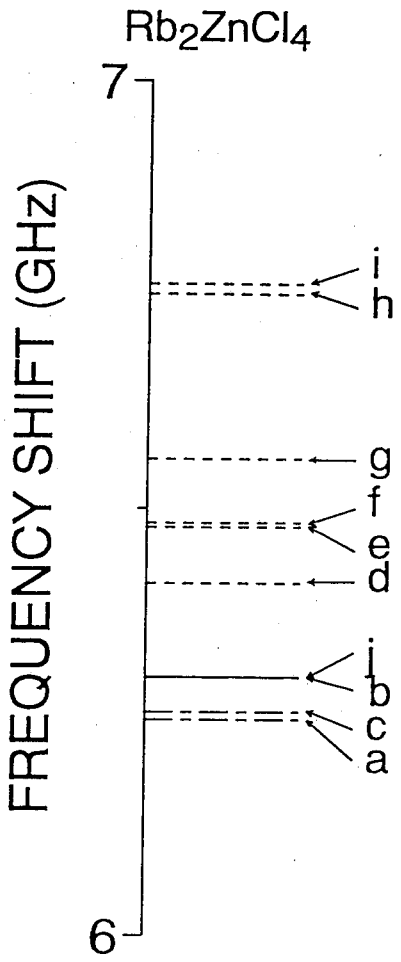

Fig. 4.2.4 Brillouin frequency shift of TA1 mode calculated in terms of the VIS model by using the refractive indices of RZC. Letters correspond to the name of the groups of the frequency shift of the LA mode.

Fig. 4.2.5.The distribution of LA mode (a) and TA1 mode (b) calculated by using the elastic stiffness tensors of RZC, RZB and ASO. The three kinds of lines indicate three groups; the solid, broken and chain lines show the group I, II and III, respectively. Alphabetical letters indicate the group of the Brillouin frequency shift.

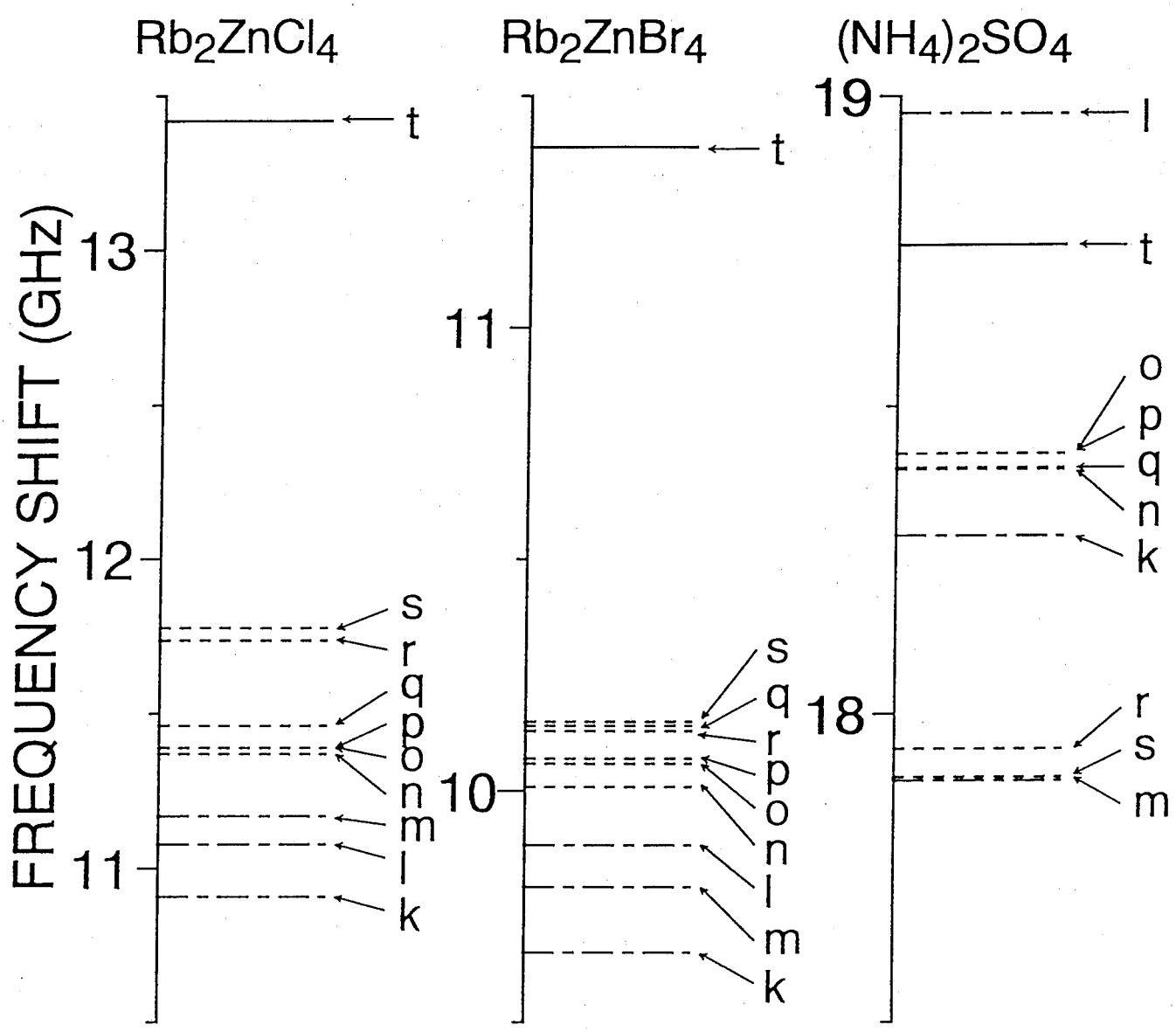
Rb2ZnCl4
Rb2ZnBr4
(NH4)2SO4
FREQUENCY SHIFT (GHz)
13
12
11
11
10
19
18
t
s
r
q
p
o
n
m
l
k

(a)

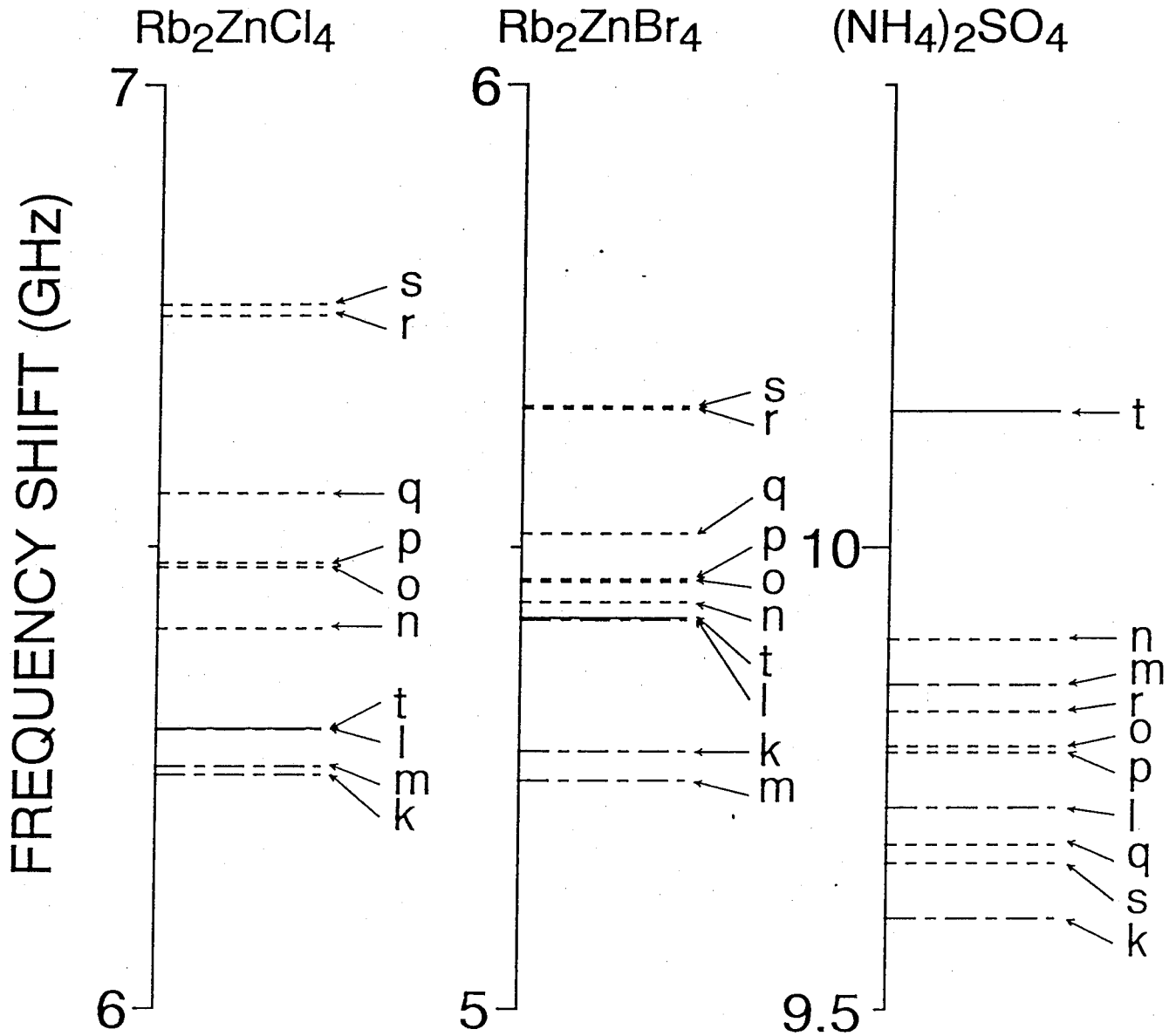
Rb2ZnCl4
Rb2ZnBr4
(NH4)2SO4
FREQUENCY SHIFT (GHz)
7
6
6
5
10
9.5
s
r
q
p
o
n
t
l
m
k
s
r
q
p
o
n
t
l
k
m
t
n
m
r
o
p
l
q
s
k

(b)

assumption of the intermediate states with the bcc and hcp structure according to the VIS model. On condition that each alphabetical letter indicates a same direction of a calculated phonon-wave vector, the distribution of LA and TA1 modes in RZC, RZB and ASO are classified into ten groups as shown in Figs.4.2.5(a) and 4.2.5(b).

In LA mode the feature of the discrete distribution of RZC and RZB of the RZC group compounds is similar to each other in contrast to ASO. To be exact, the distributions of the groups I, II and III of RZC and RZB are similar to each other, even then there are a few differences in an alphabetical order as shown in Figs.4.2.5(a) and 4.2.5(b). The characteristic distribution of the calculated results of RZC and RZB can be seen in the experimental one of KZB. This feature of distribution should be consider as the characteristic of the RZC-group compounds. That is, the good agreement between the calculated and experimental results indicates that a origin of the characteristic distribution of $\Delta\nu$ in the β phase is caused by the virtual bcc and hcp structures of the VIS model.

In TA1 mode the calculated results of RZC and RZB shown in Fig.4.2.5(b) indicate that the distribution of TA1 mode expands over about 0.5GHz. However in Fig.3.2.4(b) the experimental result of TA1 mode does not show any anomaly at T_t within the experimental error. From the difference between experimental and calculated results the experimental result in Fig.3.2.4(b) seems to show the difference between the stiffness tensors of RZC group compound and KZB compound.

In summary of this subsection, the distributions of LA and

TA1 modes are obtained by numerical calculation using the elastic stiffness tensors of RZC, RZB and ASO compounds according to the VIS model. The two distributions of the calculated results of RZC and RZB are similar to each other. And the distributions calculated are similar to that of the experimental result of KZB. The good agreement between the calculated and experimental results shows that the distribution of LA mode in the β phase is caused by the virtual bcc and hcp structures of the VIS model. On the other hand the calculated result of the TA1 mode indicates that the distribution expands over about 0.5 GHz in contrast to the experimental result which does not expand. It seems that the difference between the experimental and calculated results indicates the difference of the stiffness tensor between KZB and RZC group compound.

§ 4.3 Discussion

4.3.1 Physical meaning of VIS Model

In general a domain structure appears when the crystal changes its phase from high symmetry phase to low one. In this section, this domain structure of KZB is explained. We consider here the simplest example, a phase transition from orthorhombic to monoclinic phase as shown in Fig.4.3.1. When a crystal changes its symmetry from orthorhombic to monoclinic, two types of domains, domain-1 and domain-2, appear as shown in Fig.4.3.1. In other words there are two types of routes for atomic displacement. Namely it means that these two routes are equivalent for the orthorhombic structure.

Now we consider about the α-β transition using the as-grown single crystal. By X-ray diffraction study and Brillouin scattering study, we observed many domains appeared in the β phase crystal exposed the α-β transition. The domains are simply shown in Fig.4.3.2. These many domains, A, B, C..., should be equivalent in the β phase. The diagram means that the as-grown α phase changes to domain-A of the β phase through route-A at the α-β transition point, etc. That is, these routes, A, B, C,..., should be also equivalent each other thermodynamically. But in this case, because the α phase symmetry is lower than the β one, it is difficult to explain that these routes are equivalent thermodynamically. In order to solve this problem, we assume some virtual intermediate states (VIS model) of which symmetry is higher than the one of the β phase. The schematic illustration of this model is shown in Fig.4.3.3, where we assume one virtual intermediate state as the simplest model. The space group of the

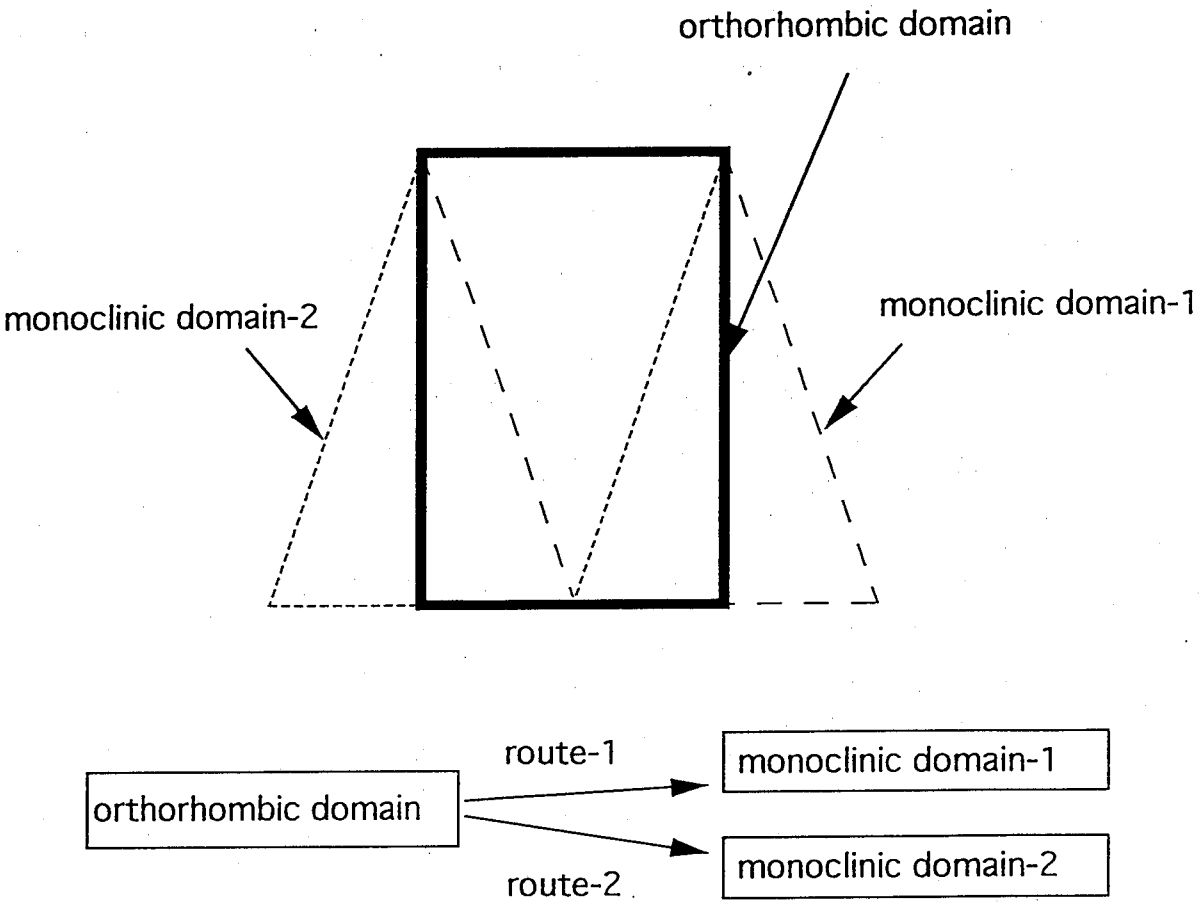

Fig. 4.3.1 Two types of monoclinic domains transformed from an orthorhombic structure. Domain 1 and 2 are derived through the route 1 and 2, respectively.

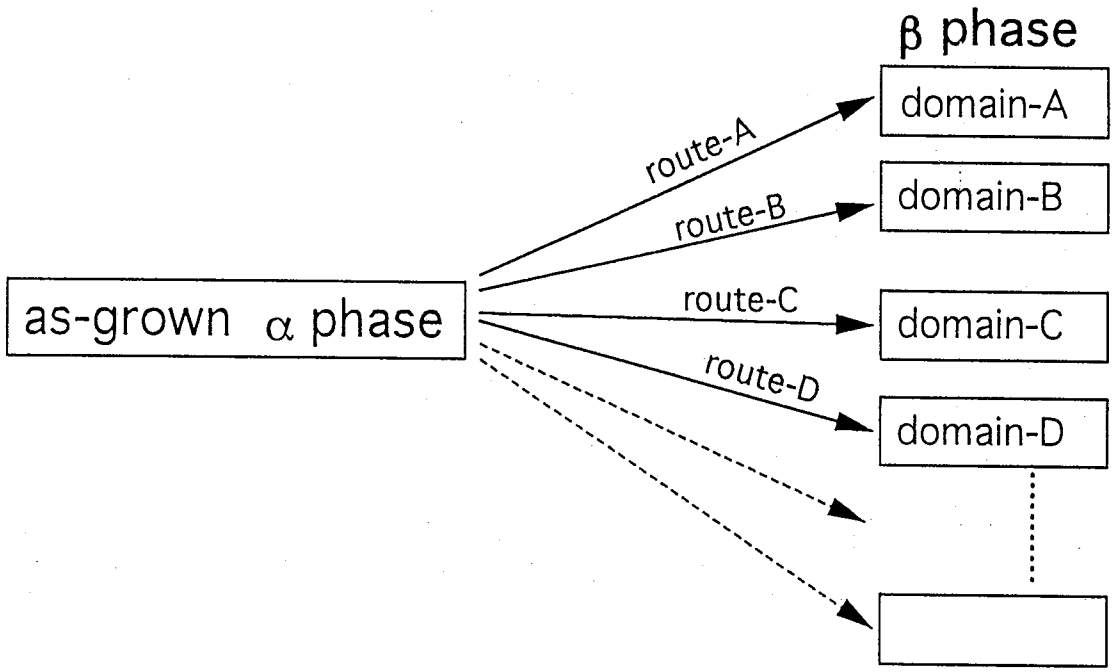

Fig. 4.3.2 Many domains of the β phase derived from as-grown single phase.

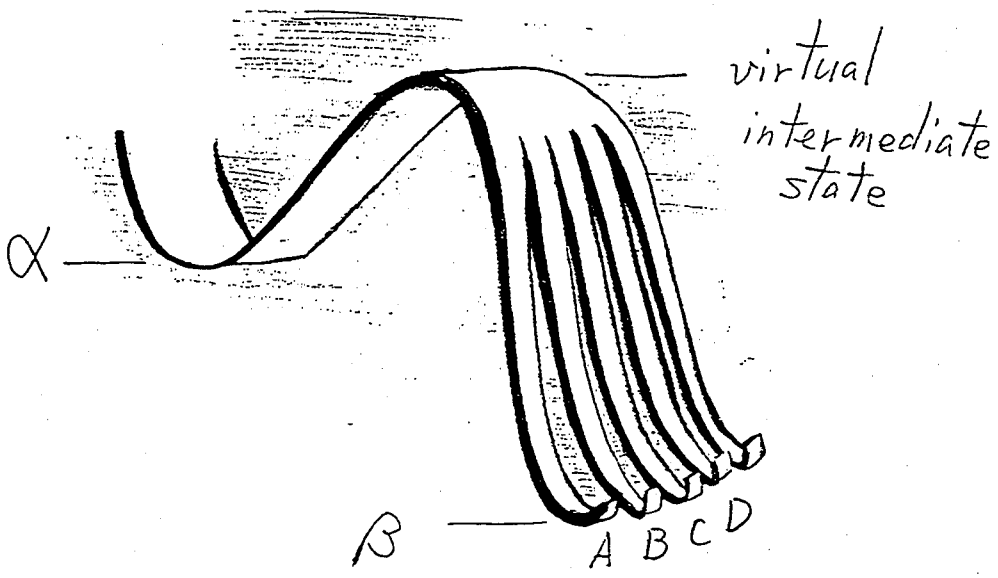

Fig. 4.3.3 The schematic illustration of single virtual intermediate state model. Letters of A, B, C, D,... indicate the names of domains in β phase. A crystal changes from the as-grown α to β phase through the virtual intermediate state.

virtual intermediate state derives thermodynamical equivalency of the domains of the β phase. Next we consider a structure of the virtual intermediate state.

4.3.2 Necessary Conditions of VIS model

The intermediate state has to satisfy following three conditions (a), (b) and (c), according to the experimental results.

(a)By X-ray diffraction study in § 3.1, the axis relations were observed as given in Table 3.1. One of the results, data 1 in Table 3.1, indicates that the b axis of the α phase (monoclinic axis, b_α) is parallel to the c axis of the β phase (pseudohexagonal axis, c_β). Namely one of domains in Fig.4.3.3 should satisfy this condition.

(b)Then from Table 3.1 we obtain the condition that there are three types of axis relations between α and β phases: the angles between b_α and c_β axes are about 0°(or 180°) of data 1, 90° of data 2 and 120°(or 60°) of data 3.

Here the results obtained by X-ray diffraction study after repetitions of heating and cooling runs does not give us any definite axis relation between the as-grown α phase and the first heated β phase as mentioned in §2.2.

(c)By Brillouin scattering study described in §4.2.1, the ten groups of frequency shift $\Delta\nu$ of the LA mode in the β phase were obtained as shown in Fig.4.2.1(b). These results were obtained by

first heating from as-grown single α phase.

4.3.3 Number of the virtual intermediate states

Next taking account of the conditions of §4.3.2, we consider about a structure of the virtual intermediate state. All space groups are generally classified into seven crystal systems; triclinic, monoclinic, orthorhombic, tetragonal, rhombohedral, hexagonal and cubic. The structure of the intermediate state should have equivalent axes more than three because of the condition (b). The structure which has the equivalent axes more than three is rhombohedral, hexagonal or cubic. However, the structures of the rhombohedral and hexagonal can not give the angle, about 90 degrees, between b_α and c_β axes contained in the condition (b), since it only gives 60° (120°). Namely we should consider the cubic structure as the virtual intermediate state. The transition from α to β phase proceeds as the following,

$$\alpha \rightarrow \text{cubic} \rightarrow \beta.$$

A cubic structure has <111>, <100> and <110> axes. Taking account of the condition (a), we get three types of axis relations as follows; (1)b_α // one of <111> axes // c_β, (2)b_α // one of <100> axes // c_β and (3)b_α // one of <110> axes // c_β. By the single virtual intermediate state model with cubic structure according to the above three conditions, a number of values of the frequency shift of the LA mode in the β phase are calculated as shown in Table 4.3.1. For example, if the α-β transition takes place according to the axis relation (1), a number of groups of the frequency shift described in § 3.2 should be three. However,

axis relation	number of LA mode
α→cubic→β <100>	3
α→cubic→β <111>	4
α→cubic→β <110>	4

Table 4.3.1. The Number of values of the frequency shift of the LA mode, according to one virtual intermediate state model of the cubic structure.

axis relation	number of LA mode
α→cubic→hexagonal→β <111>	3
α→cubic→hexagonal→β <100>	7
α→cubic→hexagonal→β <110>	10

Table 4.3.2. The Number of values of the frequency shift of the LA mode, according to two virtual intermediate states model of the cubic and hexagonal (or rhombohedral) structures.

by Brillouin scattering study we found ten groups of frequency shift of LA mode in the β phase as shown in Fig.4.2.1(b). That is, from the results of Table 4.3.1 we can not explain the experimental results by using the single virtual intermediate state model.

Then, we have to introduce two virtual intermediate states as the next simpler model. By X-ray diffraction study a 120° domain was observed as shown in data 7 of Table 3.1. From this result a hexagonal or rhombohedral structure should be selected as a virtual intermediate state in addition to a cubic structure. That is, the transition proceeds as the followings,

$$\alpha \rightarrow \text{cubic} \rightarrow \begin{matrix}\text{hexagonal} \\ \text{(or rhombohedral)}\end{matrix} \rightarrow \beta.$$

Taking account of the condition of (a), we obtain the new axis relations as follows, (4)b_α // one of <111> axes // unique axis of hexagonal (or rhombohedral) // c_β, (5)b_α // one of <100> axes // unique axis of hexagonal (or rhombohedral) // c_β and (6)b_α // one of <110> axes // unique axis of hexagonal (or rhombohedral) // c_β. According to the axis relations, (4)-(6), a number of values of the frequency shift of the LA mode in the β phase were obtained in Table 4.3.2. From the condition of (6), we found ten values of the frequency shift of LA mode successfully. This result agrees with the experimental result of Fig.4.2.1(b). Namely two virtual intermediate states must be considered for the simplest model. This result confirms the VIS model in § 4.1. The schematic illustration of the two virtual intermediate state model is given in Fig.4.3.4.

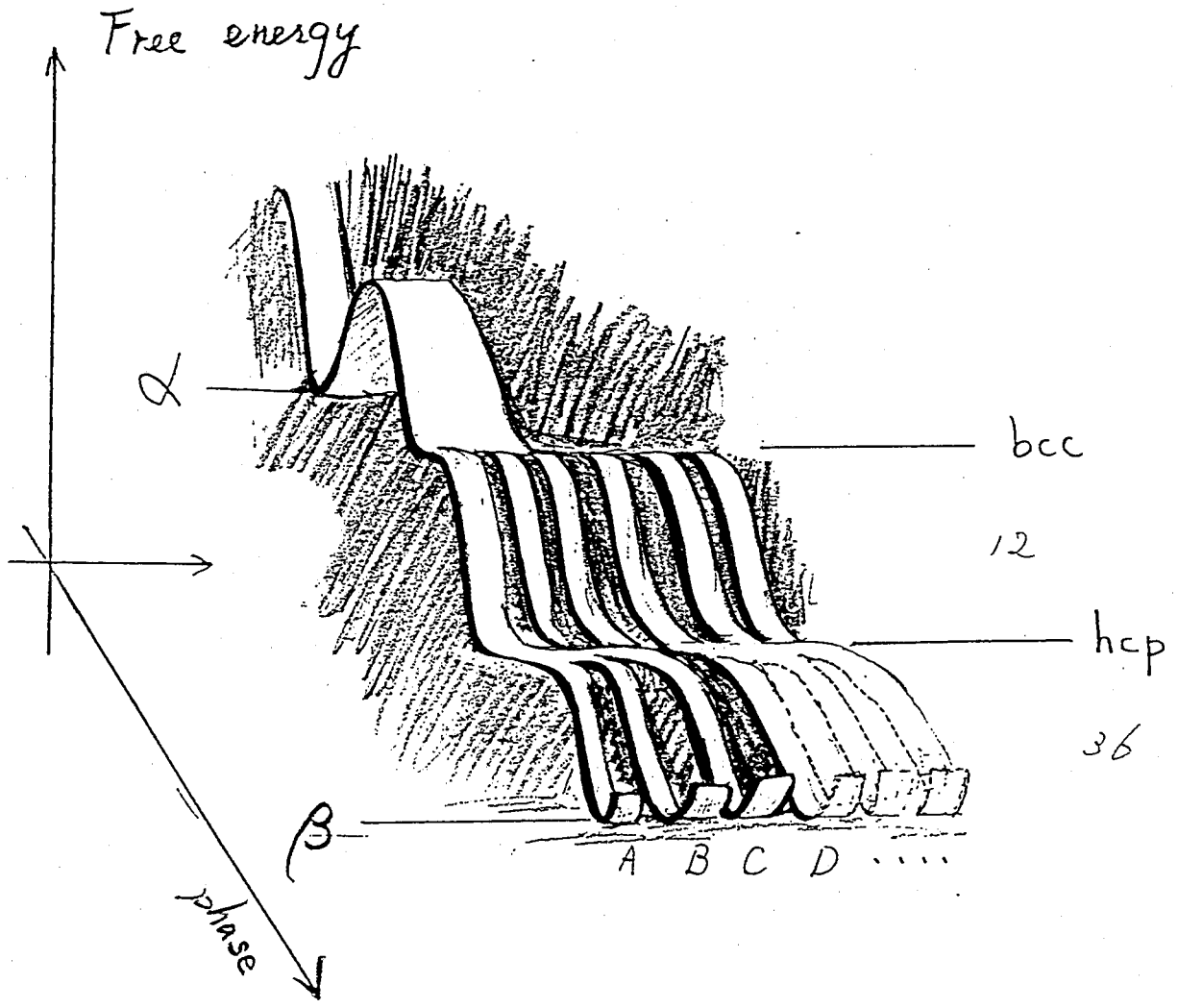

Fig. 4.3.4. The schematic illustration of the α–β transition according to the VIS model.

4.3.4 Space group of the virtual intermediate state

The space group of the cubic and hexagonal structures consistent with the condition of (6) are considered. The displacement of atoms at the α-β transition is treated according to the VIS model. Furthermore we assume two relations as follows. (1)The relation between the α phase and the virtual cubic structure, and also between the β phase and the virtual hexagonal structure have group-subgroup relations, respectively. (2)The number of formula units per cell of the cubic structure is equal to 2 as same as one of the α phase.

First we investigate the space group which satisfies the above condition (1) and the axis relation (6). The α phase has the monoclinic structure with space group $P2_1/m$. The relation between the structure and its symmetry operations is shown in Fig.4.3.5. In Fig.4.3.6 the symmetry operations of the α phase are shown in the coordinate system of cubic structure after a transition from the α phase to the virtual cubic structure. Among 36 space groups of cubic symmetry, only space group $Im\bar{3}m$ satisfies the symmetry operations indicated in Fig.4.3.6. These symmetry operations can be seen in $Im\bar{3}m$ of Fig.4.3.7. That is, the space group of the cubic structure of the virtual intermediate state is determined as $Im\bar{3}m$.

Next the space group which satisfies the conditions of (2) and the axis relation (6) are investigated. The β phase is the pseudohexagonal structure with the space group Pmcn. The structure, which is the supergroup of Pmcn and is either hexagonal or rhombohedral structure, is only hexagonal of $P6_3/mmc$ or $P6_3/mcm$. On the other hand from a structural consideration of

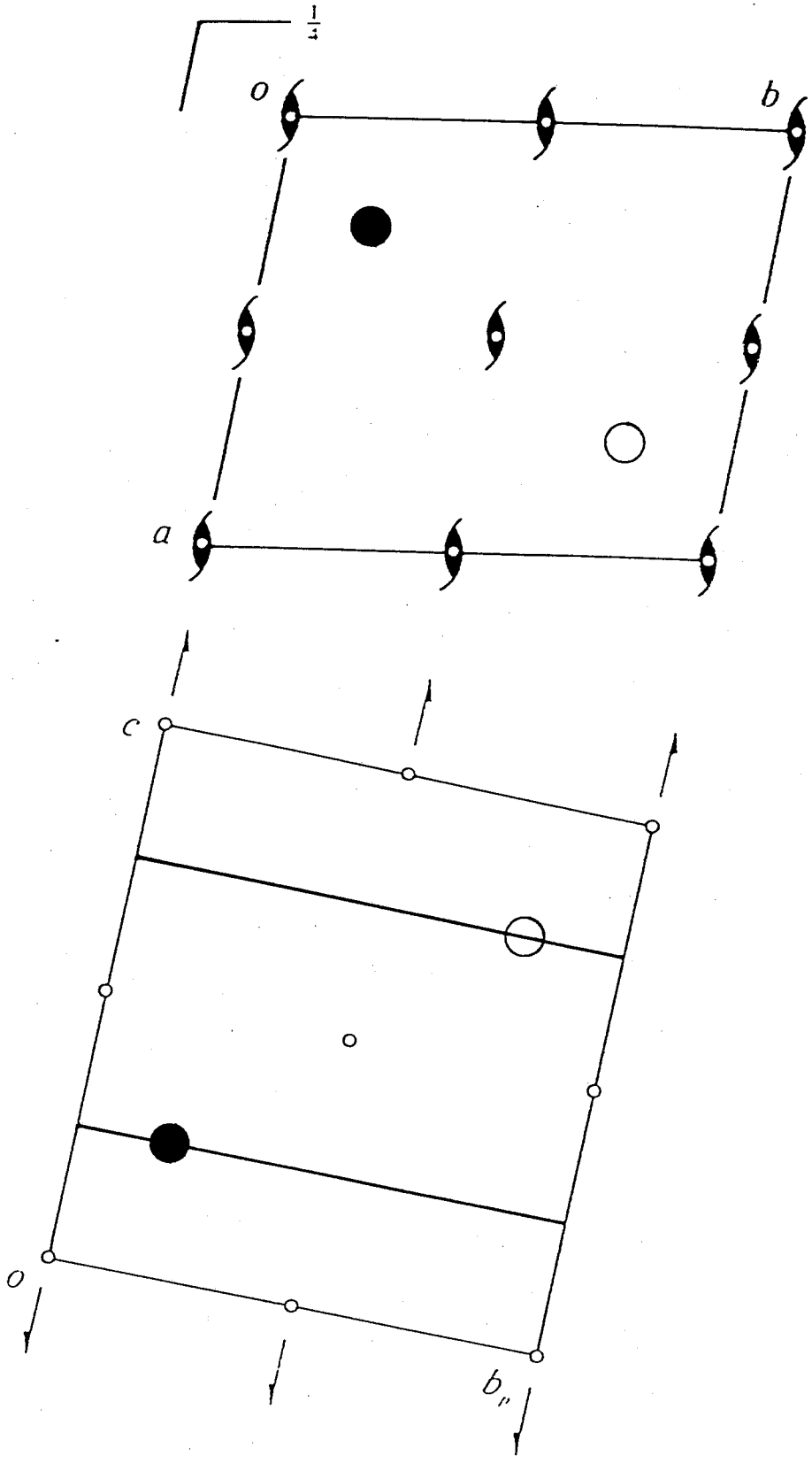

Fig. 4.3.5. The crystal structure of the α phase of the space group $P2_1/m$. Symbols of the symmetry operations are according to the International Table.[35] Large open and solid circles indicate the Zn atoms of K_2ZnBr_4.

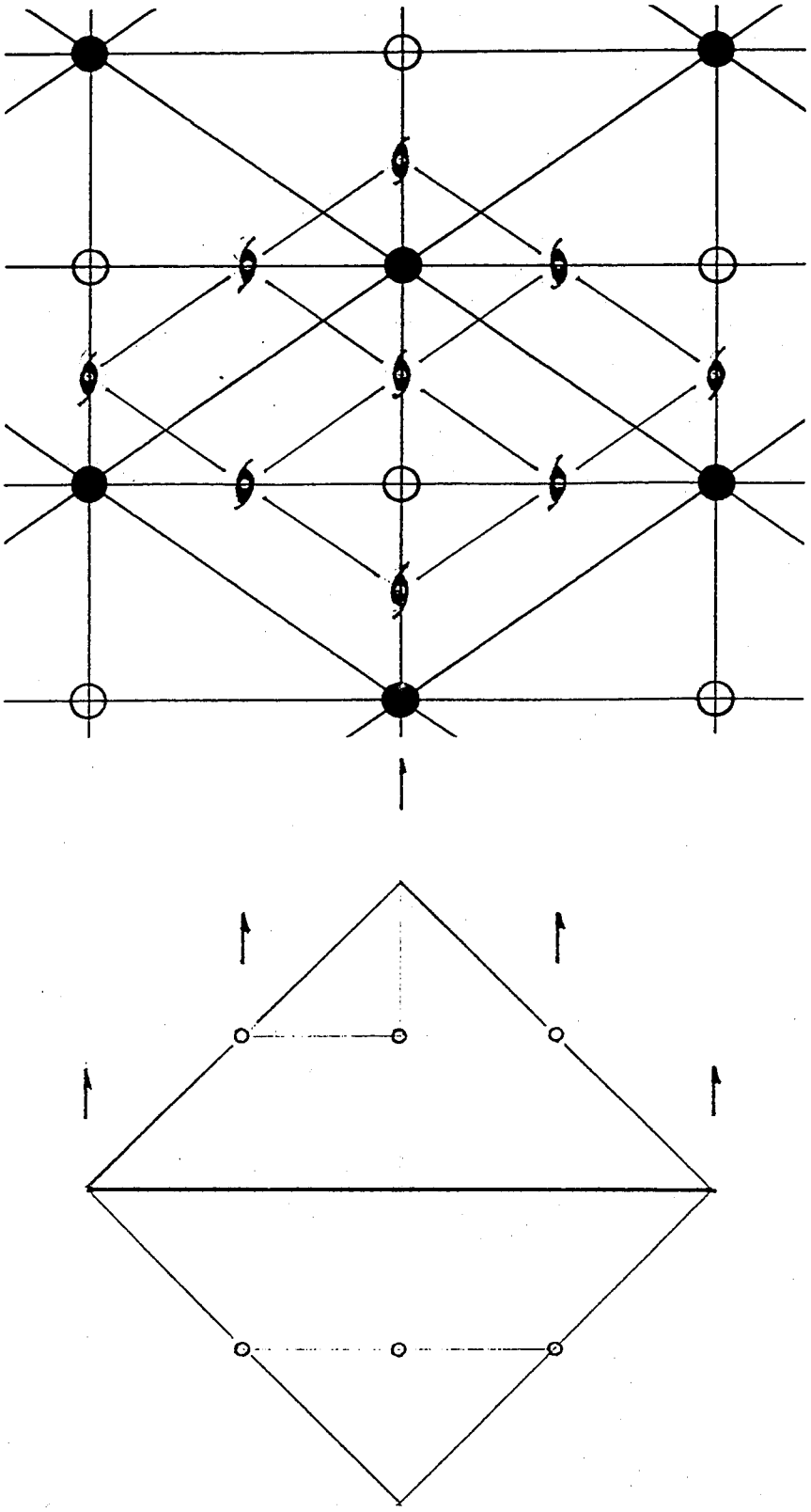

Fig.4.3.6. The symmetry operations of the space group $P2_1/m$ in cubic structure. (a) The projection from the [110] direction. (b) The projection from the [100] direction. Large open and closed circles indicate the Zn atoms in the virtual bcc structure.

$Im\bar{3}m$

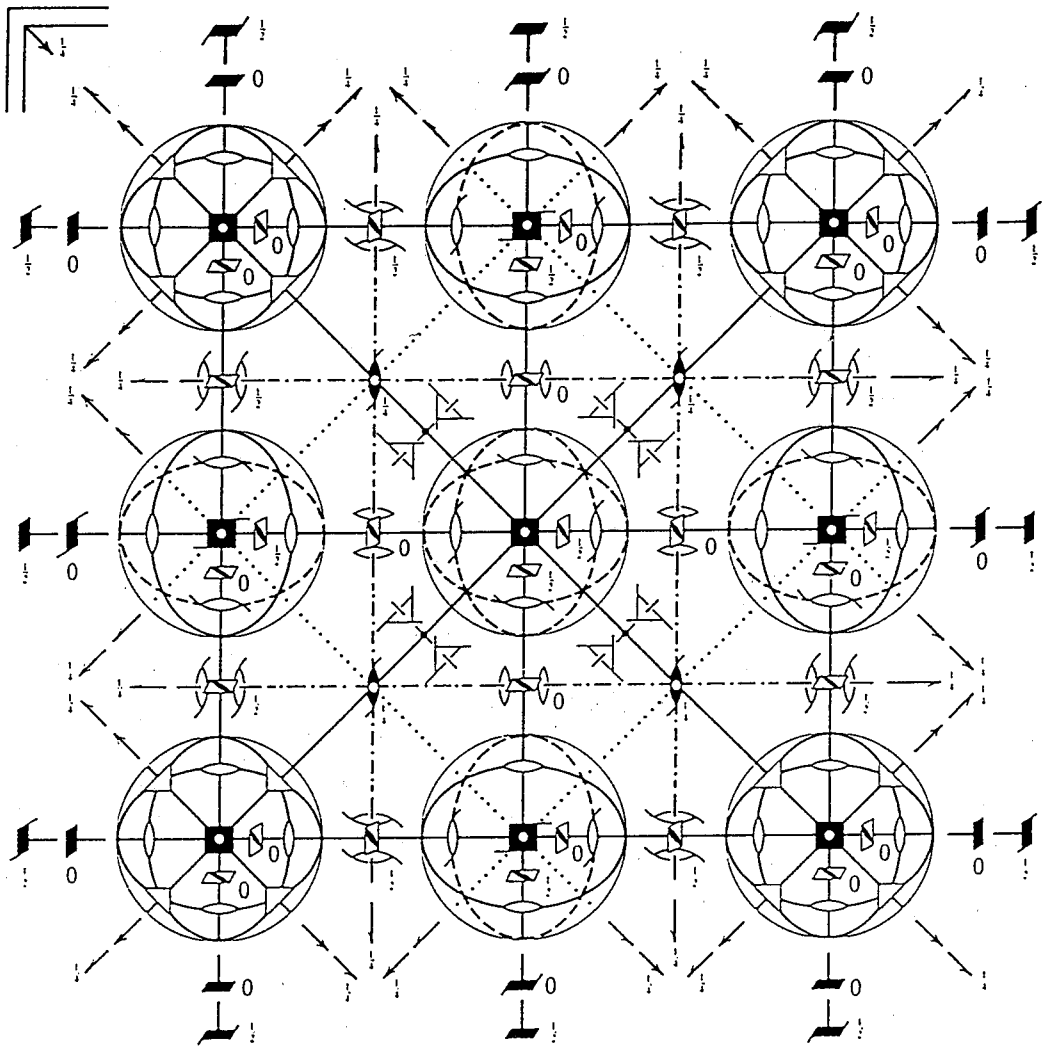

Fig. 4.3.7. Symmetry operations of the space group of Im$\bar{3}$m. [International Tables for Crystallography. Vol. A 1983][35)]

the pseudohexagonal β structure, the space group of the virtual hexagonal structure is concluded to be $P6_3/mmc$. The relation between Pmcn and $P6_3/mmc$ is shown in Fig. 4.3.8.

In summary of this section the space groups of the virtual intermediate states were determined as follows;

$$\alpha \rightarrow \underset{Im\bar{3}m}{\text{cubic (bcc)}} \rightarrow \underset{P6_3/mmc}{\text{hexagonal}} \rightarrow \beta.$$

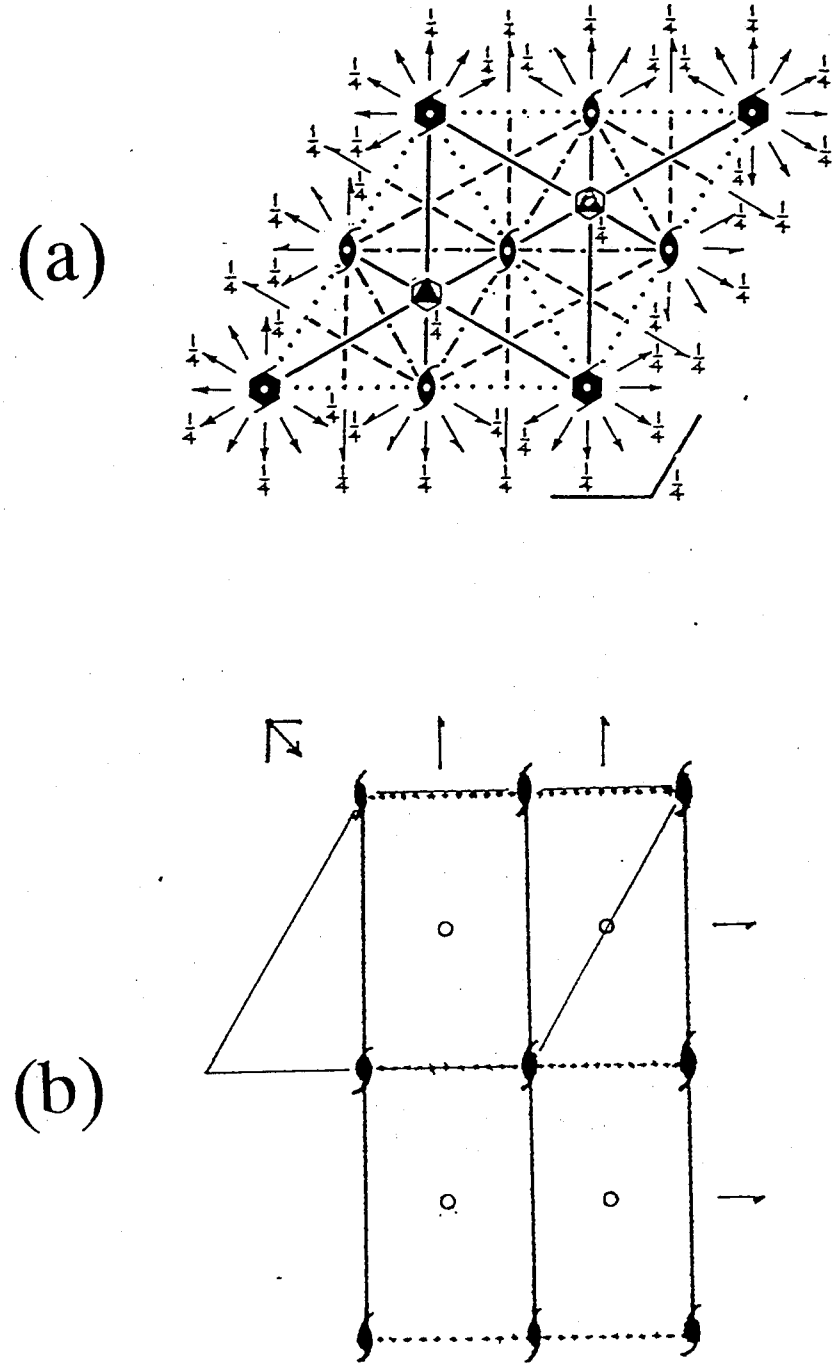

Fig.4.3.8. (a) The space group of $P6_3/mmc$. (b) The relation between the space group of $P6_3/mmc$ and Pmcn.

CHAPTER 5. CONCLUSION

By X-ray diffraction study, the axis relations were elucidated between the low temperature α and high temperature β phases. The relation indicates that the direction of crystallographic axes changes at every time passing through the transition point. For many A_2BX_4 type ferroelectrics which have β-K_2SO_4 type structure in the high temperature phase, it is widely accepted that $P6_3/mmc$ is the space group of the prototype. However, we found in the present study that the experimental result of K_2ZnBr_4 can not be explained by assuming the prototype symmetry $P6_3/mmc$. In order to explain the characteristic feature of this reconstructive α-β transition of K_2ZnBr_4, the virtual intermediate states model, the VIS model, was proposed as the phase transition mechanism. The bcc and hcp structures were considered as the virtual intermediate states.

In order to investigation the relationship between the as-grown α phase and first heated β phase, the Brillouin scattering spectra of K_2ZnBr_4 were observed as functions of temperature in both of the α and β phases. On heating the temperature dependence of the spectra in the β phase showed a clear difference in each experimental run in contrast to the good reproducibility in the α phase. Furthermore after many times of the experimental runs using the as-grown single crystal, the frequency shift of the LA mode showed a characteristic distribution in the β phase. In terms of the VIS model, the numerical analysis reveals well the experimental result.

Finally a detailed discussion was given for the VIS model taking account of both results of X-ray diffraction and the

Brillouin scattering. BY this consideration it was concluded that two states must be necessary as virtual intermediate states in the simplest case. Furthermore the space groups of the virtual intermediate states was determined as the $Im\bar{3}m$ and $P6_3/mmc$ by using an application of the group-subgroup relation.

Appendix 2.2: Elimination of Possibility of Experimental Mistakes

Two cases of experimental mistakes are discussed in the following. First, there may be a mistake of determining the unit cell. That is, the unit cell in a wrong direction was determined accidentally. This may happen when the wrong cell parameters are nearly equal to the correct cell parameters. In order to discuss this mistake, the case of the data 8 in Table 3.1 is investigated. If one β structure is equal to the other β structure in data 8, there is no mistake as above mentioned. The one β structure is compared with the other β structure by the correlation coefficient r for the structure factor observed by X-ray diffraction, where the correlation coefficient r is defined as following,

$$r = \sum_{hkl} \{[\,|F_1(h,k,l)| - \overline{F}_1\,] \times [\,|F_2(h,k,l)| - \overline{F}_2\,]\}$$
$$/\{\sum_{hkl} [\,|F_1(h,k,l)| - \overline{F}_1\,]^2 \times \sum_{hkl} [\,|F_2(h,k,l)| - \overline{F}_2\,]^2\}^{\frac{1}{2}}$$

where $F(h,k,l)$ is the structure factor and $\overline{F}$ is an average of all $|F(h,k,l)|$. Reflections satisfied $|F| > 3\sigma(|F|)$ are used in the analysis. In the case of data 8, the number of independent reflections used is 137. The calculated correlation r is 0.969. Thus we clarify that the two β structures are equal with each other and that there is no mistake in determining the unit cell.

Second, there might be a possibility that the wrong cell was assigned. The axes were determined by peak searching of twenty reflections. A unit cell might be accidentally determined by using reflections from different domains of a sample. This unit cell parameters might be almost equal to the correct unit cell parameters. However, there was no possibility of such mistake,

since other diffraction peaks were successfully observed by the use of the obtained cell-orientation matrix. Thus the two cases of mistaking the cell orientations are eliminated.

Appendix 2.3.1 Light Scattering Cell

The sample cell for light scattering measurement is shown in Fig.2.3.2. It was made of a brass block and four windows. Brass surface was made black by treating one with a aqueous solution of copper carbonate (30g), ammonia (29%, 345cc) and water (655cc). This cell was mounted on the basket made of stainless steel with goniometer like as shown in Fig.2.3.2. In order to heat a sample a manganin heater was used, C) and D) in Fig.2.3.2.

Appendix 2.3.2 Scattering Geometry for Brillouin Scattering

The magnitude of observed phonon wave vector q associated with the present Brillouin scattering experiment are calculated. Then the angle θ in Fig.A.1 is also estimated by using the refractive indices of RZC instead of KZB. The characteristic of this scattering configuration is that the magnitude of q does not change if refractive index of the crystal changes. But the magnitude depends on the index of n_s in Fig.A.1. In Fig.A.1, because of the law of Snell, we obtain

$$\sin 45°/\sin\psi=n_c/n_s. \qquad (A-1)$$

From the law of conservation of momentum, we obtain

$$q=k_s-k_i \qquad (A-2)$$

The values of k_s and k_i can be written

$$k_s\tilde{=}k_i=n_c k_o, \qquad (A-3)$$

where k_o is the wave number of the light in a vacuum. From eqs. (A-1), (A-2) and (A-3),

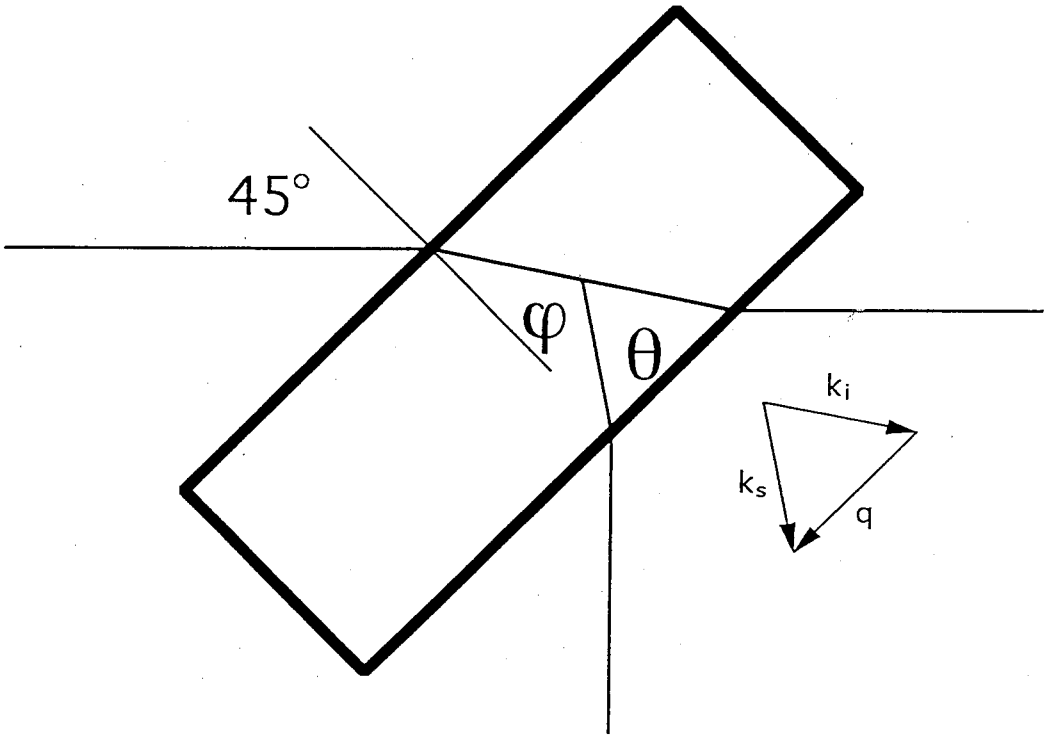

Fig. A.1. Scattering geometry.

$$q=2n_c k_o \sin\theta/2$$
$$=2n_c k_o \sin\psi$$
$$=2n_s k_o \sin 45°. \qquad \text{(A-4)}$$

thus the magnitude of q does not depend on n_c. Note that, if the refractive n_s index of silicone oil depends on temperature, the magnitude of q also depends on temperature.

By the use of the refractive index of silicone oil $n_s=1.4025$ at room temperature and $k_o=2\pi/\lambda=2\pi/514.5$ (nm^{-1}), where λ is a wave length of the Ar^+ gas laser, we obtain $q=2.4222\times10^{-2}$ [nm^{-1}]. Finally from the condition of $n_c=(n_{a,RZC}+n_{b,RZC}+n_{c,RZC})/3=1.57$ and eq. (A-1)

$$\sin\psi = 0.632 \qquad \text{(A-5)}$$

That is, $\psi=39.17$. Then we obtain $\theta=78°$.

Appendix 3.2 Mode Assignment by Inelastic Neutron Scattering

The phonon branches of KZB were observed along [010] of α phase. Single crystal of K_2ZnBr_4 was obtained by evaporation method from aqueous solutions (see §2.1). In elastic neutron scattering measurement have been carried out on $1cm^3$ samples mounted in an aluminum can at room temperature. These experiments were performed by the use of triple-axis spectrometers (TAS) of guide line 4 (G4) in the research reactor JRR-3M of JAERI (Tokai). The measurement process was remote-controlled vir a computer in the building next to the reactor hall. The Bragg peak width (FWHM) was less than 0.4° in 40'-open-40'-40' collimation. The energy scan with constant Q was performed. The inelastic neutron scattering intensity was investigated on the lines (2 0 1)-(2 1 1) and (0 4 0)-(0 5 0) whose scattering vectors Q are (2

q 1) and (0 4+q 0), respectively. Since phonon propagation vector q was nearly perpendicular to scattering vector Q=(2 q 1), and parallel to Q=(0 4+q 0), transverse (TA) modes (almost components of perpendicular to (2 0 1) plane) and longitudinal (LA) mode were observed from Q=(2 q 1) and (0 4+q 0), respectively.

The scattering intensity with constant Q=(0 4+q 0) is shown in Fig.3.2.2(a). The phonon frequency of LA and TA modes was estimated from the peak position. The dispersion relations of phonons are shown in Fig.3.2.2(b). The TA and LA modes were clearly observed. But because of a low resolution of this experimental system, we can not distinguish between TA1 and TA2 modes. Linear lines of the LA, TA1 and TA2 modes are obtained by using the results of Brillouin scattering study (§3.2) of KZB at room temperature and the magnitude of |q| described in Appendix 2.3.2)

Appendix 4.1.1: The General Concept of $P6_3/mmc$ Prototype-I

---- The α-β axis relations ----

In the case of the second order phase transition it is widely accepted that low temperature structures are induced by symmetry breaking from the high-temperature prototype phase.[9] Then, the α-β transition in K_2ZnBr_4 and K_2CoBr_4 might also be considered with the symmetry breaking from the prototype $P6_3/mmc$, because many A_2BX_4-type ferroelectric materials with space group Pmcn are considered to have space group $P6_3/mmc$ in the prototype phase.

In K_2ZnBr_4, the low temperature α phase has space group $P2_1/m$, and has a mirror plane. The space group $P6_3/mmc$ has the two kind of mirror planes, one includes the hexagonal unique axis

(case i) and the other is perpendicular to the axis (case ii). It is expected that one of the two kind of mirrors may remain as the mirror plane in $P2_1/m$. In case i the a_β-axis ($a_\beta \tilde{=} 7.68$A) becomes the b_α-axis ($b_\alpha \tilde{=} 7.50$A). In other words, the mirror plane in Pmcn becomes one in $P2_1/m$. In case ii, the unique axis in prototype $P6_3/mmc$ becomes the unique axis in the α phase, i.e. the c_β-axis ($\tilde{=} 7.22$A) becomes the b_α-axis.

In the case i, since the a_β-axis is parallel to the b_α-axis, the angle between them is either 0 or 180 degrees. Further, we must consider that the β phase is pseudo-hexagonal and the a_β-axis can turn 120 degrees about the unique c-axis. Therefore three directions of the a_β-axis are possible. However, the c_β-axis must always be perpendicular to the b_α-axis. In Table 3.1, data 2 seems to satisfy approximately the above condition. However, it is clear that data 1 and data 3 do not satisfy the above condition. Hence, the case i is not accepted generally.

Next, we consider the case ii in which the unique axis is kept at the α-β phase transition. In this model, the c_β-axis becomes the b_α-axis. That is, the angle between the c_β-axis and the b_α-axis should be 0 or 180 degrees. Investigating the experimental results in Table 3.1, we find that data 1 seems to satisfy this condition, whereas data 2 and data 3 do not. Again, this model seems not to be appropriate.

In the above two models, data 1 and data 2 can be described by using the idea of symmetry breaking from $P6_3/mmc$ while data 3 cannot be explained by assuming the space group $P6_3/mmc$ as the prototype. Indeed the situations such as data 3 were often observed and the concept that $P6_3/mmc$ is the prototype space

group is discarded.

Appendix 4.1.2: The General Concept of $P6_3/mmc$ Prototype-II

---- The β-β axis relations ----

The β-β axis relations are investigated, where β phases were obtained by repeating the β-α-β transition. If the prototype of K_2ZnBr_4 is the space group $P6_3/mmc$, the hexagonal unique axis should be always kept unchanged. The β-β axis relations given in Table I shows that data 6 and data 7 seem to keep the unique axis of pseudo-hexagonal through the β-α-β transition, while data 8 and data 9 do not. That is, data 6 is a good example that the crystal axis does not change through the β-α-β transition, while data 7 is an example that the a- and b-axes turn 120 degrees about the pseudo-hexagonal axis. Data 8 and data 9 indicate that the α-β transition can not be explained by a general theory with $P6_3/mmc$ prototype for the A_2BX_4 type ferroelectric crystals.

Though the c_β-axis can be considered not to change through the β-α-β transition in the above mentioned model, the crystal axis often turns some dozen degrees from the expected value. It is considered that this difference comes about, not because of the displacement of the crystal inside the glass capillary, but because of the essential feature of the α-β transition.

Appendix 4.1.3: Explanation of Relations between each States in VIS Model

The VIS model explains the relation between α and the bcc structures shown in Figs.4.1.1 and 4.1.2 as follows; In Fig. 4.1.2(b), the projection of the bcc structure from [110] direction is shown, where filled circles lie on the one layer and

open circles lie on the other layer shifted perpendicular to the (110) plane. The angle θ is 109.47 degrees. Fig.4.1.1 indicates the b-axis projection of the α structure and the monoclinic angle β is 108.99 degrees[2]. If a- and c-axes are equal in length and open circles move to the center of the cell drawn with solid lines in Fig.4.1.1, then the b-axis projection is approximately equal to the projection of the bcc structure (Fig.4.1.2(b)). Thus the α-structure is not so different to the bcc structure, except for its b-axis: in the α structure the axes ratios for b/a and b/c are 0.817 and 1.04, respectively. However in the bcc structure the ratios are 1.63.

The relationship between bcc and hcp unit cells is illustrated as a three dimensional picture in Fig.4.1.3. If large open circles coincide with the filled circles so as to increase the angle from 109 to 120 degrees, then the bcc structure transform to the hcp structure. This relation is known as the Burgers' model[30] which illustrates the hcp-bcc phase transition in zirconium.

Appendix 4.2: The Direction of the Observed Phonon Wave Vector

Thirty-one possible directions of observed phonon wave vector given by the VIS model were explained as follows. Here we take a count of two types axis relations (type A and type B) between bcc and hcp structures of VIS as shown in Fig.A-2 described in 4.1.2. When the bcc state changes to the hcp state, A'B'C'D'E'F' hexagon of the bcc structure transforms to ABCDEF hexagon of the hcp structure as shown in Fig.A-2 pointed out in 4.1.2. If we consider the direction of the observed wave vector

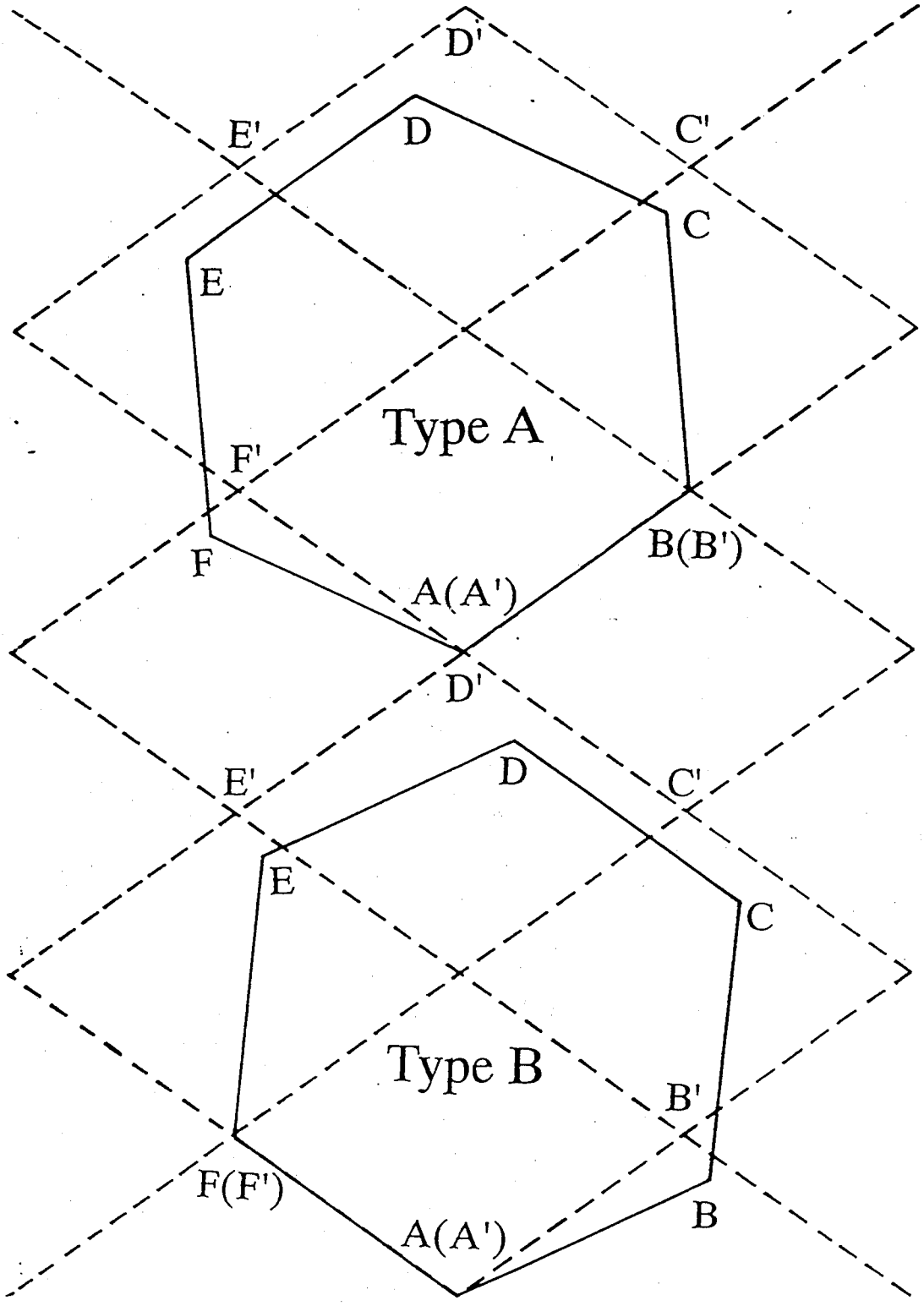

Fig. A.2. The relation between the bcc and hcp structures. Solid and broken lines cells indicate the hcp and bcc structures, respectively; bcc: the projection of the bcc structure from the [110] direction, hcp: the hcp structure projected along the unique axis. There are two equivalent types for the transformation; Type A and Type B.

in a coordinate system on the crystal structure of the β phase reconstructed by the α-β transition, the direction changes in each experimental run even then the direction of the observed phonon wave vector is fixed parallel to the b-axis of the α phase. That is, the directions of the observed phonon-wave vector in the β phase are shown in Fig.A-3 in the coordinate system of the β phase. Here the arrows in Fig.A-3 can be classified into three groups as follows. I) If an observed phonon wave vector is parallel to the A arrow, the angle between the b-axis of the α phase and the c-axis of the β phase after the α-β transition is 0 or 180 degrees [Group I]. II) The eight phonon vectors from B to I arrows indicate that the angle is 60 or 120 degrees [Group II]. III) The two phonon vectors of J and K arrows indicate that the angle is 90 degrees [Group III]. Furthermore we must consider that in the β phase the axis direction can turn 120 degrees about the c-axis of the orthorhombic β phase, since the c-axis is the pseudo-hexagonal axis.[29] That is, a total of thirty-one arrows are obtained for the directions of observed phonon wave vector. On the above conditions the model calculation of $\Delta\nu$ in the β phase can be performed, if we obtain a complete set of the elastic stiffness tensor of the β phase.

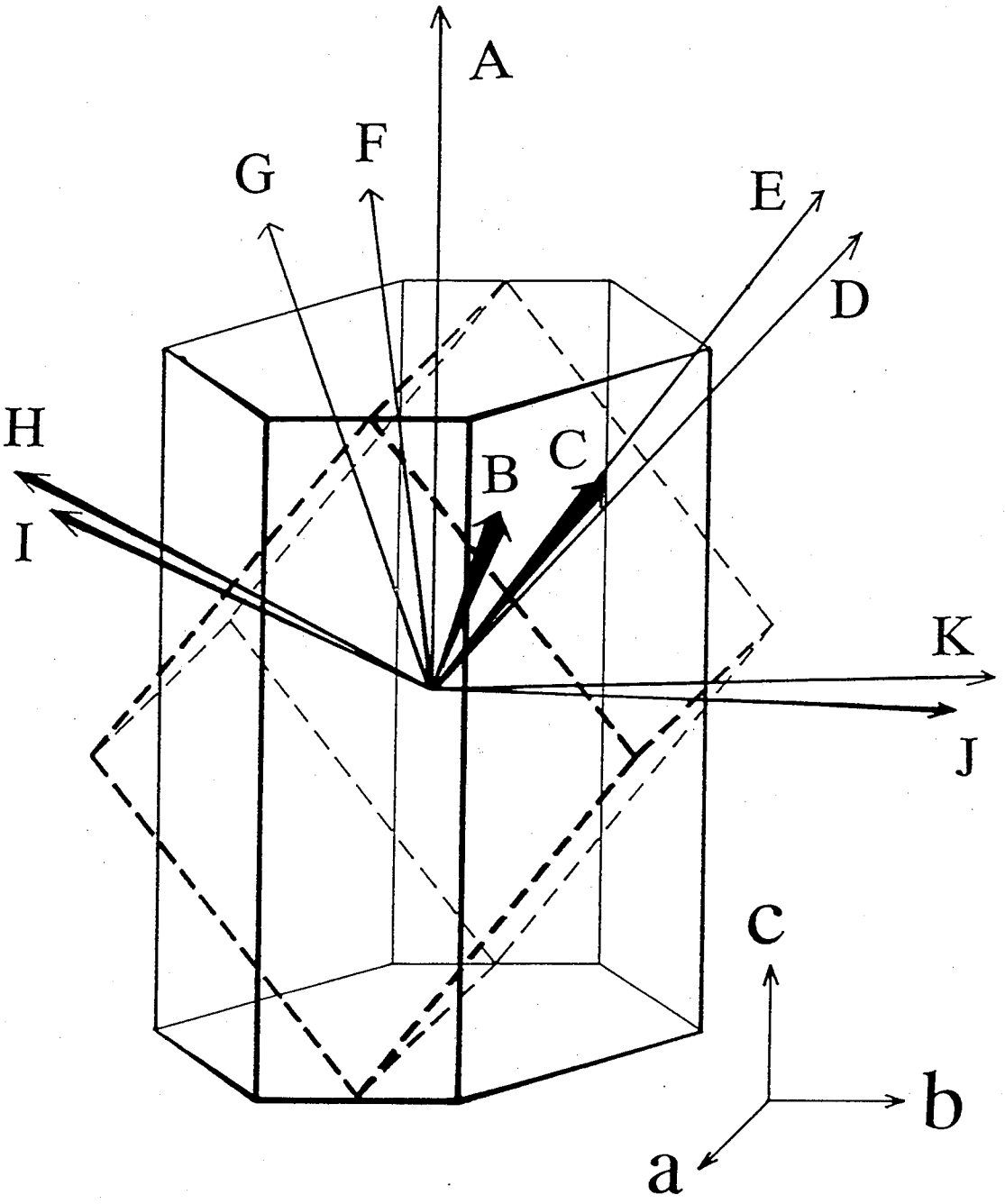

Fig. A.3 The direction of the observed phonon-wave vector in the β phase after the α-β transition in take account of the relation between the axis orientations of bcc and hcp structure of VIS. The direction are shown in a coordinate system located on the β phase reconstructed by the α-β transition. Arrows (a,b, and c) show the axis orientation of the orthorhombic β phase.

References

1)W.B.Pearson:"A Handbook of lattices spacings and structures of metals and alloys", Pergamon Press, Oxford (1967).

2)Z.Nishiyama", Martensitic Transformation", Academic Press, New-York (1979).

3)P.Toledano and V.Dmitriev: Condenced Matter News 2 (1993) 9 and references therein.

4)H.Arend, P.Muralt, S.Plesko and D.Altermatt: Ferroelectrics 24(1980)297.

5)K.Gesi:J. Phys. Soc. Jpn. 54 (1985) 3694.

6)J.D.Axe, M.Iizumi and G.Shirane: Incommensurate Phases in Dielectrics, ed.R.Blinc and A.P.Levanyuk, (North-Holland, 1986,Amsterdam)Vol.2, Chap.10 and references therein.

7)H.Z.Cummins: Phys. Rep. 185 (1990) 211.

8)T.Yamaguchi, F.Shimizu, M.Morita, H.Suzuki and S.Sawada: J. Phys. Soc. Jpn. 57 (1988) 1898.

9)H.Mashiyama, H.Kasano and T.Yamaguchi: J. Phys. Soc. Jpn. 60 (1991) 45.

10)F.Shimizu, T.Yamaguchi, H.Suzuki, M.Takashige and S.Sawada: J. Phys. Soc. Jpn. 59 (1990) 1936.

11)V.I.Pakhomov and P.M.Fedorov: Sov. Phys. Crystallogr. 17 (1973) 833.

12)H.J.Seifert and L.Staudel: Z. Anorg. Allgem. Chem. 429 (1977) 105.

13)H.W.Zandbergen,G.C.Verschoor and D.J.W.Ijdo: Acta Crystallogr. B35 (1979) 1425.

14)K.Gesi:J. Phys. Soc. Jpn. 53 (1984) 3850.

15)F.Shimizu, T.Anzai, H.Sekiguchi, M.Takeshige and S.Sawada: J.

Phys. Soc. Jpn. 63 (1994) 437.

16)H.Kasano, M.Takesada and H.Mashiyama: J. Phys. Soc. Jpn. 61 (1992) 1580.

17)H.Suzuki, F.Shimizu, M.Takashige, S.Sawada and T.Yamaguchi: J. Phys. Soc. Jpn. 59 (1990) 191.

18)H.J.Seifert and I.Al-Khudair: J. Inorg. Nucl. Chem. 37 (1975) 1625.

19)F.Shimizu, H.Suzuki, M.Takashige, S.Sawada and T.Yamaguchi: Ferroelectrics 125 (1992) 117.

20)H.Mashiyama, M.Takesada, M.Kojima and H.Kasano: Ferroelectrics 152 (1994) 313.

21)H.J.Seifert and K.H.Kischka: Thermochimica Acta 27 (1978) 85.

22)F.Shimizu, M.Takashige, S.Sawada and T.Yamaguchi: J. Phys. Soc. Jpn. 62 (1993) 2964.

23)F.Shimizu, M.Takashige, S.Sawada and T.Yamaguchi: Ferroelectrics (in press).

24)M.Takesada and H.Mashiyama: J. Phys. Soc. Jpn. 63 (1994) 2618.

25)F.Shimizu, M.Takashige and S.Sawada: Ferroelectrics (in press).

26)M.Takesada and T.Yagi: J. Phys. Soc. Jpn. 63 (1994) 1241.

27)M.Takesada, M.Yamaguchi and T.Yagi: Ferroelectrics 152 (1994) 391.

28)M.Takesada and T.Yagi: J.Phys. Soc. Jpn. 63 (1994) No.12 (in press).

29)M. Takesada and T. Yagi: Ferroelectrics (in press).

30)J. Warczewski, P. Urbanowicz and J. Kusz: Cryst. Res. Technol. 21 (1986) 131.

31)A. Sawada, Y. Makita and Y. Takagi: J. Phys. Soc. Jpn. 41 (1976) 174.

32)W. G. Burgers: Physica, 1 (1934) 561.

33)J.J.L. Horikx, A.F.M. Arts, J.I. Dijkhuis and H.W. de Wijn: Phys. Rev. B 39 (1989) 5726.

34)Y.Luspin and G.Hauret: C. R. Acad. Sc. Paris B274 (1972) 995.

35)International Tables for Crystallography. Vol. A. (1983).

36)M.Jochum, H-G Unruh and H.Barnighausen: J. Phys. C. 6 (1994) 5751.